博士論文（要約）

Applicability of unmanned aerial vehicles (UAVs) for uneven–aged forest management planning: A study in a mixed conifer–broadleaf forest in Northern Japan

(異齢林管理計画への無人航空機（UAV）の利用可能性：

北日本の針広混交林を対象として)

Jayathunga Sadeepa

ジャヤトゥンガ サデーパ

博士論文

Applicability of unmanned aerial vehicles (UAVs) for uneven–aged forest management planning: A study in a mixed conifer–broadleaf forest in Northern Japan

(異齢林管理計画への無人航空機（UAV）の利用可能性：

北日本の針広混交林を対象として)

Jayathunga Sadeepa

This dissertation is submitted in partial fulfillment of the requirements of the degree of

Doctor of philosophy in the department of Global agricultural sciences

Thesis committee

Dr. Owari Toshiaki (Chief)

Dr. Tsuyuki Satoshi

Dr. Hirata Yasumasa

Dr. Sato Tamotsu

Dr. Tatsuhara Satoshi

International Program for Agricultural development Studies (IPADS)

Department of Global Agricultural Sciences

Faculty of Agricultural and Life Sciences

The University of Tokyo

September, 2018

Table of Contents

List of Tables

List of figures

Abbreviations

%	Percentage
%RMSD	Relative Root Mean Squared Deviation
%RMSE	Relative Root Mean Squared Error
2D	Two Dimensional
3D	Three Dimensional
ABA	Area–Based Approach
AIC	Aikake Information Criteria
ALS	Airborne Laser Scanning
AOI	Area of Interest
APS–C	Advanced Photo System Type–C
asl	Above Sea Level
BA	Basal Area
BDM	Broadleaf Dominating Mixed Selection Stand
BEF	Biomass Expansion Factor
CC	Canopy Cover > 2–Meter Height
CC_{mean}	Canopy Cover > Mean Canopy Height
CDM	Conifer Dominating Mixed Selection Stand
CDM–PR	Conifer Dominating Mixed Selection Stand with Poor Regeneration
CF	Carbon Fraction
CHM	Canopy Height Model
cm	Centimeter(s)
CMOS	Complementary Metal–Oxide–Semiconductor
Co.	Company
CPU	Central Processing Unit
CST	Carbon Stock in Living Biomass
CVH	Coefficient of Variation of Canopy Height
D	Wood Density
d_0	Point Density Above 2–Meter Height
d_1, d_2, d_3 d_4, d_5 d_6, d_7 d_8, d_9	Point Density Above 1^{st}, 2^{nd}, 3^{rd}, 4^{th} , 5^{th} , 6^{th} , 7^{th} , 8^{th} and 9^{th} Height Fractions
d_{mean}	Point Density Above Mean Canopy Height
DBH	Diameter at Breast Height
D_q	Quadratic Mean Diameter at Breast Height
DSM	Digital Surface Model
DTM	Digital Terrain Model
Eq.	Equation

ETM+	Enhanced Thematic Mapper Plus
g	Gram(s)
GB	Gigabyte(s)
GCP	Ground Controlling Point
GIO	Greenhouse Gas Inventory Office of Japan
GLM	Generalized Linear Modelling
GLMM	Generalized Linear Mixed Modelling
GNSS	Global Navigation Satellite System
GPS	Global Positioning System
GPU	Graphic Processing Unit
h	Hour(s)
ha	Hectare(s)
h_{dom}	Dominant Height
IMU	Inertial Measurement Unit
Inc.	Incorporated
InSAR	Interferometric Synthetic Aperture Radar
ISO	International Organization For Standardization
kg	Kilogram(s)
kHz	Kilohertz
km	Kilometer(s)
$km\,h^{-1}$	Kilometers per Hour
LAS	Laser Format
LiDAR	Light Detection And Ranging
LOOCV	Leave–One–Out Cross Validation
Ltd.	Limited
m	Meter(s)
m^2	Squared Meter(s)
$m^2\,ha^{-1}$	Square Meter(s) per Hectare
$m^3\,ha^{-1}$	Cubic Meters per Hectare
MaxH	Maximum Canopy Height
MD	Mean Deviation
MeanH	Mean Canopy Height
$Mg\ C\ ha^{-1}$	Mega Gram Carbon per Hectare
$Mg\ C\ t–d\ m^{-1}$	Mega Gram Carbon per Total Dry Matter
min	Minute(s)
mm	Millimeter(s)

mrad	Milirad
N	Stem density
NA	Data Not Available
OS	Operating System
P10, P25, P50, P75 and P95	10^{th}, 25^{th}, 50^{th}, 75^{th} And 95^{th} Percentile of Canopy Height
PCA	Principal Component Analysis
PL	Plantation
pts.	Points
R	Root–To–Shoot Ratio
RAM	Read Only Memory
REDD+	Reducing Emissions from Deforestation and Forest Degradation–Plus
RF	Reserve Forest Area
RGB	Red, Green, Blue
RMSD	Root Mean Squared Deviation
RMSE	Root Mean Squared Error
RS	Remote Sensing
s	Second(s)
SAR	Synthetic Aperture Radar
SD	Standard Deviation
SDH	Standard Deviation of Canopy Height
SF	Sparse Forest Stand
SfM	Structure from Motion
SIFT	Scale–Invariant Feature Transform
SR	Surface Area Ratio
t–dm m^{-3}	Total Dry Matter per Cubic Meter
TIFF	Tagged Image File Format
TIN	Triangulated Irregular Network
TLS	Terrestrial Laser Scanning
UAV	Unmanned Aerial Vehicle
USA	United States of America
UTHF	University of Tokyo Hokkaido Forest
V	Merchantable Volume
VIF	Variance Inflation Factor
VLOS	Visual Line of Sight
YB	Young Broadleaf Stand
YC	Young Conifer Stand

Acknowledgement

This thesis was made possible because of the tremendous support I received from many individuals. I would like to express my heartfelt gratitude to those who paved the path for me on this journey until its successful completion.

First of all, I would like to express my deepest gratitude to my supervisors for their kind guidance and mentorship throughout this research project. Associate professor Toshiaki Owari as my principal supervisor, for providing me the opportunity and necessary research environment, and Professor Satoshi Tsuyuki as my co–supervisor for kind support in challenging steps and technical knowledge. Without their kind support and guidance, this thesis would not have been possible. Also, I would like to thank the members of my thesis committee–Dr. Yasumasa Hirata, Dr. Tamotsu Sato and Dr. Satoshi Tatsuhara–for their comments and suggestions that significantly contributed to improve this thesis.

My sincere appreciation goes to the technical staff members of the University of Tokyo Hokkaido Forest–Hiroshi Inukai, Hisatomi Kasahara, Hitomi Ogawa, Kota Kimura, Masaki Tokuni, Shinya Inukai, Takashi Inoue, Yoshinori Eguchi, Yuji Nakagawa, Yuji Niwa, and Yukihiro Koike–for their contribution in field and UAV data collection. This work was supported by JSPS KAKENHI grant numbers 15K14751, 16H04946, and 17H01516. Also, this study used Juro Kawachi Memorial dataset of forest spatial information.

Chapter 3 and 4 of this dissertation were benefited from anonymous reviewers whose critical comments improved my work further during the journal publication process. I am grateful to the faculty members of Department of Global Agricultural Sciences and the University of Tokyo Forests for their valuable comments during seminars. I wish to thank members of Tsuyuki–semi for their comments and suggestions during seminars. I'd like to acknowledge the assistance given by my colleague Chen Tai Shen in the statistical analyses.

I'd like to make a special acknowledgement of my deeply felt gratitude to Professor Kensuke Okada, as the IPADS program coordinator, for his kind support throughout the study period.

I sincerely thank all the others who assisted me in various ways during my study period (2015–2018), but not specifically mentioned above.

At last, but not least I am so grateful to my family, for their encouragement, strength and support from the beginning to the end of this research study for its successful completion.

Jayathunga Sadeepa

6 September, 2018

Abstract

Conventional remote sensing (RS) techniques such as satellite RS, airborne laser surveying (ALS), synthetic aperture radar (SAR) and interferometric SAR (InSAR) have limited applicability in operational forest management at local scale because they often require trade–offs between resolution, scale, frequency and cost. By addressing the limitations of conventional remote sensing platforms, fixed–wing unmanned aerial vehicles (UAVs) may bridge the gap between the need for an effective method for data acquisitions and the efforts associated with ground surveys. Previous studies have shown that digital photogrammetric techniques such as structure from motion (SfM) are capable of successfully reconstructing three–dimensional (3D) forest canopy using fixed–wing UAV imagery over even–aged plantations, and forest types with simple structural arrangements, e.g., boreal forests, and woodlands. Although fixed–wing UAV photogrammetry has great potential in forestry applications, its applicability in uneven–aged forest management planning has not been studied intensively. Thus, the aim of this study is to explore how fixed–wing UAV photogrammetry can be incorporated into uneven–aged forest management planning in mixed conifer–broadleaf forests. This thesis comprises seven Chapters including four main Chapters to address four research questions.

Three forest management Compartments (43, 45 and 48) that are located in the University of Tokyo Hokkiado Forest (UTHF) were chosen as the area of interest (AOI). These Compartments comprised forest areas with varying levels of forest structural and spatial complexity. High resolution RGB aerial imagery were acquired over the AOI using a Trimble UX5 fixed–wing UAV platform. These imagery were subjected to a photogrammetric processing using a digital photogrammetric software package to build 3D point clouds and orthomosaics. Then commonly used canopy models, e.g., canopy height models (CHMs), and structural metrics, e.g., height, density, and height variation metrics, were derived using 3D point cloud data. Also, an image metric that explains the broadleaf vegetation cover percentage was calculated using the spectral information contained in the orthomosaics.

The first research question, i.e., how accurate the UAV–photogrammetric products are?, was addressed in Chapter 3 using UAV, ALS and field data from Compartment 43 and 48. The accuracy of UAV–SfM products, i.e., 3D point clouds, CHMs, and structural metrics were evaluated by comparing them to ALS derived 3D point clouds, CHMs and structural metrics, respectively. Then the utility of UAV–SfM structural metrics for estimating forest structural attributes, e.g., dominant height (h_{dom}), basal area (BA), quadratic mean diameter at breast height (Dq), and stem density (N), was examined by employing generalized linear modelling (GLM). Also, the impact of terrain conditions, e.g., altitude, slope, aspect, and forest structural complexity e.g., as explained by canopy height, roughness, and cover, on the performance of the UAV–SfM CHM was explored using GLM. The results demonstrated that apart from the poorly reconstructed small canopy gaps, UAV–SfM point clouds, CHMs, and structural metrics have a comparable accuracy to ALS observations. Also, UAV–SfM data provided similar results to ALS in terms of the area–based estimations of the commonly used forest structural attributes. Relative root mean squared error (%RMSE) values of UAV–SfM estimated h_{dom}, BA, Dq, and N were 7.4%, 18.7%, 12.1%, and 22.7%, respectively. Further, the terrain condition did not show statistically significant association with the performance of the UAV–SfM CHM whereas forest structural attributes that explained the vertical and horizontal variations of the forest canopy were significantly associated with the performance of the UAV–SfM CHM, e.g., canopy height and roughness showed positive coefficient while canopy cover showed a negative coefficient. In Chapter 3 of this thesis, it was demonstrated that although there are differences between ALS and UAV–photogrammetry technique, fixed–wing UAV–photogrammetric products developed over uneven–aged mixed conifer–broadleaf forests perform well in reconstructing forest canopy structure and predicting forest structural attributes that are commonly used in forestry applications. Nevertheless, the performance of UAV–SfM CHM is likely to be influenced by the structural complexity of the forest canopy.

The second research question, i.e., what type of quantitative forest information can be retrieved using UAV photogrammetric products?, was addressed in the Chapters 4. First, the utility of fixed–wing UAV–photogrammetry in estimating widely used forest resource information, e.g., merchantable volume (V) and carbon stock in living biomass (CST), was tested using regression

modelling of field measurements, and UAV–SfM structural and image metrics calculated at plot–level. Also, the spatial distributions of UAV–SfM estimated V and CST were mapped over Compartment 43 and 48. UAV–SfM results, e.g., plot–level estimates and spatial distribution maps of V and CST, were then compared to ALS results to get better understanding on the accuracy of the UAV–SfM estimations. Plot–level validation of UAV–SfM estimated V revealed a RMSE of 39.8 m^3 ha^{-1} and a %RMSE of 16.7%, whereas the RMSE and %RMSE vales for UAV–SfM estimated CST were 14.3 Mg C ha^{-1} and 17.4%, respectively. The image metric (broadleaf vegetation cover percentage) that was included in the regression analysis showed a statistically significant association with both V and CST, and provided an additional explanatory power. Nevertheless, RMSE values did not significantly change after adding the image metric into the regression analysis, e.g., %RMSE was reduced by 1.9% for V estimation, and 1.5% for CST estimation. Furthermore, the obtained UAV–SfM estimates were comparable to ALS estimates (relative RMSE of ALS estimations were 16.4% and 16.7% for V and CST, respectively). The spatial distributions of V and CST could be successfully mapped using UAV–SfM data and their stand– and landscape–level variations could be identified with a comparable accuracy to ALS observations. Therefore, the potential of fixed–wing UAV–photogrammetry to capture the fine scale spatial variation of V and CST in uneven–aged forests that are subjected to silvicultural practices and natural disturbances over time was further confirmed in the Chapter 4 of this thesis.

The utility of UAV photogrammetry to characterize forest canopy structure was examined in Chapter 5 to answer the third research question, i.e., how UAV–photogrammetric products can be used to characterize forest canopy structure and vegetation types?. Seven structural metrics derived from UAV–SfM data, e.g., 95th percentile of canopy height (P95), mean canopy height (MeanH), standard deviation of canopy height (SDH), coefficient of variation of canopy height, surface area ratio (SR), canopy cover > 2 m height (CC), and canopy cover > mean height (CC_{mean}), were compared to field measurements, e.g., h_{dom}, BA, Dq, standard deviation of diameter at breast height, CST, N, and proportion of broadleaf stem density, using univariate (Pearson correlation coefficients) and multivariate analyses (Principal component analysis–PCA). Then twelve subsets (each including three UAV–SfM metrics, i.e., a metrics that explained height measurement, a metric

that explained height variation and a metric that explained canopy cover) were defined and PCA ordinations were produced. These twelve PCA ordinations were compared to the PCA ordinations of four base combinations, i.e., all the field metrics, all the UAV–SfM structural metrics, all the field and UAV–SfM metrics, and all the ALS metrics, to examine if a subsect of UAV–SfM structural metrics is capable of capturing the vertical and horizontal variations of the uneven–aged forest canopy structure as explained by all the field and ALS structural metrics. After identifying the appropriate subsect of UAV–SfM structural metrics through PCA ordination comparison, the subsect of UAV–SfM structural metrics was coupled with the broadleaf vegetation cover percentage metric to classify the predominant forest structure types in Compartment 43 and 48. Unsupervised *k*–means clustering algorithm was used for the classification. Lastly, the spatial distribution of the identified forest structure types were mapped. The results demonstrated that all the chosen UAV–SfM structural metrics have significant correlations with at least one field measurement of forest canopy structure. Also, all the PCA ordinations of the UAV–SfM metric subsets were correlated to the PCA ordinations of the base combinations. Subset that comprised MeanH, SDH, and CC showed the strongest correlations with the PCA ordinations of all the base combinations, suggesting that this particular subset is capable of characterizing the vertical and horizontal variations of the forest canopy structure at the AOI. Forest canopy structure classification identified five predominant forest structure types: short, open canopy, conifer dominating structures; short, dense canopy, broadleaf dominating structures; tall, close canopy, broadleaf dominating structures; very tall, close canopy, conifer dominating structures with relatively high variation of canopy height; and very tall, close canopy, conifer dominating structures with relatively low variation of canopy height. Results also revealed that the remotely sensed forest structure types have relationship to the conventional forest stand classification maps. In Chapter 5, it is concluded that the structural and spectral information retrieved from fixed–wing UAV–photogrammetric products are capable of characterizing the vertical and horizontal variations of the forest canopy structure, discriminating broadleaf and conifer vegetation types, and identifying predominant forest canopy structure types in uneven–aged mixed conifer–broadleaf forests without ground sampling data.

Several major limitations, i.e., bias, resource intensiveness and lack of spatially explicit data, are often associated with the conventional ground data acquisition and uneven–aged forest management planning. Thus, in Chapter 6 of this thesis, it is discussed how the fixed–wing UAV platforms can be used to overcome major limitations of the conventional data collection method and support uneven–age forest management planning. This was demonstrated by conducting a case study in the UTHF, particularly by providing empirical evidences for the forest management Compartment 45 which is scheduled to be managed in 2018. Detailed investigation revealed several stages in the forest management planning process of UTHF that can benefit from fixed–wing UAV–photogrammetry, e.g., forest stand classification, forest inventorying, harvesting and restoration planning, and carbon management. First, the utility of UAV–SfM data for forest stand classification of Compartment 45 was tested and the UAV results were compared with the conventional stand classification map (prepared using ground based observations). Then the utility of UAV–SfM derived structural metrics for forest inventorying, e.g., to estimate BA, Dq, V, and CST, was examined for Compartment 45 using the regression equations developed in Chapter 3 and 4 of this thesis. Finally, the potential of V and CST information of Compartment 45 in the harvesting decision making processes were examined. The results revealed that UAV–SfM data are promising to discriminate broadleaf dominating mixed stands, young broadleaf stands, and sparse forest stands. However, misclassifications were often occurred when classifying conifer dominating mixed stands, conifer dominating mixed stands with poor regeneration, and reserve forest area as their delineations are not solely based on the forest canopy vegetation structure. Regression equations developed using the UAV–SfM and field data of Compartment 43 and 48 performed well in terms of area–based estimation of forest structural attributes of Compartment 45, e.g., %RMSE values were 15.0%, 12.3%, 12.9%, and 12.6% for BA, Dq, V, and CST, respectively. Also, the spatial distributions of V and CST could be accurately mapped over Compartment 45 using UAV–SfM data. UAV–SfM estimated V had a good potential to be used in the forest harvesting decision making in uneven–aged forest management planning. In this thesis, CST which has huge importance at local–, national–, regional– and global–level is proposed as a new indicator to be incorporated into future management planning for identification of restoration sites, and for carbon management at forest enterprise level

because UAV–SfM estimated CST information at local–level has huge potential to contribute to national–level carbon management and reporting. Chapter 6 of this thesis showed that fixed–wing UAV data is capable of minimizing efforts and time spent for convention data collection methods by providing detailed and accurate complementary data source that can be utilized in important stages of the forest management planning of the UTHF.

Overall, the results of this thesis demonstrated that fixed–wing UAVs are an efficient data collection method in forestry applications, hence capable of supporting precision forestry at local–level. Particularly, they can contribute to the existing data collection and management planning processes by providing detailed, accurate and spatially explicit forest information, e.g., stand delineation, forest inventory, and forest canopy structural complexity. Nevertheless, the conventional method cannot be replaced by UAV photogrammetric data due to some limitations of photogrammetry, e.g., poor penetration ability into the canopy, and lack of information about understorey and regeneration that also play an important role in forest management decision making. Therefore, it is concluded that fixed–wing UAV–photogrammetry has a good potential in uneven–aged forest management planning as a complementary data source to improve efficiency, minimize resource requirement, and enhance precision of the data. Future research should target to explore how the limitations of fixed–wing UAV–photogrammetry can be overcome, e.g., if the limitations could be overcome when fixed–wing UAV–photogrammetry is combined with other data sources such as terrestrial laser scanning (TLS), and if results can be improved when UAV platforms are used with other sensor types such as LiDAR.

Chapter 1

Introduction

1.1. Background

1.1.1. Importance of forest management planning

In addition to the supply of timber and non–timber forest resources, forests provide a multitude of ecological functions, e.g., nutrient cycling, carbon sequestration, maintenance of wildlife habitats and biodiversity, pollution absorption and regulation of supply and quality of water, and social benefits to humankind, e.g., recreation. Climate change, the most important environmental issue of the twenty–first century, has significant implications for the resource management including natural resources such as forests (Apps, 2001; Boisvenue and Running, 2006; Millar et al., 2007; Noss, 2001). Therefore, forest management strategies should aim to deal with future challenges that forest ecosystems might face under changing climatic conditions as well (Keenan, 2015; Lindner et al., 2014; Messier and Puettmann, 2011; Nelson et al., 2016; Poteete and Ostrom, 2004).

Forests play a key role in the increasing levels of atmospheric carbon because they act as both carbon sinks (carbon accumulation through photosynthesis) and sources (due to decomposition, respiration, and harvesting) (Houghton et al., 1999; Klein et al., 2013; Nabuurs et al., 2008). Therefore, great importance is often ascribed to forest management in various conventions and protocols (e.g., Kyoto Protocol) because it can provide opportunities for the sustainable use of forest resources (Bawa and Seidler, 1998). It also provides a pathway for the protection of forests and reduction of emissions, and supports climate change mitigation initiatives like REDD+ by addressing forest degradation and deforestation, while enhancing the direct benefits to human society and the environment at the regional and global levels (Lindenmayer et al., 2000). The unexpectedly large impact of forest management on global vegetation biomass that was recently reported (Erb et al., 2017) further highlights the significance of sustainable forest management.

Currently, there is a gradual shift from pure even–aged management to uneven–aged management of forests throughout the world as a result of the increasing criticisms on the even–aged silviculture, particularly considering the strong and mostly negative impacts of clear–felling on visual landscapes, habitat quality, and outdoor recreation (Kuuluvainen et al., 2012; Monserud and Sterba, 1996; Pukkala et al., 2011). In uneven–aged forest management, the management consists of a range of methods, in which the forest cover is only partially removed (Kuuluvainen et al., 2012), hence sometimes referred to as continuous cover forestry (Pommerening and Murphy, 2004). Basically, uneven–aged forest management aims to create and maintain stands with uneven tree age structure through selection harvesting, i.e., removal of individual trees (single tree selection) or as groups (group selection) (Kuuluvainen et al., 2012; Nyland, 2002; Pukkala et al., 2011).

A well–planned forest management strategy can provide opportunities for sustainable utilization of uneven–aged forest resources (Bawa and Seidler, 1998; MacDicken et al., 2015), and contribute to climate change mitigation aims (Nelson et al., 2016) by maintaining and preserving existing forest resources, increasing the area of forest cover, and increasing the carbon stocks on the forested landscapes. Hence, great importance is often ascribed to uneven–aged forest management (Bettinger et al., 2017; Davis and Johnson, 1987; Erb et al., 2017; MacDicken et al., 2015; Sabogal et al., 2013). The goal of uneven–aged forest management is getting diversified to support revenue streams (Cambero and Sowlati, 2014; Merilä et al., 2014) while contributing to ecological services (Boyd and Banzhaf, 2007; Johnson and Curtis, 2001; Lindenmayer et al., 2001; Lowrance et al., 1997), carbon management (Jandl et al., 2007; Naughton–Treves and Wendland, 2014; Seidl et al., 2014), and expanded recreational opportunities (White, 2017; Wilkes–Allemann et al., 2015).

However, to achieve the goals of uneven–aged forest management and to promote sustainable utilization of forest resources, decisions must be made in a complex, ever–changing environment where a wide variety of stakeholders and groups have a role to play. Management planning is the most critical phase of forest management (Bettinger et al., 2017; Davis and Johnson, 1987) as the objectives are set, and the course of actions for achieving those objectives are determined during this phase. This is particularly true for uneven–aged forest management, because with proper management planning uneven–aged management has the potential to become fully

competitive with existing even–aged management. Uneven–aged forest management planning requires substantial amounts of data that can inform the quantitative and qualitative information about forest resources (Kuuluvainen et al., 2012; Monserud and Sterba, 1996; Pukkala et al., 2011). Particularly uneven–aged forest management planning requires information for forest resource inventorying, forest structure characterization, vegetation composition identification and forest monitoring. However, acquisition of accurate and up–to–date data using ground surveys is often resource–intensive and lacks spatial distributions, and sometimes the data acquisition could be biased. Hence, there's a demand for an innovative and effective method to obtain accurate data in a cost–effective manner (Franklin and Van Pelt, 2004; Kane et al., 2010b).

1.1.2. Role of remote sensing technology in forest management planning

The wide availability of remote sensing (RS) technology, i.e., technique of acquiring information about an object of interest or phenomenon without making physical contact with the object (Campbell, 2002), in recent decades, continuous advancements made in RS sensors and platforms, and varying spectral, spatial, and temporal resolutions of RS data, has provided innovative avenues for forest managers to use RS data in combination with field data, as an alternative data source, to obtain spatially explicit information that are required for forest management planning (e.g., Brosofske et al., 2014; Hall et al., 2006; White et al., 2013; Wulder et al., 2013). There are various sources of RS data that are acquired using active and passive sensors, e.g., optical sensors, synthetic aperture radar (SAR), interferometric SAR (InSAR), and light detection and ranging (LiDAR), and different types of platforms, e.g., satellite, and airborne platforms.

Satellite–borne optical sensors may have limited applicability in operational forest management because they often require trade–offs between resolution, scale, frequency and cost. Although other active RS techniques such as airborne LiDAR, SAR and InSAR have been proven to effectively provide data that complement field–based measurements by yielding three–dimensional (3D) canopy reconstruction and more accurate information about forest resources (Ho Tong Minh et al., 2016; Hyyppä et al., 2012; Kumar et al., 2017; Yoga et al., 2017), their application

in forest management is often hindered by high acquisition costs. By addressing these limitations of conventional remote sensing techniques, unmanned aerial vehicles (UAVs), i.e., a fine–scale remote sensing technique emerging as an alternative to airborne and satellite platforms, may bridge the gap between the need for an cost–effective method for data acquisition, and the considerable efforts associated with ground surveys (Matese et al., 2015; Puliti et al., 2017; Thiel and Schmullius, 2017; Torresan et al., 2017).

UAV platforms have key advantages of (1) flexibility to host different kind of sensors, (e.g., Franklin et al., 2017; Wallace et al., 2016), (2) decentralization of data acquisition to plan flight sessions as per requirement and to avoid problems such as cloud cover (e.g., Puliti et al., 2017, 2015; Zahawi et al., 2015), (3) potential for obtaining data with high spatial and temporal resolution (e.g., Cunliffe et al., 2016; Thiel and Schmullius, 2017), and (4) low material and operational costs (e.g., Anderson and Gaston, 2013; Nex and Remondino, 2014; Puliti et al., 2017). Currently, three types of small UAV platforms (UAV platforms weigh < 5 kg and widely used for scientific research) are available on the market: (1) multi–rotor, (2) single–rotor that is similar in design and structure to a helicopter, and (3) fixed–wing UAVs (Nex and Remondino, 2014; Watts et al., 2012). Single–rotor UAVs (in comparison to multi–rotor UAVs) have the advantage of efficient power consumption but they have limited agility, higher complexity, operational risk and product costs.

Compared to multi–rotor UAVs, fixed–wing models could be superior in forestry applications because of several factors, including (1) faster flying speeds that allow them to cover large areas without being influenced by wind resistance or bad weather as easily as multi–rotors, (2) long endurance and an extended battery life that enable them to cover many miles in a single session, (3) ability to carry heavier payloads, and (4) capability to fly at higher altitudes that permit a greater visual line of sight (VLOS) range. Thus, fixed–wing UAVs may enable efficient data collection over relatively larger areas and are a viable option for forestry applications, including operational forest management that requires geo–referenced imagery at comparatively large scales. Particularly, fixed–wing UAVs could be an appropriate data acquisition method where extensive field data collection can be costly, field locations can be inaccessible, or the use of RS to complement the field sampling is advisable (Puliti et al., 2017). High–resolution imagery acquired using UAV platforms can be

utilized to extract fundamental characteristics such as tone, texture, pattern, shape and association (Anderson and Gaston, 2013; Bohlin et al., 2017; Getzin et al., 2014; Torresan et al., 2016). Also, the digital photogrammetric techniques such as structure from motion (SfM) are capable of successfully developing 3D point clouds from UAV imagery.

Digital photogrammetry and SfM

Photogrammetry is generally the use of photography for surveying. It facilitates the production of maps and geographic databases from aerial photographs (Kasser and Egels, 2002). It is simply defined as any measuring technique allowing the modelling of a 3D space using two–dimensional (2D) images. Aimé Laussedat, a military engineer in France, is known as the inventor of photogrammetry. However, the term "Photogrammetry" was first introduced in 1867 by Albrecht Meydenbauer (Albertz, 2007). Stereo–photogrammetry is one of the widely applied photogrammetric methods. In stereo–photogrammetry, the 3D structure can be resolved from a series of overlapping, offset images. In the early stages, the 3D location of points within a scene was determined manually using the 3D location and pose of the camera(s), or the 3D locations of a series of known control points. Since the introduction of the discipline of photogrammetry, it has been continuously evolved and remarkably improved to the most recent innovation of the digital photogrammetry, i.e., based on the fundamental concepts of traditional photogrammetry but also involves comprehensive use of digital tools, and takes advantage of the automated processes. Digital photogrammetry has significantly cut costs, reduced processing time and allowed even non–experts to successfully utilize photogrammetry for various purposes (Kasser and Egels, 2002). Also the developments in Global Navigational Satellite System (GNSS) and Inertial Measurement Units (IMU) have also significantly contributed the high positional accuracy of digital photogrammetric techniques while the introduction of graphic processing units (GPUs) increased the computational capabilities in graphic processing.

SfM technique, developed in 1990s based on the same basic concepts of stereoscopic photogrammetry, is one of the widely used digital photogrammetric techniques. SfM operates to provide automatic definition of the geometry of a scene, camera positions and orientation without

prior specifications of the targets with known 3D positions. The 3D positions are solved simultaneously using a highly redundant, iterative bundle adjustment procedure, based on a database of features automatically extracted from a set of multiple overlapping images (Snavely et al., 2008; Westoby et al., 2012). Thus the SfM approach consists of, (1) matching features that were automatically identified in multiple images, (2) tracking those features from image to image, and (3) refining the camera positions and object coordinates iteratively using non–linear least–squares minimization (Snavely et al., 2008). However, this process of SfM lacks the scale and orientation provided by ground–control coordinates and the 3D point clouds are generated in a relative 'image–space' with an absolute coordinate system (Westoby et al., 2012). Therefore, the SfM image–space coordinates required to be transformed by using a small number of known ground controls points (GCPs) e.g., identified clearly visible features in both the resulting point cloud and in the field, or physical targets (ideally with a high contrast and clearly defined centroid) that were deployed in the field before acquiring images. SfM takes the advantage of the computer vision and the automatic feature–matching algorithms. Therefore, the recent improvements in computer vision algorithms such as the Scale Invariant Feature Transform (SIFT) (Leberl et al., 2010) and parallel bundle adjustments on GPUs have improved the ability to match image features in many overlapping photographs (100s–1000s), and generate 3D point clouds over large areas (Leberl et al., 2010; Wolf and Dewitt, 2000), making SfM ideally suited for aerial imagery acquired using UAVs. Today, many commercial and open source software, e.g., IMAGINE Photogrammetry (Hexagon Geospatial, Alabama, USA), PHOTOMOD (RACURS, Moscow, Russia), Trimble Inpho (Trimble Geospatial Inc, California, USA), Agisoft PhotoScan (Agisoft LLC, St Petersburg, Russia), pix4D (pix4D Inc., Lausanne, Switzerland), and MicMac (open source) are available to perform SfM from imagery acquired using various sensors, thus made SfM a low–cost, effective tool for many applications including forest management planning.

1.1.3. Application of fixed–wing UAV photogrammetry in uneven–aged forests

In the early years, researchers have used digital photogrammetry of aerial imagery acquired using manned platforms such as aircrafts or helicopters, e.g., Baltsavias et al. (2008); Järnstedt et al. (2012); Nurminen et al. (2013); Vastaranta et al. (2013), but later shifted towards the digital photogrammetry of UAV imagery. Particularly, with the wide availability of low–cost UAV platforms in the market in recent years, forestry applications of UAVs has gained significant popularity (Hernández–Clemente et al. 2014; Torresan et al., 2017; Watts et al., 2012).

Several attempts have been made to use UAVs for various forestry applications, with some promising results reported, e.g., biophysical parameter estimation (Chianucci et al., 2016; Iizuka et al., 2017; Puliti et al., 2015; Zarco–Tejada et al., 2014), forest resource inventorying (Kachamba et al., 2016; Puliti et al., 2017), forest structure characterization (Alonzo et al., 2018; Messinger et al., 2016; Wallace et al., 2016), tree species identification (Baena et al., 2017; Cunliffe et al., 2016; Franklin et al., 2017; Gini et al., 2014; Michez et al., 2016), forest health monitoring (Dash et al., 2017; Lehmann et al., 2015; Näsi et al., 2015; Smigaj et al., 2015), forest dynamics monitoring (Aicardi et al., 2016; Pierzchała et al., 2014; Zahawi et al., 2015), and forest fire detection (de Dios et al., 2011; Ghamry et al., 2016; Yuan et al., 2015). Majority of the studies were focused on the estimation of forest biophysical parameters such as height, basal area (BA), tree density, diameter at breast height (DBH) etc., while a few also attempted to estimate volume, biomass and carbon stocks for forest resource assessment. Also, most of the studies used rotary–wing UAVs and conducted in even–aged, and well–managed forest areas. Studies that used fixed–wing UAV photogrammetry in uneven–aged forests are listed in Table 1.1.

Most of the existing studies examined how fixed–wing UAV photogrammetry could be used for estimating forest structural attributes and inventorying in uneven–aged forests. Lisein et al. (2013) is the only study that compared UAV structural metrics to LiDAR structural metrics. Nevertheless, their comparison was limited to height metrics such as mean height, 25^{th}, 50^{th}, 75^{th}, 95^{th}, 99^{th} and 100^{th} percentile heights (Pearson correlations with LiDAR height metrics ≥ 0.85) at

window level. Estimation of dominant height showed the lowest error, e.g., relative RMSE value ≥ 3.5 % (Lisein et al., 2013; Puliti et al., 2015), while relative RMSE values reported for other forest structural attribute estimations were comparatively larger, e.g., for mean height ≥ 13.3% (Puliti et al., 2015; Tuominen et al., 2015), BA ≥ 14.9% (Puliti et al., 2015; Tuominen et al., 2015), for stem volume ≥ 15.0% (Puliti et al., 2015; Tuominen et al., 2015; Puliti et al., 2017), for mean diameter = 20.1% (Tuominen et al., 2015), for stem density = 39.2% (Puliti et al., 2015), and for biomass = 46.7% (Kachamba et al., 2016). In the previous studies that used spectral information (e.g., mean and SD of band values) in the regression modelling of structural attributes, spectral metrics could improve the results only to a limited degree indicating the need of further research efforts to effectively utilize spectral information contained in UAV imagery (Puliti et al., 2015; Tuominen et al., 2015). A cost–benefit analysis of the UAV based inventory was conducted in a 7,330 ha forest area by Puliti et al. (2017) and reported that UAV has huge potential to be a cost–effective tool for large scale forest resource assessments.

Few studies attempted to characterize forest canopy structural and species attributes such as canopy gaps, leaf area index, and species composition in uneven–aged forests using fixed–wing UAV photogrammetry, and use such information to predict forest biodiversity and disturbance measures, e.g., Getzin et al. (2014) concluded that very high resolution UAV imagery could successfully capture canopy gaps as small as 1 m^2 and their variations, and Chianucci et al. (2016) demonstrated that true color UAV images could provide accurate estimates of leaf area index in beech forests with dense canopy cover but tend to overestimate the canopy cover because of the failure to capture small within–crown gaps. Michez et al. (2014) developed an approach to differentiate deciduous riparian forest species (*Alnus glutinosa*, other riparian, *Picea abies*, *Acer pseudoplatanus*, and *Quercus* spp.), and reported promising results (79.5% accuracy for the forests under pressure by farm activities and 84.1% for the unmanaged and undisturbed forest sands).

Table 1.1: Studies that used fixed–wing UAV photogrammetry in uneven–aged forests. (NA: data not available)

	Forest type and vegetation composition	**Country**	**UAV platform**	**Sensor**	**Objective(s) of study**
Lisein et al. (2013)	Uneven–aged broadleaf forests dominated by *Quercus robur* and *Q. petraea*	Belgium	Gatewing X100 (Trimble Navigation Ltd., California, USA)	GR Digital III camera (Ricoh Ltd., Tokyo, Japan)	Estimating dominant height at stand and individual tree level and comparing with airborne LiDAR estimates.
Getzin et al. (2012)	Deciduous forests dominated by *Fagus sylvatica*	Germany	Carolo P200 (Mavionics GmbH, Germany)	NA	Quantifying gap spatial patterns in managed and non–managed forest areas.
Getzin et al. (2014)	*F. sylvatica* dominated deciduous and mixed deciduous/coniferous forest	Germany	Carolo P200 (Mavionics GmbH, Germany)	NA	Assessing understorey biodiversity using high resolution imagery acquired from UAVs.
Puliti et al. (2015)	Boreal forest with *P. abies*, *Pinus sylvestri*. and *Betula pubescens*	Norway	eBee (Sensefly Ltd., Cheseaux–Losanne, Switzerland)	Canon S110 camera (Canon Inc., Tokyo, Japan)	Estimating Lorey's mean height, dominant height, tree density, basal area and volume.
Tuominen et al. (2015)	Forest area dominated by *P. sylvestris*, *P. abies*, *Larix* spp., *B. pendula* and *B. pubescens*	Finland	Gatewing X100 (Trimble Navigation Ltd., California, USA)	RICOH GR Digital III camera (Ricoh Ltd., Tokyo, Japan)	Testing the photogrammetric canopy height model and estimating forest inventory variables.

Chianucci et al. (2016)	Mountain forest dominated by *F. sylvatica*	Italy	eBee (Sensefly Ltd., Cheseaux–Losanne, Switzerl and)	Canon Power Shot/ELPH 110 (Canon Inc., Tokyo, Japan)	Estimating forest canopy attributes from true color images acquired using an UAV.
Kachamba et al. (2016)	Woodlands dominated by *Julbernadia globiflora*, *Diplorhychus condylocarpon* and *Combretum zeyheri*	Malawi	eBee (Sensefly Ltd., Cheseaux–Losanne, Switzerland)	Canon IXUS127 HS camera (Canon Inc., Tokyo, Japan)	Estimating biomass using UAV derived point cloud data and comparing the impact of digital terrain models.
Michez et al. (2016)	Riparian forest of *A. glutinosa*	Belgium	Gatewing X100 (Trimble Navigation Ltd., California, USA)	GR3 and R3 camera (Ricoh Ltd., Tokyo, Japan)	Developing an approach to differentiate deciduous riparian forest species under different pressure conditions and health state.
Puliti et al. (2017)	Forest area dominated by *P. abies*, *P. sylvestris*, and *B. pubescens*	Norway	eBee (Sensefly Ltd., Cheseaux–Losanne, Switzerland)	Canon IXUS/ELPH camera (Canon Inc., Tokyo, Japan)	Understanding how UAVs can be used as sampling tools in large scale inventories.

1.2. Objectives of the study

Although the previous studies using fixed–wing UAVs (Table 1.1) reported promising results, and highlighted their potential in forestry sector, applicability of fixed–wing UAVs in forest management planning has not been intensively examined. Thus, several important questions are yet to be addressed. Based on the existing knowledge, I have identified four critical research questions; (1) How accurate the UAV photogrammetric products in uneven–aged forestry applications are?, (2) What type of quantitative forest inventory information can be retrieved using UAV photogrammetric products?, (3) How can we use UAV photogrammetric products to characterize forest canopy structure and vegetation types?, and (4) How can forest managers incorporate information retrieved using UAV photogrammetry for uneven–aged forest management planning? Addressing these research questions would significantly contribute to the advancement of the knowledge on UAV photogrammetry in uneven–aged forestry applications. Therefore, the overall aim of this study is to explore how we can incorporate fixed–wing UAV system for uneven–aged forest management planning. Based on the four research questions discussed above, four specific objectives were set out to achieve the main aim of the study.

First objective was to evaluate the accuracy of UAV photogrammetric products in comparison to airborne LiDAR data. Except for the handful of studies summarized in Table 1.1, majority of exiting studies have tested the utility of fixed–wing UAVs in even–aged plantations, well–managed forests, or boreal and woodland forests that have simple structures (Torresan et al., 2016; White et al., 2013). Thus, the robustness of the fixed–wing UAV photogrammetry over heterogeneous forests, and the extent to which the results of the existing studies are representative of uneven–aged forests with multi–layered arrangements and complex structures are uncertain and requires better understanding. This is particularly true for mixed conifer–broadleaf forests in northern Japan that represent the transition zone between the temperate forests and boreal forests, and subject to various anthropogenic (e.g. selection harvesting) and natural disturbances (e.g., typhoon damage). Therefore, the performance of the UAV photogrammetric products were assessed in this study to confirm their accuracy and robustness in uneven–aged forests. Airborne LiDAR data,

i.e., a well–established, intensively–researched and one of the most accurate data sources, was used as the reference data set. Also the forest structural attributes estimated using UAV photogrammetric products were validated using field measurements.

Second objective was to retrieve quantitative forest inventory information, e.g., volume and carbon stock. Uneven–aged forest management planning demands for a substantial amount of spatially explicit data and information. Existing literature suggests that fixed–wing UAV platforms could represent a viable option to provide such data and information at the forest enterprise level, where they can be used as part of the sampling strategy to obtain wall–to–wall data in a cost–effective manner (Puliti et al., 2017). However, studies that tested the utility of fixed–wing UAV photogrammetry for data collection at forest enterprise level is limited in literature, Puliti et al., (2017) is the only study that used fixed–wing UAV for large–scale forest inventorying. Spectral and structural information were extracted from UAV photogrammetric products to estimate widely used forest inventory information, i.e., volume and carbon stock. The UAV photogrammetric estimates were compared to airborne LiDAR estimates to get better understanding.

UAV imagery can be used to obtain both spectral and structural information that are important to characterize forest canopy structure and vegetation type, hence have the advantage that other 3D data sources such as airborne LiDAR do not possess. Structural information of the UAV photogrammetric products have been studied intensively using both individual tree– and area– based approaches. Nevertheless, very few studies have used the spectral information contained in UAV photogrammetric products in combination with structural information (e.g., Puliti et al., 2015; Tuominen et al., 2015), and there is a need to better understand how we can effectively exploit the spectral information contained in UAV imagery. Also, the studies that attempted to characterize the forest structure by using multivariate analyses are limited in literature. Alonzo et al., (2018) studied forest structure and vegetation composition simultaneously in a boreal forest but still lacked the multivariate analysis to characterize multi–faceted forest structure. Thus, the third objective was to characterize forest structure and vegetation types using structural and spectral information contained in UAV data. In this study, the UAV photogrammetric structural attributes that are capable of quantifying forest canopy structure were identified by comparing them to field measurements and

airborne LiDAR data, and the multi–faceted forest canopy structure and vegetation types were characterized and mapped using multivariate statistical analyses.

Fourth objective was to explore how the UAV retrieved information can be applied for uneven–aged forest management planning at forest enterprise level. Although, some of the existing literature have addressed several aspects of fixed–wing UAV photogrammetry that could be immensely important in forest management planning (Puliti et al., 2017; Torresan et al., 2017; Tuominen et al., 2015), there still persists a knowledge gap between fixed–wing UAV photogrammetry and uneven–aged forest management planning. In this study, I attempted to fill this knowledge gap by proposing how to incorporate fixed–wing UAV system for uneven–aged forest management. Upon successfully addressing the above mentioned important questions systematically, it could be possible to propose a method to incorporate UAV system into uneven–aged forest management planning. The information retrieved in the second, and third sections were utilized to propose how UAV photogrammetry can be incorporated into uneven–aged forest management planning at forest enterprise level.

1.3. Organization of the thesis

The outline of the research is summarized in Figure 1.1. After providing the background to this research study, the research questions and objectives (Chapter 1), information about the study site and data is presented (Chapter 2). Chapter 3-6 address the main research questions of this study. Field data used in this study comprised of two types, forest inventory data and stand classification maps of Compartment 43, 45, and 48 of UTHF. Forest inventory data were used to calculate the plot–level forest biophysical attributes. Airborne laser scanning data (ALS) data, i.e., Digital terrain model (DTM), and point cloud data were used to calculate plot–level structural metrics and to develop canopy height models (CHMs). Fixed–wing UAV imagery that were collected over the study area were subjected to photogrammetric processing to produce UAV photogrammetric point cloud and orthomosaic. Similarly, plot–level structural metrics and CHMs were derived using normalized UAV photogrammetric point cloud. An image metric was calculated using the UAV orthomosaic. In Chapter 3, UAV derived structural metrics and CHMs derived for Compartment 43 and 48 were compared with LiDAR structural metrics and CHMs to evaluate the performance of UAV photogrammetric products. In Chapter 4, the field measured plot–level volume and carbon stock of Compartment 43 and 48 were related to the RS derived metrics through regression modelling. RS estimated volume and carbon stock were validated using the field estimated volume and carbon stock. Also, UAV estimated volume and carbon stock were compared to LiDAR estimated volume and carbon stock. In Chapter 5, plot–level UAV structural and image metrics were compared to plot–level field forest biophysical attributes of Compartment 43 and 48 using univariate and multivariate statistical analyses. Also, forest canopy structure and vegetation types were classified, and the spatial distributions of forest structure types were mapped in this Chapter. The utility of the information retrieved in Chapters 3-5 for forest management planning of Compartment 45 was explored in Chapter 6. The major findings of this study and their contribution to the existing knowledge are discussed in Chapter 7. Also, the study is concluded, the limitations of the study are summarized, and new directions for future research work are stated in the later part of the Chapter 7.

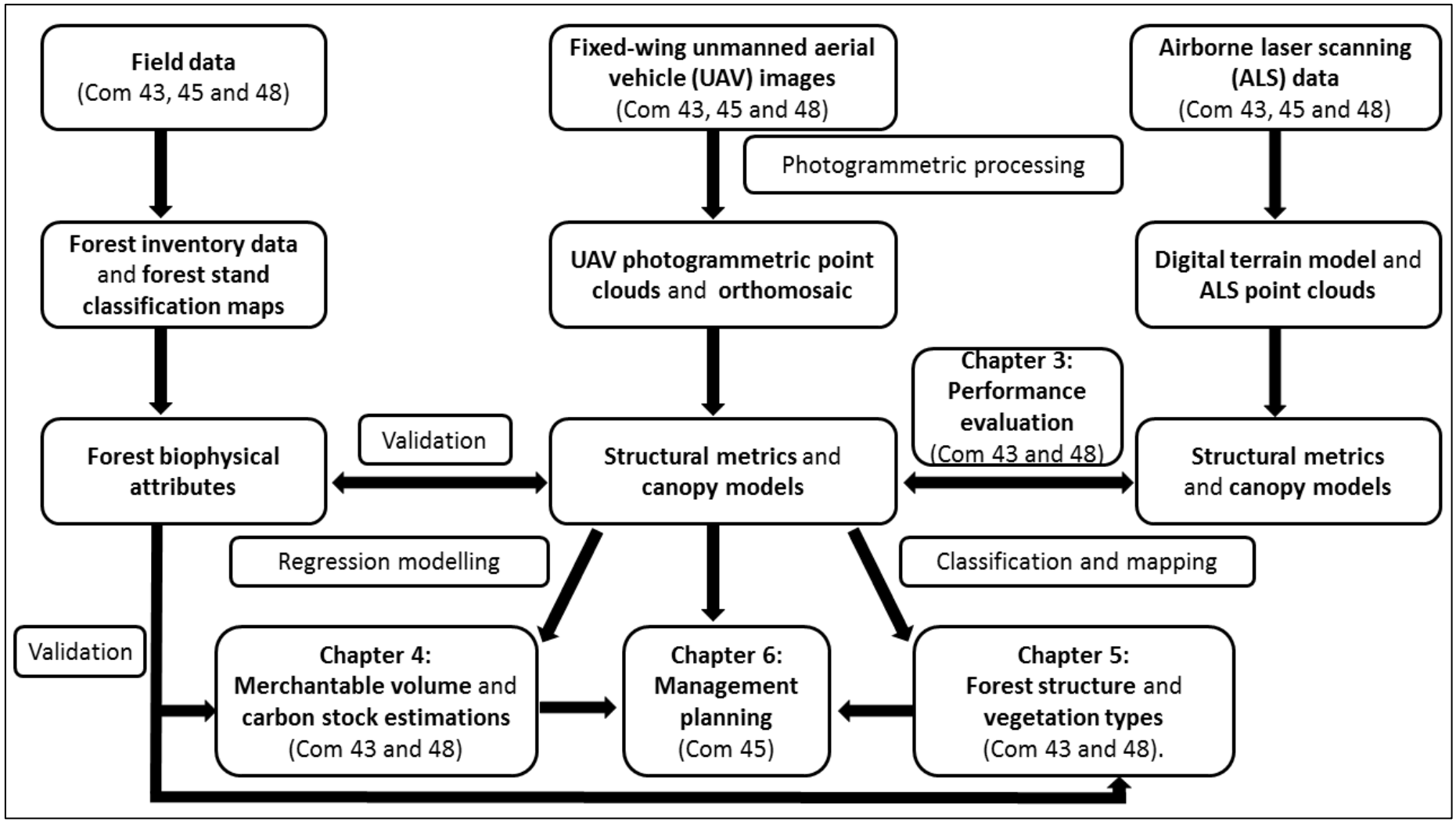

Figure 1.1: Research outline

Chapter 2

Study site and Data

2.1. Study site

This study was carried out in the University of Tokyo (UTHF) Hokkaido Forest (Figure 2.1), where forest management activities such as selection harvesting and enrichment planting are practiced. The UTHF is located in Furano City in the central part of Hokkaido Island in Northern Japan (43° 10–20′ North, 142° 18–40′ East, 189–1,459 m a.s.l), and has a total area of 22,715 ha. The mean temperature was 6.4°C and precipitation was 1,297 mm at the arboretum (230 m a.s.l) 2001–2008. Snow covers the ground from late November to early April, with a maximum depth of about 1 m (Owari et al., 2011). The UTHF is a pan–mixed conifer–broadleaf forest (Tatewaki, 1958) that represents the transition zone between cool–temperate broadleaf forests and subboreal coniferous forests. *Abies sachalinensis*, one of the dominant tree species in the pan–mixed forest type, grows here at a wide range of elevations (200 to about 1,200 m a.s.l) (The University of Tokyo Hokkaido Forest, 2017). Other common tree species include *Picea jezoensis*, *P. glehnii*, *Fraxinus mandshurica*, *Kalopanax septemlobus*, *Quercus crispula*, *Betula maximowicziana*, *Taxus cuspidata*, and *Tilia japonica* (Horie et al., 2013). The forest floor is often occupied by dwarf bamboo (*Sasa senanensis* and *S. kurilensis*).

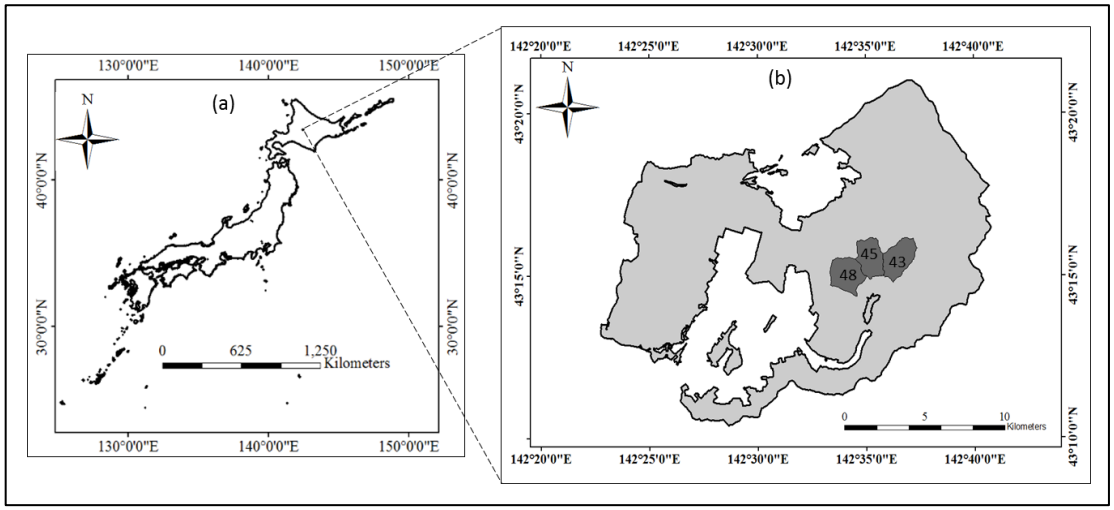

Figure 2.1: (a) Location of the UTHF in Japan, and (b) the location of the AOI in the UTHF. Coordinate system: UTM zone 54N.

The area of interest (AOI) included three forest management Compartments (43, 45 and 48) (Figure 2.2) which were scheduled for management in 2016, 2018 and 2017, respectively. The size of Compartment 43, 45, and 48 are 335 ha, 304 ha, and 340 ha, respectively. The elevation of the AOI ranges from 400 to 820 m a.s.l (Figure 2.3). Major tree species found in this area include *A. sachalinensis*, *P. jezoensis*, *B. ermanii*, *T. japonica*, and *P. glehnii*. These Compartments comprises forest areas with different levels of canopy structural and spatial complexity, which had developed as a result of previous disturbances (silvicultural practices and wind damage). A significant amount of the forest area in these three Compartments is secondary forest recovering from the heavy typhoon damage in 1981.

The forest management in UTHF

Two major silvicultural activities are practiced in the forest management of UTHF; (1) selection harvesting, and (2) restoration of disturbed forest areas.

The rotation of harvesting is either 15 or 20 years. The selection harvesting process is illustrated in Figure 2.4. The harvesting process includes 4 steps;

1) Forest stand classification: The forest stand classification is conducted by the experienced technical staff members of the UTHF based on the field observations. The basic criteria used to classify forest stand types is attached as Appendix 1. Before going into the field for stand classification work, the technical staff members gather prior knowledge and information about the forest stand types and management history, e.g., visual assessments of available aerial imagery, studying previous forest stand classification maps of the relevant Compartments, and referring to the management history.
2) Forest inventory: After stand classification, a stratified sampling is applied to the relevant forest management Compartment based on the stand types and the area occupied, and sample plots are established. Then forest inventory information is collected from sample plots, and volume is calculated based on the collected field data.
3) Decision making on the harvesting: The harvesting rate (10–30%) for mature stand types with adequate growing stock is decided by the technical staff members of the UTHF based on the growth rate of each stand type.
4) Harvesting: Trees to be harvested are identified on the field and marked by the technical staff members. Auction process through stumpage sales is used to get competitive prices for the standing trees to be harvested. The buyers of the standing trees use contractors for the harvesting process. An inspection is conducted during and after harvesting by the technical staff members of the UTHF.

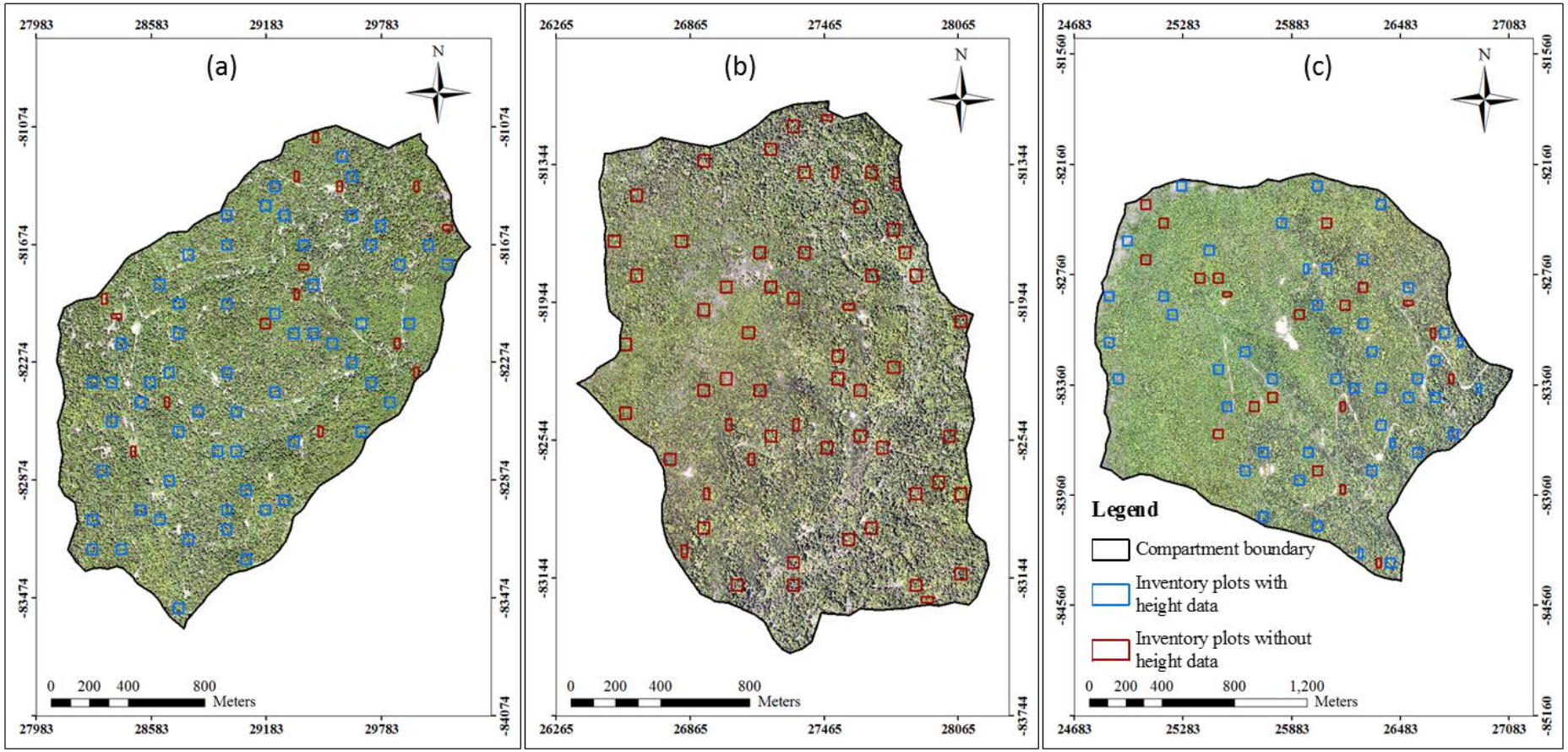

Figure 2.2: UAV aerial orthomosaic (0.5 m pixel resolution) of Compartment 43 (a), 45 (b), and 48 (c) acquired in June, 2017. The locations of sample plots in each Compartment are also shown. Coordinate system: JGD2000 Japan–19 zone XII.

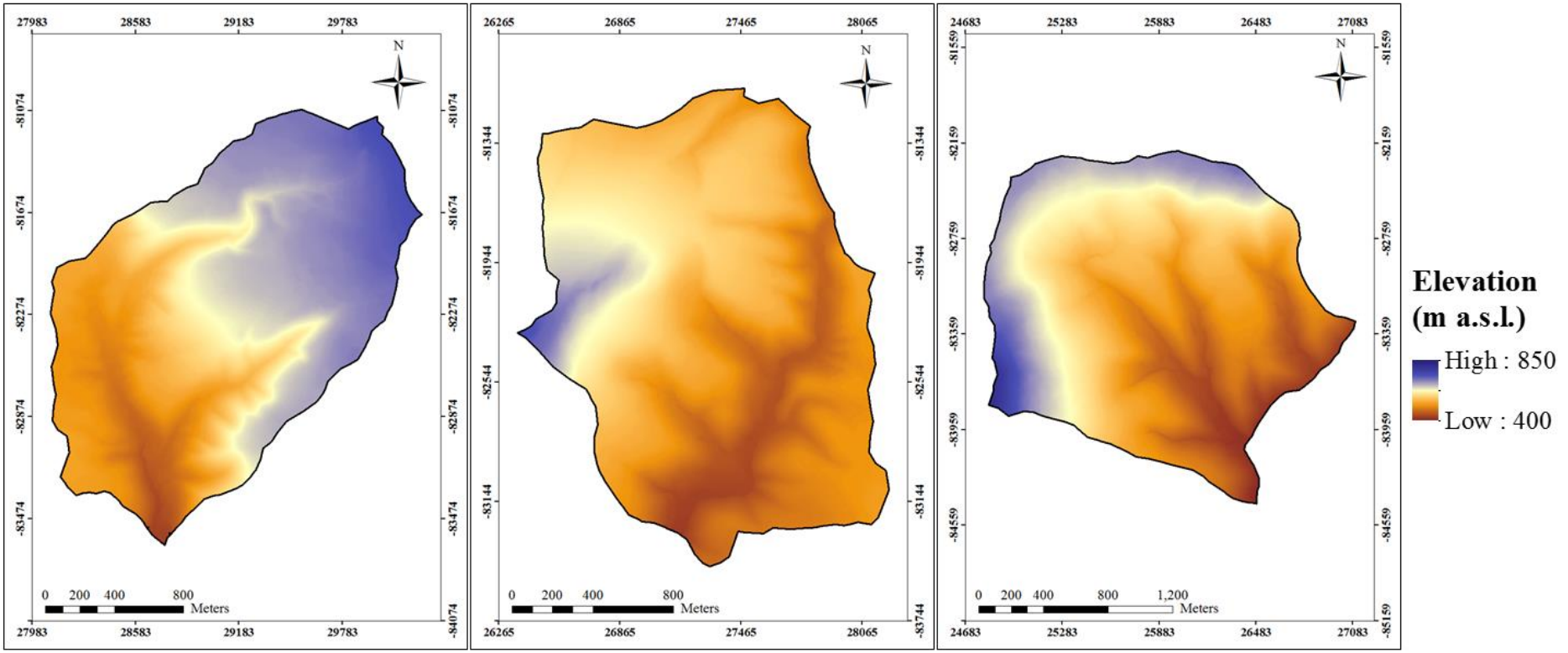

Figure 2.3: $LiDAR_{DTM}$ (1 m pixel resolution) of the AOI. Coordinate system: JGD2000 Japan–19 zone XII.

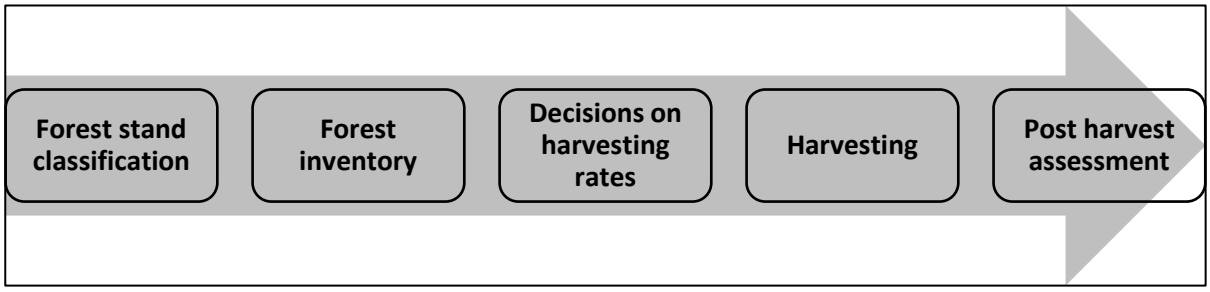

Figure 2.4: Selection harvesting process of the UTHF

The restoration activities are conducted mainly in the heavily disturbed areas of forest (typhoon or fire damaged). The potential area identification is mainly based on the field observations during the stand classification phase, in post–harvesting assessment or following a major disturbance such as typhoon.

The most recent forest stand type classifications of Compartments 43 (2016), Compartment 45 (2018), and Compartment 48 (2017) are illustrated in Figure 2.5. The definitions of stand types are summarized in Table 2.1. Stand definitions were developed based on the stand delineation guidelines provided in the 13th forest management plan of UTHF 2011–2020 (Appendix 1).

Table 2.1: Definitions of the forest stand types.

Stand type			Definition
Selection harvesting stands	Broadleaf–dominated mixed stand	BDM	Stand with an inadequate amount of natural regeneration but an adequate amount of marketable hardwood timber. Further silvicultural operations are required after recurrent selection harvesting.
	Conifer–dominated mixed stand	CDM	Stand with an adequate amount of conifer (fir) natural regeneration and marketable softwood timber. Sustainable selection harvesting is possible.
	Conifer–dominated mixed stand with poor regeneration	CDM–PR	Stand with an inadequate amount of conifer natural regeneration but an adequate amount of marketable softwood timber. Further silvicultural operations are required after recurrent selection harvesting.
Young–growth stands	Young conifer	YC	Stand with an adequate amount of conifer natural regeneration but an inadequate amount of marketable timber. Harvesting is not conducted to nurture existing young trees.
	Young broadleaf	YB	Stand with an adequate amount of broadleaf natural regeneration but an inadequate amount of marketable timber. Harvesting is not conducted to nurture existing young trees.
Sparse forest		SF	Stand with an inadequate amount of natural regeneration and marketable timber. Characterized by wider canopy gaps. Either silvicultural operations are not feasible (unmanaged) or further operations are required followed by selection harvesting (managed).
Reserve forest		RF	Forest areas that are excluded from silvicultural operations on the basis of environmental conditions or accessibility. Includes riparian forests, forest areas on steep slopes, high altitudes, or ridges.
Plantation		PL	Areas that were subjected to silvicultural soil scarification and replantation after heavy typhoon damage.

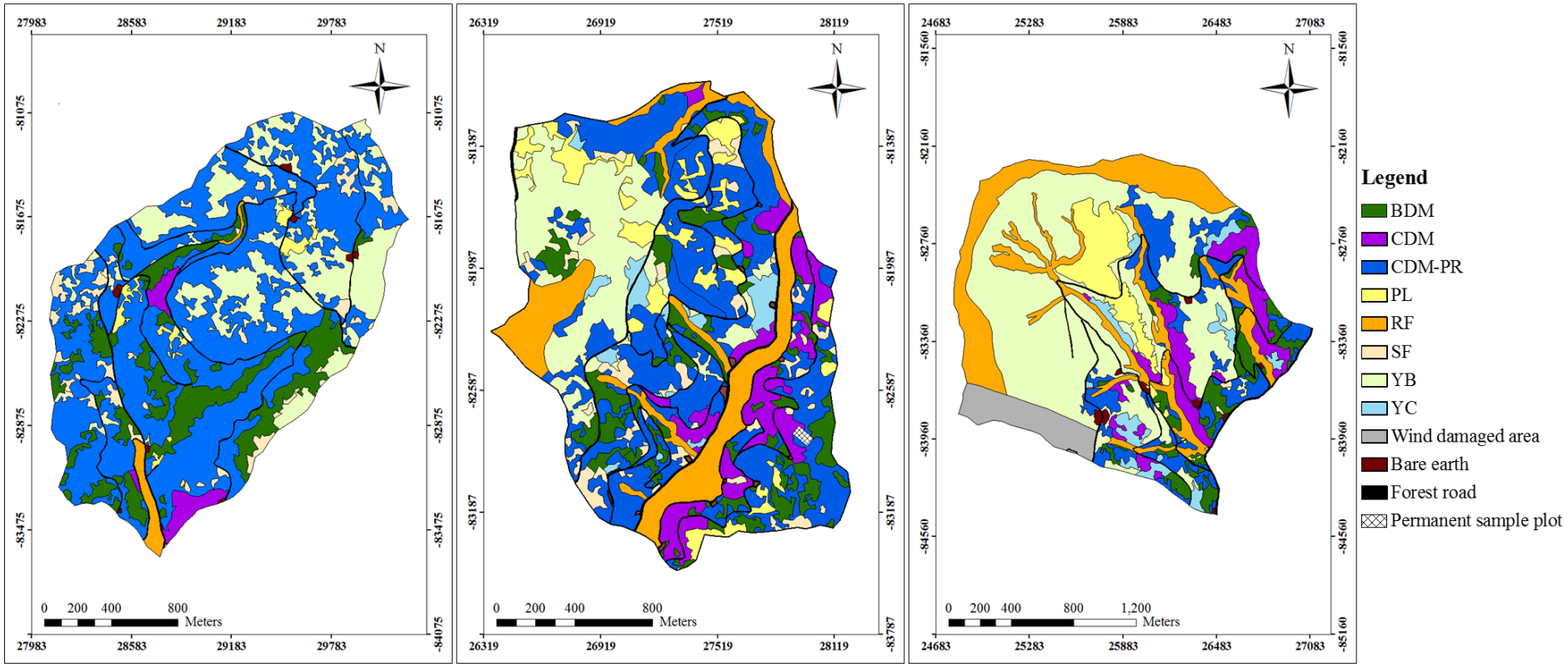

Figure 2.5: Stand classification maps of the AOI; Compartment 43 (left), Compartment 45 (center), and Compartment 48 (right). The maps were produced based on the field observations and visual interpretations in February 2016 (Compartment 43), February 2018 (Compartment 45), and February 2017 (Compartment 48). Source: UTHF. Coordinate system: JGD2000 Japan–19 zone XII.

2.2. Field Data

I used forest inventory data sets of March 2016, 2017, and 2018 that were collected by technical staff members of the UTHF. 193 sample plots (157 plots of 50 m x 50 m, 36 plots of 50 m x 25 m) that were located inside the forest Compartments 43, 45 and 48 were chosen for this study. These sample plots represented the major forest stand types of the study area i.e., BDM, CDM, CDM–PR, RF, SF, YB, and YC. The area of PL was excluded from the inventory (common inventory practice of UTHF), based on the assumption that the volume would be negligible for a very young plantation; hence, no sample plots were chosen for PL. One corner position of the sample plots were determined by Trimble Pro6H (Trimble Navigation, CA, USA) differential global positioning system (GPS) that collects global navigation satellite system (GNSS) information. Remaining three corners of the plot were marked using an analog compass and a Truepulse laser range finder (Laser Technology Inc., Colorado, USA). In each plot, the DBH (measured using a caliper with 2 cm intervals), and species name of all trees with DBH $\geq$ 5 cm were recorded. The inventory datasets did not include any tree height measurements. Therefore, soon after completing the forest inventorying, I conducted a separate field survey of 105 sample plots (chosen from the original inventory plots) with the assistance of the technical staff members of the UTHF. For Compartment 43, 59 sample plots (all plots with size of 50 x 50 m) were chosen whereas 46 sample plots (40 plots of 50 x 50 m, and 6 plots of 25 x 50 m) were chosen for Compartment 48. Tree height data were collected in March 2016 (Compartment 43) and March 2017 (Compartment 48) from eight largest trees in each selected sample plot. The top and bottom of each individual tree was measured using a Vertex laser hypsometer (Haglof, Inc., Långsele, Sweden) to get the actual tree height. Three measurements were taken without changing the standing position, and the average of the three measurements was noted as the induvial tree height.

Usually, volume and carbon stock are expressed according to various specifications. In this study, I refer to the gross merchantable volume (V), i.e., the stem volume of a tree including defective and decayed wood (Maezawa et al., 1968), and carbon stock in living biomass (CST) i.e., the carbon in living biomass, including stem, stump, branches, bark, seeds, foliage, and live roots

with a diameter > 2 mm (Food and Agriculture Organization of the United Nations, 2015), to comply with the definitions used by the greenhouse gas inventory office of Japan (GIO). The V of individual trees was calculated from DBH values using one variable V tariff for the UTHF. Equation 2.1 shows the volume equations used to develop the tariff for conifers species in UTHF (Maezawa and Kawahara, 1986). The equations 2.2–2.5 developed for *Fraxinus mandschurica* (DBH < 80 cm), *Fraxinus mandschurica* (DBH ≥ 80 cm), other broadleaf species (DBH < 80 cm), and other broadleaf species (DBH ≥ 80 cm), respectively (Maezawa et al., 1968).

$$\log V = -3.7789 + 2.4437 \log d, \quad \text{Eq. (2.1)}$$

$$\log V = -3.7400 + 2.4572 \log d, \quad \text{Eq. (2.2)}$$

$$\mathrm{V} = -12.56 + 2.265\,\mathrm{d}, \quad \text{Eq. (2.3)}$$

$$\log V = -3.7844 + 2.4189 \log d, \quad \text{Eq. (2.4)}$$

$$\mathrm{V} = -8.62 + 0.190\,\mathrm{d}, \quad \text{Eq. (2.5)}$$

where V is the merchantable volume, d is the DBH. CST was calculated using the following allometric equation (National greenhouse gas inventory report of Japan, 2017):

$$CST = \sum_j \{[V_j \times D_j \times BEF_j] \times (1 + R_j) \times CF\}, \quad \text{Eq. (2.6)}$$

where *CST* is the carbon stock in living biomass (Mg C ha^{-1}); *V* is the merchantable volume (m^3 ha^{-1}); *D* is the wood density (t–d.m. m^{-3}); *BEF* is the biomass expansion factor for the conversion of volume; *R* is the root–to–shoot ratio; *CF* is the carbon fraction of dry matter (Mg C t–d.m.$^{-1}$); and *j* is the tree species. The value of *CF* was assumed to be a constant of 0.51 Mg C t–d.m.$^{-1}$ for conifer species and 0.48 Mg C t–d.m.$^{-1}$ for broadleaf species as suggested by GIO (National greenhouse gas inventory report of Japan, 2017). The BEF, D, and R values used in this study are summarized in Table 2.2.

Table 2.2: Biomass expansion factor (*BEF*), root–to–shoot ratio (R), and wood density (*D*) for tree species. Note: *BEF* is for > 20 years of age.

Species	**BEF**	**R**	**D (t–d.m. m^{-3})**
A. sachalinensis	1.38	0.21	0.318
P. jezoensis	1.48	0.23	0.357
T. cuspidata	1.23	0.20	0.454
P. glehnii	1.67	0.21	0.362
Larix kaempferi	1.15	0.29	0.404
Other conifer spp.	1.32	0.34	0.352
Populus tremula	1.18	0.26	0.291
Betula spp.	1.31	0.26	0.468
Alnus hirsuta	1.25	0.26	0.454
Quercus spp.	1.26	0.26	0.624
Ulmus davidiana	1.18	0.26	0.494
Magnolia obovata	1.18	0.26	0.386
Phellodendron amurense	1.18	0.26	0.344
Acer spp.	1.18	0.26	0.519
Tilia spp.	1.18	0.26	0.369
Kalopanax septemlobus	1.18	0.26	0.398
Other broadleaf spp.	1.26	0.26	0.624

Source: National greenhouse gas inventory report of Japan (2017).

A summary of forest structural characteristics of the AOI is provided in Table 2.3 and 2.4.

Table 2.3: Summary statistics for plots located in Compartment 43, 45, and 48 (n = 193)

		Compartment 43 (n = 71)			Compartment 45 (n = 58)			Compartment 48 (n = 64)		
		Range	Average	SD	Range	Average	SD	Range	Average	SD
Mean DBH	cm	6.4–33.6	17.3	6.0	8.0–39.4	17.7	6.5	6.4–23.6	14.5	4.1
BA	$m^2\ ha^{-1}$	5.2–51.9	34.3	8.5	10.2–48.4	34.1	8.7	3.2–50.2	26.0	10.4
V	$m^3\ ha^{-1}$	20.5–426.4	278.4	92.1	66.1–439.7	292.1	89.3	24.1–461.8	203.8	100.7
CST	Mg C ha^{-1}	7.2–148.1	94.3	30.8	24.0–147.9	102.2	30.1	8.3–149.4	71.6	33.5
Stem density (N)	ha^{-1}	276–5816	1227	1052	216–3884	1056	756	48–4636	1166	736
Broadleaf stem proportion		0.25–0.98	0.67	0.19	0.27–0.99	0.63	0.16	0.27–0.99	0.71	0.22

Note: All the trees with DBH ≥ 5 cm were used for calculations.

Table 2.4: Summary statistics for plots with height data (n = 105).

		Compartment 43 (n = 59)			Compartment 48 (n = 46)		
		Range	Average	SD	Range	Average	SD
h_{dom}	m	13.9–31.2	25.5	3.5	10.4–30.0	22.0	4.3
Mean DBH	cm	6.4–33.6	17.9	5.5	8.1 –23.6	14.9	4.1
BA	m^2 ha^{-1}	9.7–51.9	36.2	7.3	3.8–44.0	27.6	10.5
V	m^3 ha^{-1}	63.0–426.4	297.9	83.6	24.1–395.6	220.8	101.4
CST	Mg C ha^{-1}	22.6–148.1	100.7	27.7	8.3–133.2	78.0	34.3
N	ha^{-1}	276–5816	1160	998	208–2564	1101	595
Broadleaf stem proportion		0.25–0.98	0.64	0.18	0.29–0.98	0.71	0.21

Note: All the trees with DBH ≥ 5 cm were used for calculations.

2.3. Remote sensing data

2.3.1. Airborne LiDAR data

LiDAR data over the AOI were acquired under leaf–on conditions in September 2015 using an Optec Orion M300 sensor (Teledyne Technologies, Ontario, Canada) mounted on a helicopter. Specifications of LiDAR data are summarized in Table 2.5. The Optec Orion M300 sensor is capable of capturing up to 4 range measurements, including first, second, third, and last returns. Initial processing of LiDAR data was conducted by the data provider (Hokkaido Aero Asahi Corp., Japan), including classification of points into ground and non–ground classes using TerraScan software (2000–2016 Arttu Soininen, Terrasolid), and the data were delivered in LAS format (Coordinate system: JGD2000 Japan–19 zone XII/ GSIGEO 2000 geoid). LiDAR ground points were used to develop the LiDAR digital terrain model ($LiDAR_{DTM}$) and the first returns of the LiDAR vegetation points were used to calculate structural metrics.

Table 2.5: Specifications of LiDAR data.

Parameter	Description
Nominal flying height	600 m
Flying speed	140 km h^{-1}
Course overlap	50%
Pulse rate	100 kHz
Scan angle	±20°
Beam divergence	0.16 mrad
Point density	11.7 pts. per m^2

2.3.2. UAV imagery

2.3.2.1. UAV equipment and payload

UAV images were acquired using a Trimble UX5 (Trimble Navigation, CA, USA) small fixed–wing UAV platform (Figure 2.6) that weighs about 2.5 kg with its payload and that was equipped with a lithium–polymer electric battery allowing for a maximum flight time of ~50 min. The UAV was equipped with an on–board GNSS system to provide rough positioning. For this study, the UX5 was equipped with a Sony NEX–5T 16.1 megapixel RGB camera (Sony Corp., Tokyo, Japan) with an APS–C 23.5 × 15.6 mm CMOS image sensor as the payload. The camera weighs approximately 218 g (110.8 × 58.8 × 32.5 mm) and has a shutter speed of 1/4,000 s, a focal length of 15 mm, and an ISO that adapts to the light conditions of each shot. These camera settings ensured optimal exposure and prevented images from being affected by motion. Based on the weather condition of the image acquisition days, actual shutter speed of the camera was changed between 1/1,600 s and 1/2,000 s.

Figure 2.6: Trimble UX5 fixed–wing UAV used in this study and its accessories.

2.3.2.2. UAV imagery collection: Planning and implementation

UAV imagery was collected on 17 and 18 September 2015 for Compartment 43 and on 2 September 2016 for Compartment 48. Another set of UAV imagery were acquired on 5–7 June 2017 for all the three Compartments. Altitude (the angle between horizon and the center of the sun including refraction) and the azimuth (the angle between the meridional plane of the earth and the vertical plane of the sun) during September 2015 UAV data acquisition were 34°–46°and 154°–235°, respectively whereas they were 39°–51°and 150°–238°, respectively, for September 2016 UAV data acquisition. Altitude of 50°– 64°and azimuth of 138°–253° were recorded for June 2017 UAV data acquisitions. Image acquisition was composed of three phases: the planning phase, the field phase, and flight missions. In the planning phase, flight simulation software package (Trimble access aerial imaging) was used to obtain a plan for flight implementation. The main input parameters required in the planning phase were flight altitude, flying speed, working area and image overlap. Flight altitude and longitudinal and lateral overlaps were set to 500 m, 90%, and 80%, respectively for 2015 and 2016 data acquisitions. Flying speed was 80 km h^{-1}. Flight planning window and parameters used for 2017 data acquisition are shown in Figure 2.7. However, the defined flight altitude, longitudinal and lateral overlap were only indicative, as it was subjected to slight changes during actual flight because of wind, and the differences between the simulated and actual flight

paths. The home points (take–off and landing points) and ground control points (GCPs) were located in available open areas.

Figure 2.7: Picture showing the flight planning window of the Trimble access aerial imaging software package (Trimble Navigation, CA, USA). Details shown are for June, 2017 data acquisition.

The field phase included marking GCPs on the ground and measuring their positions. 50 × 50 cm targets with a black–and–white checkerboard pattern were used as GCPs to ensure the greatest possible contrast in the images (Figure 2.8). After fixing the GCP targets to the ground, their center position was determined using the Trimble Pro6H differential GPS that collects GNSS data. The nearest official reference point was used as the base station. Later, field–recorded coordinates were post–processed using correction data from the base station.

Figure 2.8: View of a GCP on ground (left) and in UAV aerial imagery (right).

The weather was stable during all the days of image collection. All the images were acquired during the noon time. For each flight, the UAV took off, ascended to the predetermined flight altitude, flew a parallel track course under GPS control, and then automatically returned to and landed at the launch site. The camera was triggered automatically based on the predefined flight plan, and images were stored in jpeg format. Although the manufacturer stated maximum flight time is ~50 minutes, the actual maximum flight time during the data acquisition was ~25 minutes, thus at least 4 flights were required to complete the data acquisition of one compartment. After each UAV flight, images (Figure 2.9) were downloaded to a field laptop. After trimming the unwanted photos, the resulting images were subsequently used in the SfM processing workflow. The UAV images had an image resolution of 4,912 × 3,264 and a ground resolution of 14 cm per pixel.

Figure 2.9: Original UAV aerial imagery acquired on 17th September 2015 (left) and 6th June 2017 (right) over Compartment 43.

2.3.2.3. Photogrammetric processing of UAV imagery

I used Agisoft PhotoScan Professional Edition 1.3.2 (Agisoft LLC, St. Petersburg, Russia) to generate 3D dense point clouds, as it has proven effective for the production of dense and accurate point clouds over forested areas (Dandois and Ellis, 2010; Puliti et al., 2015). PhotoScan offers a user–friendly workflow that combines proprietary algorithms based on computer vision SfM and stereo–matching for image alignment and 3D reconstruction (Verhoeven et al., 2012). This workflow consists of two stages: image alignment and point cloud densification. To avoid unsatisfactory 3D reconstruction, I selected parameters for each stage based on the results of an initial analysis of a small area via forward sequential selection (Järnstedt et al., 2012; Remondino et al., 2014; Wong, et al., 2016).

The first stage of processing, image alignment, consists of sparse reconstruction of the 3D geometry by detection and matching of image feature points in overlapping images using SfM techniques. In this stage, I used the highest image matching option, a key point limit of 40,000 and a tie point limit of 4,000. Absolute orientation was successful for all the input images. In order to optimize the image matching, tie points in the sparse point cloud that were generated in the initial alignment were manually edited by deleting mislocated points based on three criteria: reprojection error, reconstruction uncertainty, and projection accuracy. This optimization did not significantly reduce the final number of tie points. To allow for more accurate model reconstruction, I then optimized the camera orientation and internal parameters using GCPs (At least 8 GCPs were used for each Compartment). Optimization was conducted for focal length in the x and y dimensions (fx, fy), principal point coordinates (cx, cy), radial distortion coefficients (k1, k2, k3), and tangential distortion coefficients (p1, p2).

In the second stage of processing, point cloud densification, the software calculates depth information for images and combines all points into a single dense point cloud. To build the dense point cloud, I selected a medium quality that downscaled the image size from the original image by a factor of 8 (bilinear resampling) to avoid excessive processing time. In addition, mild depth filtering was used to remove outliers and reduce noise. The resulting dense point cloud was then used to build a mesh which was later used to develop an orthomosaic. PhotoScan uses bilinear

interpolation during orthomosaic generation process. Finally, the dense point cloud (point density > 5.4 pts. per m^2) and the orthomosaic (0.5 m pixel resolution) were exported in LAS and TIFF formats (Coordinate system: JGD2000 Japan–19 zone XII/ GSIGEO 2000 geoid), respectively, for further processing. PhotoScan was installed on a workstation with an Intel Core i5–4670 CPU at 3.4 GHz, 16 GB RAM, 64–bit OS, and NVIDIA Quadro K2000 GPU. A total processing time of about 36 h of continuous computation was needed for each Compartment to complete the processing.

2.4. Pre–processing of RS data

2.4.1. Generation of CHMs

2.4.1.1. Generation of LiDAR canopy height

The CHMs were generated using Fusion software package(version 3.60) (McGaughey, 2016). LiDAR non–ground points and their z values were used to derive the LiDAR digital surface model ($LiDAR_{DSM}$) using the maximum z value of the point cloud within a 1 × 1 m grid used as the DSM height for that grid cell. A 1 m grid was chosen considering the average tree crown size in the study area and the point density values of RS data. I built the LiDAR digital terrain model ($LiDAR_{DTM}$, 1 m pixel resolution) using a triangulated irregular network (TIN) constructed from LiDAR ground points using Delaunay triangulation. Then I calculated the LiDAR canopy height model ($LiDAR_{CHM}$) by subtracting $LiDAR_{DTM}$ from $LiDAR_{DSM}$.

2.4.1.2. Generation of UAV–SfM canopy height

I used UAV–SfM points and their z values to derive the UAV–SfM digital surface model ($UAV–SfM_{DSM}$, 1 m pixel resolution) following the same procedure as for $LiDAR_{DSM}$ generation. No void filling was used to construct more accurate models. Several studies have highlighted the need for a precise DTM to generate an accurate CHM from SfM (Dandois and Ellis, 2010; Lisein et al., 2013). To reconstruct the precise ground terrain using the SfM point cloud, the ground must be visible from multiple locations. However, this is challenging in forest areas with dense canopy cover (Wallace et al., 2016). Therefore, I used $LiDAR_{DTM}$ to normalize absolute heights in this study, such that I

subtracted $LiDAR_{DTM}$ from $UAV–SfM_{DSM}$ to obtain the UAV–SfM canopy height model ($UAV–SfM_{CHM}$, 1 m pixel resolution).

2.4.2. Calculation of forest structural and vegetation metrics

Although forest canopies are multifaceted, they are commonly studied using the dominant characteristics of canopy, e.g., canopy structure and vegetation type. Therefore, canopy structural metrics were extracted using 3D RS data while an image metric that explains the broadleaf cover percentage was extracted using the spectral information contained in UAV–SfM orthomosaic.

2.4.2.1. Calculation of forest structural metrics

Prior to calculation of structural metrics from LiDAR and UAV–SfM point clouds, their absolute height values were normalized using $LiDAR_{DTM}$. Previous forestry studies have assessed the accuracy of remote sensing techniques by extracting various structural metrics that play major roles in forest management and other ecological applications, e.g., Kane et al. (2010b); Lefsky et al. (2002); Moran et al. (2018); Parker et al. (2004); Tompalski et al. (2018). I calculated the RS structural metrics that were widely used in previous studies (described in Table 2.6) for all the sample plots (n = 193) using normalized LiDAR and UAV–SfM point cloud data. The *cloudmetrics* and *Gridmetrics* functions of the FUSION software package (version 3.60) (McGaughey, 2016) was used to extract plot–level metrics, and grid–level metrics (grid size: 50 m), respectively. I computed all metrics using only points with heights greater than 2 m to eliminate ground and understorey vegetation (e.g., *Sasa* spp.) returns.

Table 2.6: Description of structural metrics used in this study.

Metric category	Structural metric	Abbreviation	Unit	Description
Height metrics	Maximum height	MaxH	m	Maximum height of all points in the sample plot/grid cell.
	Mean height	MeanH	m	Mean height of all points in the sample plot/grid cell.
	Percentile of canopy height	P10, P25, P50, P75, and P95	m	10^{th}, 25^{th}, 50^{th}, 75^{th} and 95^{th} percentile heights of all points in the sample plot/grid cell.
Height variation metrics	Standard deviation of canopy height	SDH	m	Standard deviation of point heights in the sample plot/grid cell. Also known as the rugosity index (Parker et al., 2004)
	Coefficient of variation of canopy height	CVH		Ratio of standard deviation of canopy height to the mean canopy height.
	Skewness	Skew		A measure of the asymmetry of the probability distribution of point heights in sample plot/grid cell about its mean.
	Kurtosis	Kurt		A measure of the "tailedness" of the probability distribution of point heights in the sample plot/grid cell.
	Surface area ratio	SR		Ratio of 3D canopy surface to the 2D planiteric area of the sample plot/grid cell. Also known as “rumple index” (Parker et al., 2004).
Canopy cover metrics	Canopy cover	CC		Number of 1 m pixels in sample plot/grid cell with height > 2 m to the total number of pixels in the sample plot/grid cell.
	Canopy cover above mean height	CC_m		Number of 1 m pixels in sample plot/grid cell with height > mean height to the total number of pixels in the sample plot/grid cell.

Canopy density metrics	d_1, d_2, d_3, d_4, d_5, d_6, d_7, d_8, and d_9	Proportion of points above 1^{st}, 2^{nd}, …, 9^{th} height fractions to the total number of points in a sample plot/grid cell.
	d_0	Proportion of points above 2 m height to the total number of points in a sample plot/grid cell.
	d_{mean}	Proportion of points above mean height to the total number of points in a sample plot/grid cell.

Note: Height metrics were calculated using only points with height > 2 m to eliminate ground and understory returns. Only first returns of LiDAR data were used for LiDAR structural metric calculation.

2.4.2.2. Calculation of the image metric

The proportion of broadleaf cover is considered as a fundamental variable in the characterization of mixed forests (Hame et al., 1997). To effectively use the spectral information contained in UAV imagery, and to produce a meaningful metric, I quantified the proportion of broadleaf cover using a UAV–SfM–exported high–resolution aerial orthomosaics. First, the land cover, i.e., broadleaf species, conifer species, sasa bamboo, bare earth, and canopy gaps, and their spectral values, were checked to produce training samples. The training samples were produced based on the visual interpretation of the aerial imagery. Then, supervised classification (using the maximum likelihood method) of the three visible light bands of the orthomosaics (0.5 m pixel resolution) was applied using the TNTmips Pro (2017) software package (Microimages, Raymond, USA) to classify the orthomosaics into five classes; broadleaf vegetation, conifer vegetation, Sasa bamboo, bare earth, and canopy gaps. UAV orthomosaics produced from the September 2015 (Compartment 43), September 2016 (Compartment 48), and June 2017 (Compartments 43, 45 and 48) data acquisitions were classified separately. A 3 × 3 moving window was applied for hole–filling of the classified classes. A separate set of ground–truth sample points was then used to assess the accuracy of the classification. Validation sample points were derived based on the visual interpretation of the 0.5 m resolution aerial imagery. The same procedure was followed for all the UAV datasets to assess their accuracy. Orthomosaics from June had a high accuracy in species classification, e.g., the overall accuracy of the classification of the June UAV orthomosaic was 90.6%. The users' and producers' broadleaf vegetation cover accuracies were > 97%. Orthomosaics from June 2017 had a high accuracy for classification, and were therefore exclusively used for the calculation of broadleaf vegetation cover. Number of training sample points, classification maps, and the accuracy assessment of classification for compartment 43, 45 and 48 are presented as Appendix 2. The broadleaf vegetation cover of each plot/grid was calculated as the percentage of pixels classified as broadleaf cover in each plot/grid relative to the total number of pixels.

Chapter 3

Evaluation of the performance of UAV photogrammetric products in comparison to airborne LiDAR data.

3.1. Introduction

3.1.1. Background

Forest canopy plays an important role as a biotic habitat (Nadkarni, 1994), an area of high photosynthetic capacity (Carswell et al., 2000), an indicator of biodiversity (Lindenmayer et al., 2001; McElhinny et al., 2006, 2005) and a gauge of forest health (Levesque and King, 2003). However, our understanding of forest canopy structure may be constrained in some important ways (e.g., structural and spatial complexity of the canopy at the landscape level) when the studies of the forest canopy are based on data collected through field surveys within a small set of sample plots that are often selected subjectively (Franklin and Van Pelt, 2004; Kane et al., 2010b). In addition, characterization of the 3D structure of the forest canopy using conventional field survey data is challenging because of physical access and resource requirements (Barker and Pinard, 2001; Lowman and Wittman, 1996).

By providing varying spatial, spectral, and temporal resolution as well as effective means of 3D canopy reconstruction, the use of RS technology addresses these issues. RS has also proven an effective means of studying forest canopy structure, as it often complements existing ground–based techniques by contributing reliable, detailed information on various aspects of the complex forest canopy (Kane et al., 2010a; Ma et al., 2001; Xie et al., 2008). In particular, recent advances in RS technology, ALS, digital photogrammetry, and UAV systems, have enabled efficient data collection and fully automated reconstruction of forest canopy surfaces over large spatial areas (Hyyppä et al., 2012; Leberl et al., 2010; Lisein et al., 2013; Torresan et al., 2017; Wulder et al., 2013).

ALS is an active RS technique that uses a LiDAR sensor, which emits a laser beam across the flight path at an operator–specified angle and receives the reflected energy. This technique allows

users to determine the distance from the sensor to a target object using either discrete return or continuous wave systems. LiDAR measurements have proven to be more successful than other remote sensing options at reconstructing 3D forest canopy structure and more accurate at predicting structural attributes, particularly when acquired with satisfactory point densities (Hyyppä et al., 2012; Wulder et al., 2013). In addition, this method provides otherwise unavailable scientific insights by allowing for detailed and novel structural measurements (Lefsky et al., 2002; Parker et al., 2004). Therefore, the application of LiDAR measurements to analyzing forest canopy structure has been researched intensively in terms of both the area–based approach (ABA) and individual tree–based methods, e.g., Hyyppä et al. (2012); Maltamo et al. (2005); Næsset (2002); Næsset et al. (2004); Reitberger et al. (2008). Nonetheless, the main limitations of ALS in practice are the high acquisition cost, which limits its application to operational forest management, and the absence of spectral data that can lead to other important information, such as species identification.

Digital photogrammetric techniques such as SfM also facilitate 3D modelling of forest canopy structure, hence many recent studies have taken advantage of it, e.g. Grenzdörffer et al. (2008); Jaakkola et al. (2017); Näsi et al. (2015). Also, several previous studies attempted to compare photogrammetric products i.e., point clouds, CHMs and structural metrics with LiDAR data (Lisein et al., 2013; Thiel and Schmullius, 2017; Wallace et al., 2016; White et al., 2015; Wong, et al., 2016).

Particularly fixed–wing UAV photogrammetry could provide a low–cost remote sensing alternative to airborne and satellite remote sensing and enable the production of cost–effective data with an unrivalled combination of spatial and temporal resolution at local scales (e.g., for areas the size of traditional forest plots up to the size of forest Compartments) (Matese et al., 2015). Although fixed–wing UAVs have great potential for use in forestry applications, very few studies have involved detailed analyses of point clouds or canopy surface models built from fixed–wing UAV photogrammetry at comparatively large scales, such as the forest management Compartment level, and even fewer studies have used fixed–wing UAV imagery to estimate forest structural attributes (e.g., Lisein et al., 2013; Puliti et al., 2015; Tuominen et al., 2015). Applications and the robustness of fixed–wing UAV photogrammetry has also not been studied intensively over a range of forest types, such as mixed conifer–broadleaf forests. In this Chapter, I address these issues.

3.1.2. Purpose

This Chapter aims to assess the performance of image–based point clouds derived from fixed–wing UAV imagery captured over a mixed conifer–broadleaf forest with varying levels of canopy structural complexity. First, I conducted a detailed evaluation of UAV photogrammetric outputs by comparing UAV–SfM–derived CHMs and structural metrics to LiDAR–derived CHMs, and structural metrics, respectively. I used LiDAR data as a reference data set to assess the performance of UAV–SfM, as LiDAR data is considered reliable for forestry applications for two main reasons: (1) the non–clustering effect of LiDAR data leads to accurate estimation of forest structural attributes and (2) the data have a proven ability to reconstruct 3D canopy structure with high accuracy for a variety of forest types (Gobakken et al., 2015; Müller et al., 2014; White et al., 2015; Wong, et al., 2016). Second, I assessed the utility of UAV–SfM–derived point clouds for estimating several forest structural attributes that are commonly used in forestry applications. Finally, I examined the effects of forest canopy structural metrics and terrain conditions on the performance of the UAV–SfM canopy model.

3.2. Materials and methods

3.2.1. Study site and data

Field data, LiDAR data and UAV imagery that were acquired in September 2015 and September 2016 of Compartment 43 and 48 were used in this Chapter.

3.2.2. Data Analysis

Figure 3.1 illustrates a flowchart that shows the methodology followed in this Chapter.

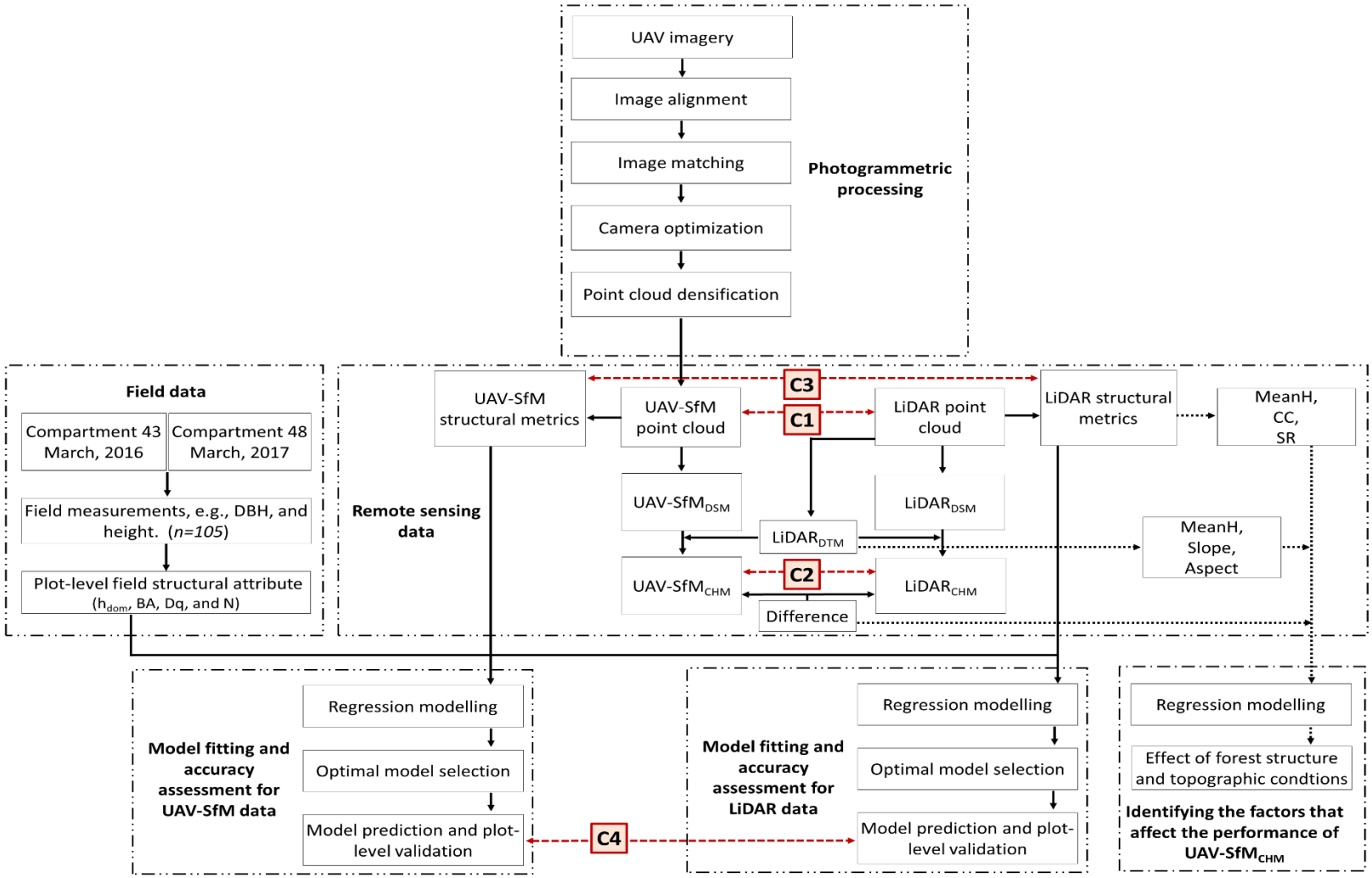

Figure 3.1: Flowchart of the methodology. C1, C2, C3, and C4 denote the comparisons between point clouds, CHMs, structural metrics, and predictions of plot–level forest structural attributes.

3.2.2.1. Field metric calculation

Plot–level field structural attributes, i.e., h_{dom}, BA, quadratic mean DBH (Dq), N, and proportion of conifer stems were calculated for the 105 sample plots with tree height data (59 plots for Compartment 43, and 46 plots for Compartment 48). A summary of the forest structural characteristics of the AOI is provided in Table 3.1.

Table 3.1: Forest structural characteristics at the study site (n = 105).

Forest structural attribute	**Compartment 43** **Average (SD) values**	**Compartment 48** **Average (SD) values**
Dominant height (m)	25.5 (3.5)	22.0 (4.3)
Quadratic mean DBH (cm)	32.3 (4.6)	14.9 (4.1)
Basal area ($m^2\,ha^{-1}$)	32.2 (9.6)	24.4 (11.0)
Stem density (ha^{-1})	324 (93)	366 (102)
Proportion of conifer stems	0.46 (0.16)	0.26 (0.20)

Note: Only trees with DBH ≥ 14 cm was used.

3.2.2.2. Processing of RS data

Photogrammetric processing of UAV imagery to obtain UAV–SfM point cloud is described in Section 2.3.2.3. CHMs and structural metrics were then derived using RS data, i.e., airborne LiDAR and UAV–SfM point clouds (described in Sections 2.4).

3.2.2.3. Comparison of LiDAR and UAV–SfM products

In order to assess the accuracy of the UAV–SfM products in detail and to thoroughly evaluate the differences between the UAV–SfM and LiDAR products, I used CHMs and plot–level structural metrics that were generated from UAV–SfM and LiDAR point cloud data.

First $LiDAR_{CHM}$ and SfM_{CHM} were compared both visually and statistically. The differences between the $LiDAR_{CHM}$ and SfM_{CHM} results were evaluated through direct comparisons of pixel values (i.e., subtraction of UAV–SfM_{CHM} from $LiDAR_{CHM}$) for insight into their altimetric differences at the pixel level.

To enable comparison of LiDAR and UAV–SfM metrics and assess their agreement, I calculated the mean difference (MD), which indicates whether the UAV–SfM metrics are generally greater or smaller than the corresponding LiDAR metric values, and the root mean squared deviation (RMSD), which indicates the average difference between metric values and clarifies the magnitude of the differences between LiDAR and UAV–SfM metric values using the equations given below.

$$MD = \frac{\sum_{i=1}^{n}((LiDAR)_i - (UAV\text{-}SfM)_i)}{n} \qquad \text{Eq. (3.1)}$$

$$RMSD = \sqrt{\frac{\sum_{i=1}^{n}((LiDAR)_i - (UAV\text{-}SfM)_i)^2}{n}} \qquad \text{Eq. (3.2)}$$

where n is the number of sample plots, and $(LiDAR)_i$ and $(UAV\text{-}SfM)_i$ are the LiDAR metric value and UAV–SfM metric value, respectively.

To assess the degree of association between metric values, I also calculated the Pearson correlation coefficient between LiDAR and UAV–SfM metric values. Finally, the presence or absence of statistically significant differences between metric mean values was tested using paired two–sample t tests.

3.2.2.4. Evaluation of the utility of UAV–SfM–derived point cloud products and plot–level validation of forest canopy structural metrics

To evaluate the utility of UAV–SfM–derived point cloud products for estimating plot–level forest structural attributes, I used generalized linear model (GLM) analysis. Based on similar published studies, I selected a subset of structural metrics (Table 2.5), that showed strong correlations with plot–level forest canopy structural metrics, to be used as predictor variables in my models. First plot–level field forest structural attributes, i.e. h_{dom}, BA, D_q and N, were related to the RS derived structural metrics using regression analysis. Then the stepwise variable selection was carried out, and the final model was selected based on Akaike's information criterion (AIC). In addition, the selection of predictor variables was penalized for collinearity using the variance inflation factor (VIF). The accuracy of the predictions was validated at the plot level using leave–one–out cross–validation (LOOCV). The root mean square error (RMSE), relative root mean square error (%RMSE), and bias were determined using the following equations.

$$RMSE = \sqrt{\frac{\sum_{i=1}^{n}(y_i - \hat{y}_i)^2}{n}} \qquad \text{Eq. (3.3)}$$

$$\%RMSE = \left(\frac{RMSE}{\bar{y}}\right) \times 100 \qquad \text{Eq. (3.4)}$$

$$Bias = \frac{\sum_{i=1}^{n}(y_i - \hat{y}_i)}{n} \qquad \text{Eq. (3.5)}$$

where n is the number of field plots, y_i, is the observed value, $\hat{y}_i$, predicted value and $\bar{y}$ is the mean of n observed values.

I used the terms "MD" (equation 3.1) and "RMSD" (equation 3.2) instead of "bias" and "RMSE" when UAV–SfM data is compared to LiDAR data (as the reference data) to avoid the confusion that UAV–SfM data is being compared to reference data but not to field data. When comparison involves the UAV–SfM predictions of forest structural attributes and field data, the terms "bias" (equation 3.5) and "RMSE" (equation 3.3 and 3.4) were used exclusively.

3.2.2.5. Identification of factors that affect the performance of UAV–SfM$_{CHM}$

I examined the effects of canopy structural complexity and topographic conditions on the performance of UAV–SfM$_{CHM}$, as these factors affect the performance of digital photogrammetry in forested areas (Baltsavias et al., 2008; Wong, et al., 2016). LiDAR structural metrics are strongly correlated with variation in vertical and horizontal forest structure at the stand level and hence explain the structural complexity of the overall forest canopy (Jayathunga et al., 2018; Kane et al., 2010b). Therefore, I selected several plot–level LiDAR structural metrics described in the previous section, including MeanH, CC, and SR to determine the influence of stand structure on the RMSD of canopy height. I also tested the effects of ground conditions such as elevation, slope (calculated as the maximum rate of change in z value from one cell to its neighbors), and aspect (which identifies the downslope direction of the maximum rate of change in the value of each cell in relation to its neighbors) that were calculated using LiDAR$_{DTM}$. Compartment was also included as an explanatory variable in the modelling, as stand and site conditions were not identical between the two Compartments. I performed multivariate data analysis using GLM with all metrics input as fixed components (Compartment and aspect were inputted as categorical factors, whereas all other metrics

were inputted as numerical values) to test the statistical significance of each factor as it affects the performance of UAV–SfM_{CHM}.

3.3. Results

3.3.1. Comparison of LiDAR and UAV–SfM outputs

3.3.1.1. LiDAR and UAV–SfM point cloud properties

A transect of the LiDAR and photogrammetric point clouds is shown in Figure 3.2 for illustration purposes. Unlike laser pulses, which penetrate the forest canopy to better account for small gaps and peaks, the photogrammetric point cloud had limited capacity to reconstruct small gaps and peaks. The number of points that represented the ground was very low in the photogrammetric point cloud and restricted to areas where large gaps were present or where bare earth was clearly visible from the sky.

3.3.1.2. LiDAR and UAV–SfM CHMs

$LiDAR_{CHM}$, UAV–SfM_{CHM}, and the canopy height difference model for Compartments 43 and 48 are shown in Figure 3.3. $LiDAR_{CHM}$ and UAV–SfM_{CHM} generally showed good agreement, which suggests that the overall quality of the reconstruction was consistent.

RMSD and MD for the study area were 3.9 and –0.70 m, respectively. The RMSD value for Compartment 43 (3.8 m) was lower than that for Compartment 48 (4.0 m). Furthermore, Compartment 43 showed a positive MD of 0.03 m, whereas a negative MD of 1.4 m was observed for Compartment 48. A histogram comparing CHMs over the study area is shown in Figure 3.4. Over the entire study area, 43.9%, 66.7%, and 79.7% of the height values were within ±1, ±2, and ±3 m of the corresponding reference point in $LIDAR_{CHM}$, respectively.

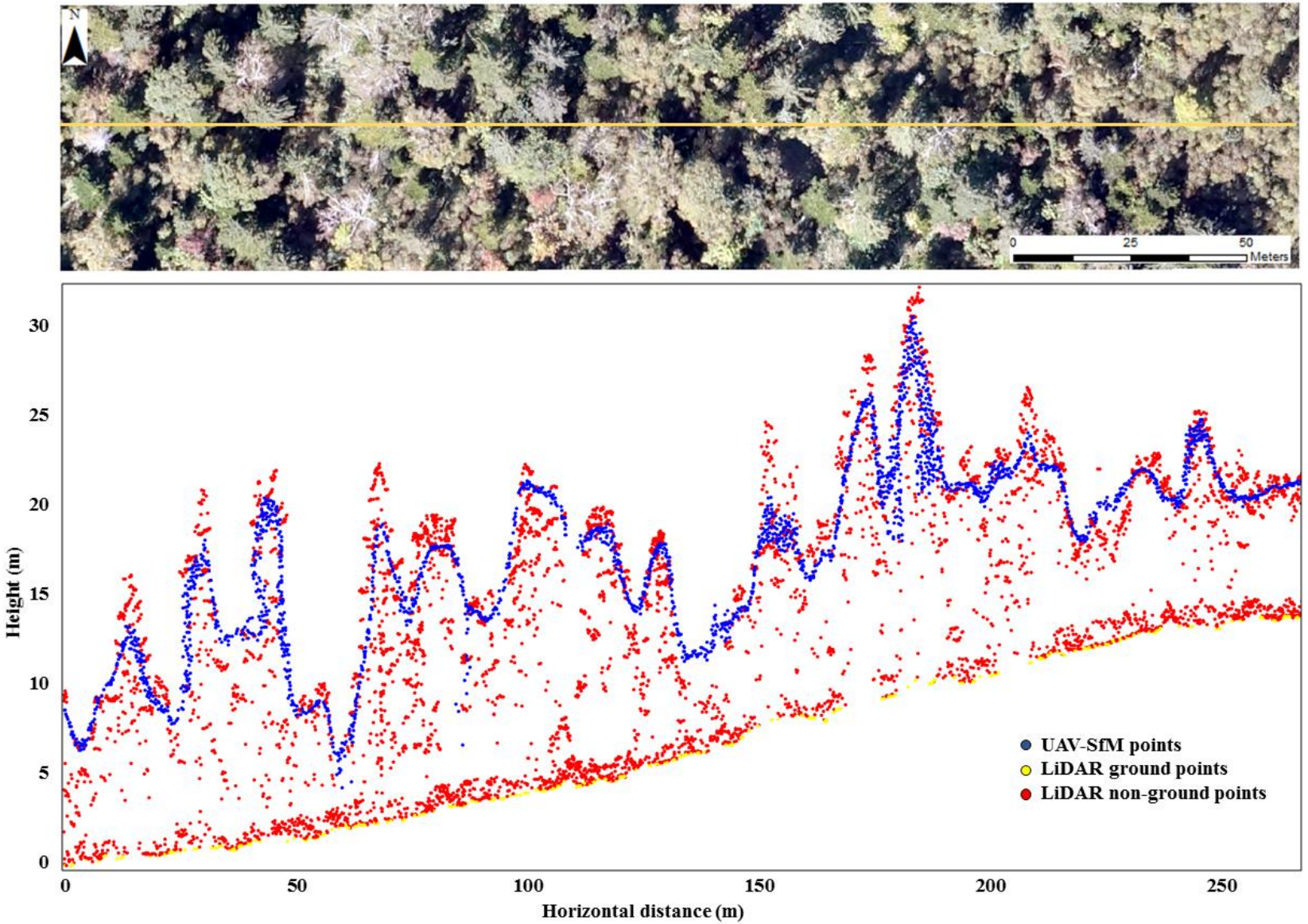

Figure 3.2: Illustration of UAV–SfM and LiDAR point clouds.

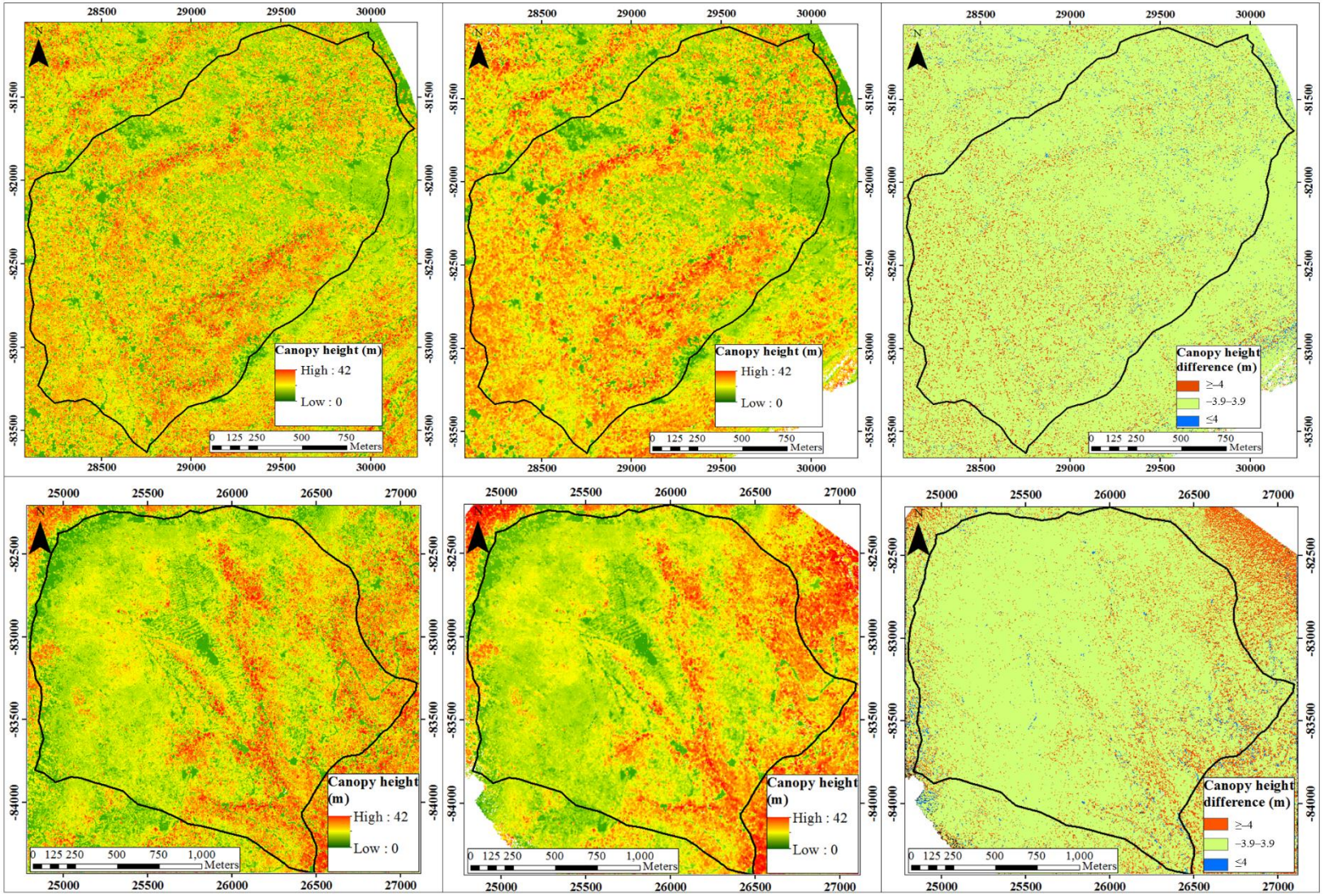

Figure 3.3: LiDAR canopy height model ($LiDAR_{CHM}$), UAV–SfM canopy height model ($UAV–SfM_{CHM}$) and height difference (Δh) between $LiDAR_{CHM}$ and $UAV–SfM_{CHM}$ of Compartment 43 (Top panel from left to right) and Compartment 48 (Bottom panel from left to right and) (1 m pixel resolution).

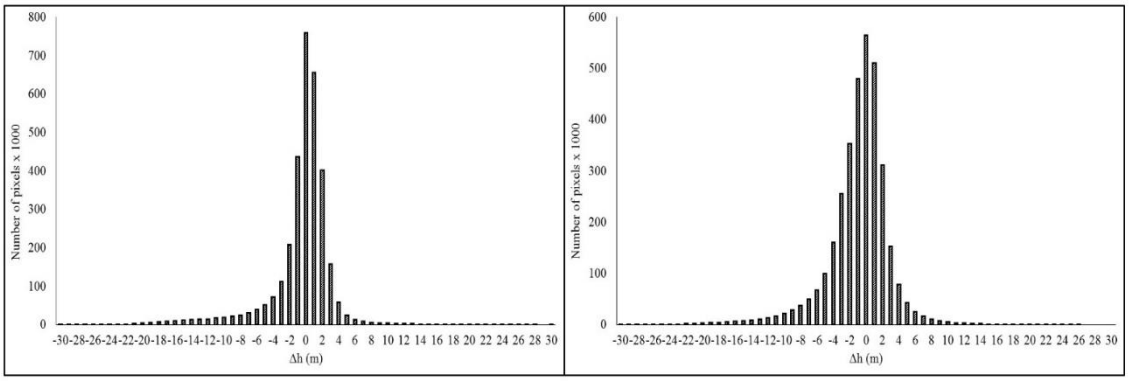

Figure 3.4: Histogram showing the frequency of pixel values. Δh is the difference between $LiDAR_{CHM}$ and $UAV–SfM_{CHM}$.[1]

Overestimations (in comparison to LiDAR data) by greater than 4 m made up 3.7% of the data, whereas underestimations by less than 4 m accounted for 9.3% of the results. The proportion of pixels with no data, mainly because of shadows, was estimated at 0.6% over the study area. Overall, canopy height differences between $LiDAR_{CHM}$ and $UAV–SfM_{CHM}$ were within the range of ±4 m for the majority of the area (88.3% for Compartment 43, 84.5% for Compartment 48, and 86.4% for both Compartments). In–depth visual comparison highlighted several differences, examples of which are shown in Figure 3.5. First, large positive differences were observed where occlusions were present, such as some isolated tree crowns that were absent from the photogrammetric canopy surface model despite being well represented in the aerial images (Figure 3.5a). Second, large negative differences in canopy height occurred mainly where the UAV–SfM technique failed to accurately reconstruct small gaps (Figure 3.5b). Third, the visual quality of the $UAV–SfM_{CHM}$ varied by stand, species, and tree density, e.g., mixed stands suffered more from the smoothing effect induced by dense point matching (Figure 3.5a, 3.5c, and 3.5d).Further comparison of $LiDAR_{CHM}$ and $UAV–SfM_{CHM}$ at the plot level is shown in Figure 3.6. Small gaps and tree tops were better represented by $LiDAR_{CHM}$. Crowns were generally wider and less defined in UAV–

[1] The total numbers of pixels (1 m resolution) for compartments 43 and 48 were 3,348,801 and 3,390,657, respectively.

SfM_{CHM} in comparison to $LiDAR_{CHM}$. UAV–SfM_{CHM} was overestimated when $LiDAR_{CHM}$ values were close to zero (Figure 3.6d and 3.6h).

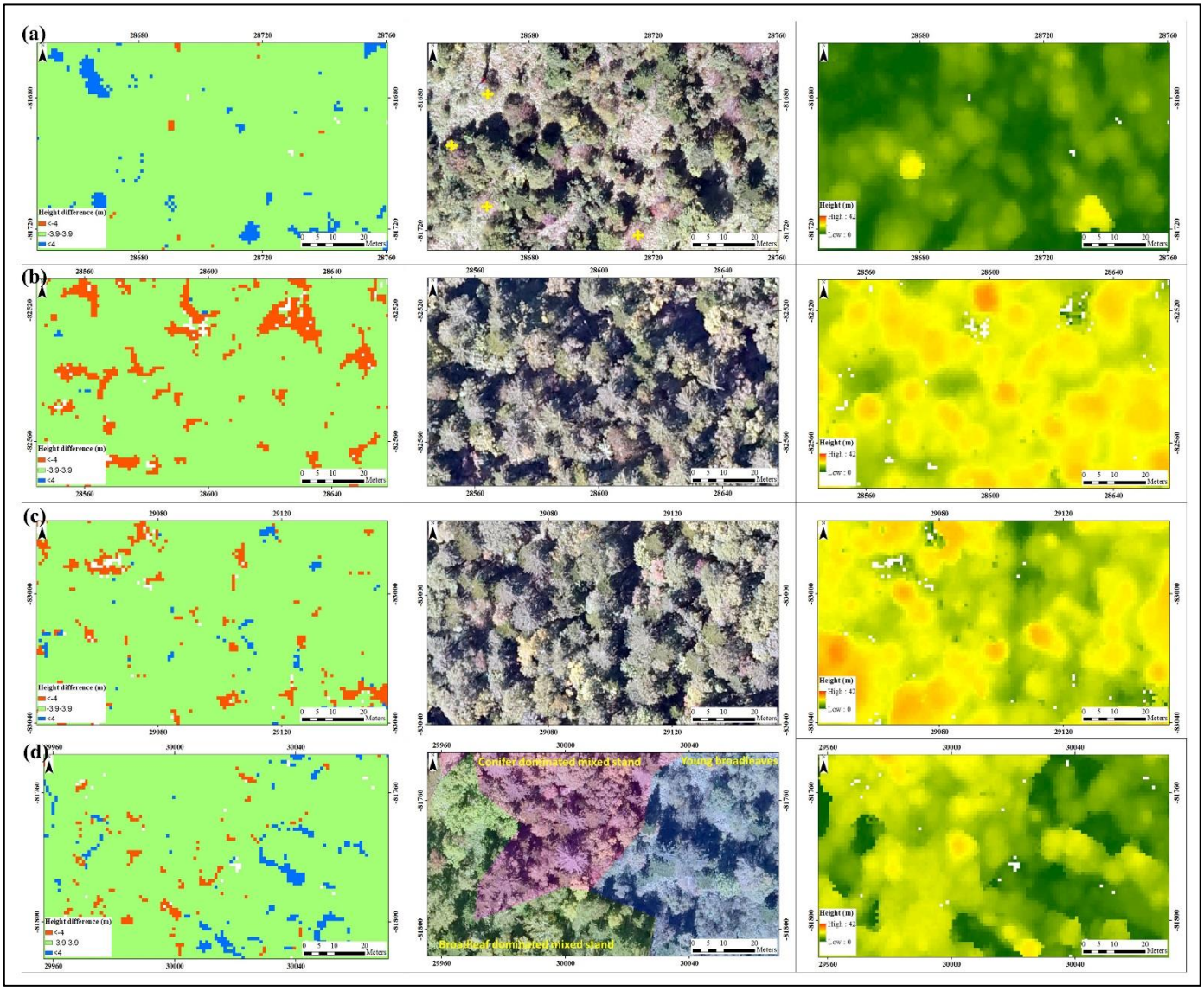

Figure 3.5: Close–up view of the height difference model (left column), aerial orthophoto (centre column), and UAV–SfM_{CHM} (right column) for visual comparison. (a) Forest stand with low tree density and more isolated trees, yellow cross icons in the aerial orthophoto indicate occluded tree crowns; (b) forest stand with numerous small canopy gaps; (c) mixed forest stand with mature broadleaf and conifer trees; and (d) mixed stands and young broadleaf stand. White pixels represent areas of the UAV–SfM_{CHM} with no data.

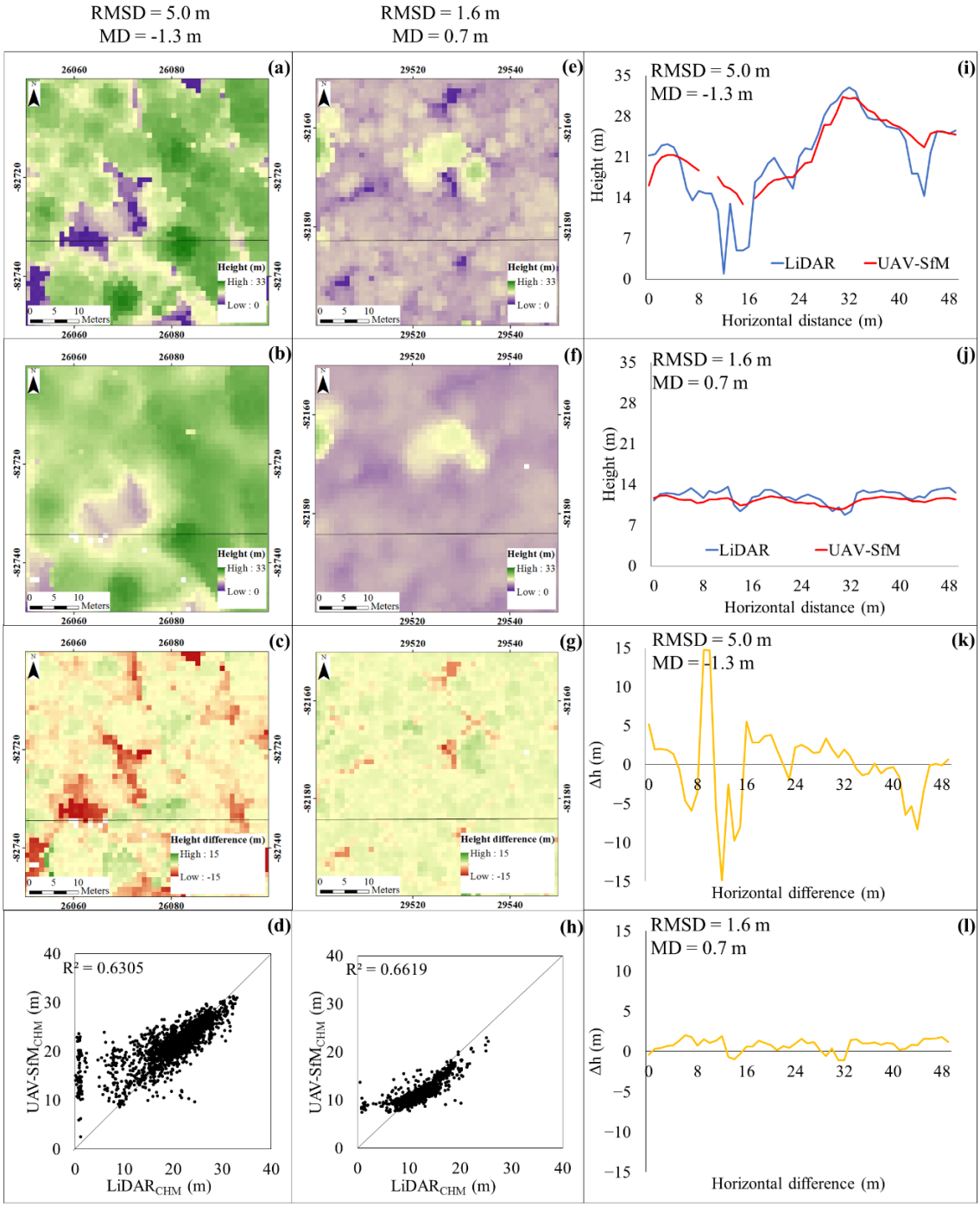

Figure 3.6: Evaluation of the differences between LiDAR$_{CHM}$ and UAV–SfM$_{CHM}$. The two plots with the lowest and highest RMSD values are shown for visual comparison (1 m pixel resolution). (a), (b), (c), (d), (i), and (k) show LiDAR$_{CHM}$, UAV–SfM$_{CHM}$, difference in height between LiDAR$_{CHM}$ and UAV–SfM$_{CHM}$, scatter plot of LiDAR$_{CHM}$ and UAV–SfM$_{CHM}$, cross–sectional profile of LiDAR$_{CHM}$ and UAV–SfM$_{CHM}$ and cross–sectional profile of the difference of a plot with highest RMSD values, respectively. (e), (f), (g), (h), (j), and (l) show LiDAR$_{CHM}$, UAV–SfM$_{CHM}$, difference in height between LiDAR$_{CHM}$ and UAV–SfM$_{CHM}$, scatter plot of LiDAR$_{CHM}$ and UAV–SfM$_{CHM}$, cross–sectional profile of LiDAR$_{CHM}$ and UAV–SfM$_{CHM}$ and cross–sectional profile of the difference of a plot with lowest RMSD values, respectively.

3.3.1.3. Comparison of structural metrics derived from photogrammetric products

Comparisons of LiDAR and UAV–SfM forest structural attributes are summarized in Table 3.2 and Figure 3.7. Although most of the variation was random, several common trends can be easily identified. Height metrics that represent the upper layers of the canopy (e.g., MaxH, P95, and P75) were underestimated, whereas height metrics that represent the middle and lower layers of the canopy (MeanH, P10, P25, and P50) were overestimated by the UAV–SfM technique.

In general, LiDAR and UAV–SfM values for all canopy height metrics showed strong correlations that were significant at the 0.01 confidence level (correlation coefficients $\geq$ 0.74). MeanH and P95, which are commonly used to characterize structural complexity of the forest canopy, showed strong correlations between LiDAR and UAV–SfM values (0.95 for mean height and 0.96 for P95) and comparatively lower RMSD values (1.5 m for mean height and 1.5 m for P95). In addition, the SDH, which is often used to represent the vertical variation in the canopy, showed good agreement (correlation coefficient = 0.74) between the two methods, with an MD of 1.2 m and RMSD of 1.4 m. Aside from the LiDAR and UAV–SfM means of Skew and P75, no statistically significant differences were found between LiDAR and UAV–SfM means of height metrics at the 0.01 confidence level.

Note that all density metrics that represent the canopy cover at different strata were overestimated by the UAV–SfM technique, which indicates the poor canopy penetration capacity of UAV–SfM data relative to LiDAR data. However, there were no statistically significant differences between mean values of LiDAR and UAV–SfM density metrics at the 0.01 confidence level, except for density above the minimum canopy height of 2 m (d_0). When I examine the d_{mean}, it is evident that there was somewhat better agreement between LiDAR and UAV–SfM values, with MD, RMSD, and correlation coefficient values of –0.02, 0.06, and 0.74, respectively (Table 3.4). For the SR (the ratio of the 3D canopy surface area to the 2D planimetric ground area that represents canopy roughness), correlation coefficient values were generally low. The mean SR estimated using the UAV–SfM technique was 3.6, which was significantly lower than its LiDAR counterpart of 5.0, although no statistically significant difference was found at the 0.01 confidence level.

Table 3.2: Results of metric comparisons.

Structural metrics	Compartment 43				Compartment 48			
	LiDAR Mean (SD)	UAV–SfM Mean (SD)	MD (SD of difference)	RMSD	LiDAR Mean (SD)	UAV–SfM Mean (SD)	MD (SD of difference)	RMSD
MaxH (m)	30.0 (3.7)	27.1 (3.5)	3.0 (1.1)	2.7	25.4 (4.5)	24.4 (4.4)	1.1 (1.9)	2.2
MeanH (m)	16.8 (3.2)	17.1 (3.5)	–0.29 (0.93)	1.1	13.9 (3.4)	15.4 (4.3)	–1.5 (1.3)	2.3
SDH (m)	5.2 (1.0)	3.9 (1.2)	1.3 (0.78)	1.5	4.2 (0.9)	3.2 (0.87)	1.0 (0.77)	1.2
CVH (m)	0.32 (0.06)	0.24 (0.09)	0.08 (0.10)	0.13	0.31 (0.06)	0.22 (0.10)	0.09 (0.06)	0.08
Skew	–0.46 (0.56)	–0.35 (0.68)	–0.12 (0.42)	0.69	–0.22 (0.53)	–0.15 (0.73)	–0.07 (0.52)	0.70
Kurt	3.3 (0.88)	3.6 (1.3)	–0.38 (0.98)	1.5	3.2 (0.73)	3.7 (1.6)	–0.42 (1.4)	2.4
P10 (m)	9.5 (2.5)	12.0 (3.8)	–2.5 (2.1)	3.4	8.3 (2.5)	11.3 (4.2)	–3.0 (2.1)	3.8
P25 (m)	13.7 (3.3)	14.7 (3.7)	–1.03 (1.40)	2.1	11.3 (3.3)	13.4 (4.5)	–2.1 (1.6)	2.8
P50 (m)	17.4 (3.7)	17.4 (3.8)	0.03 (0.74)	0.80	14.2 (3.8)	15.5 (4.6)	–1.3 (1.2)	2.1
P75 (m)	20.4 (3.9)	19.7 (3.8)	0.70 (0.62)	0.91	16.8 (4.1)	17.5 (4.5)	1.1 (0.07)	1.7
P95 (m)	24.3 (3.5)	22.9 (3.5)	1.4 (0.57)	1.2	20.4 (4.1)	20.5 (4.4)	1.4 (0.40)	2.0
d_0	0.94 (0.05)	0.99 (0.04)	–0.05 (0.03)	0.05	0.91 (0.15)	1.00 (0.00)	–0.09 (0.15)	0.34
d_1	0.92 (0.06)	0.97 (0.07)	–0.05 (0.04)	0.06	0.89 (0.16)	0.98 (0.04)	–0.10 (0.12)	0.28
d_2	0.89 (0.08)	0.95 (0.10)	–0.06 (0.04)	0.07	0.85 (0.18)	0.94 (0.14)	–0.10 (0.06)	0.12
d_3	0.85 (0.11)	0.93 (0.14)	–0.07 (0.06)	0.09	0.79 (0.21)	0.91 (0.18)	–0.12 (0.06)	0.14
d_4	0.78 (0.16)	0.87 (0.21)	–0.09 (0.07)	0.10	0.70 (0.24)	0.84 (0.23)	–0.15 (0.06)	0.15
d_5	0.71 (0.21)	0.80 (0.27)	–0.09 (0.07)	0.11	0.58 (0.27)	0.73 (0.30)	–0.15 (0.08)	0.16
d_6	0.63 (0.23)	0.73 (0.29)	–0.10 (0.08)	0.14	0.46 (0.29)	0.59 (0.36)	–0.13 (0.10)	0.16
d_7	0.55 (0.23)	0.64 (0.29)	–0.08 (0.09)	0.14	0.34 (0.26)	0.47 (0.37)	–0.12 (0.13)	0.22
d_8	0.45 (0.21)	0.50 (0.26)	–0.05 (0.09)	0.12	0.24 (0.22)	0.35 (0.32)	–0.11 (0.14)	0.25
d_9	0.33 (0.18)	0.33 (0.21)	0.00 (0.06)	0.07	0.14 (0.15)	0.22 (0.25)	–0.08 (0.14)	0.24
d_{mean}	0.51 (0.06)	0.52 (0.06)	–0.01 (0.04)	0.05	0.48 (0.10)	0.51 (0.06)	–0.03 (0.07)	0.11
SR	5.3 (0.54)	3.67 (0.28)	1.6 (0.43)	1.2	4.7 (0.44)	3.5 (0.19)	1.3 (0.40)	0.97

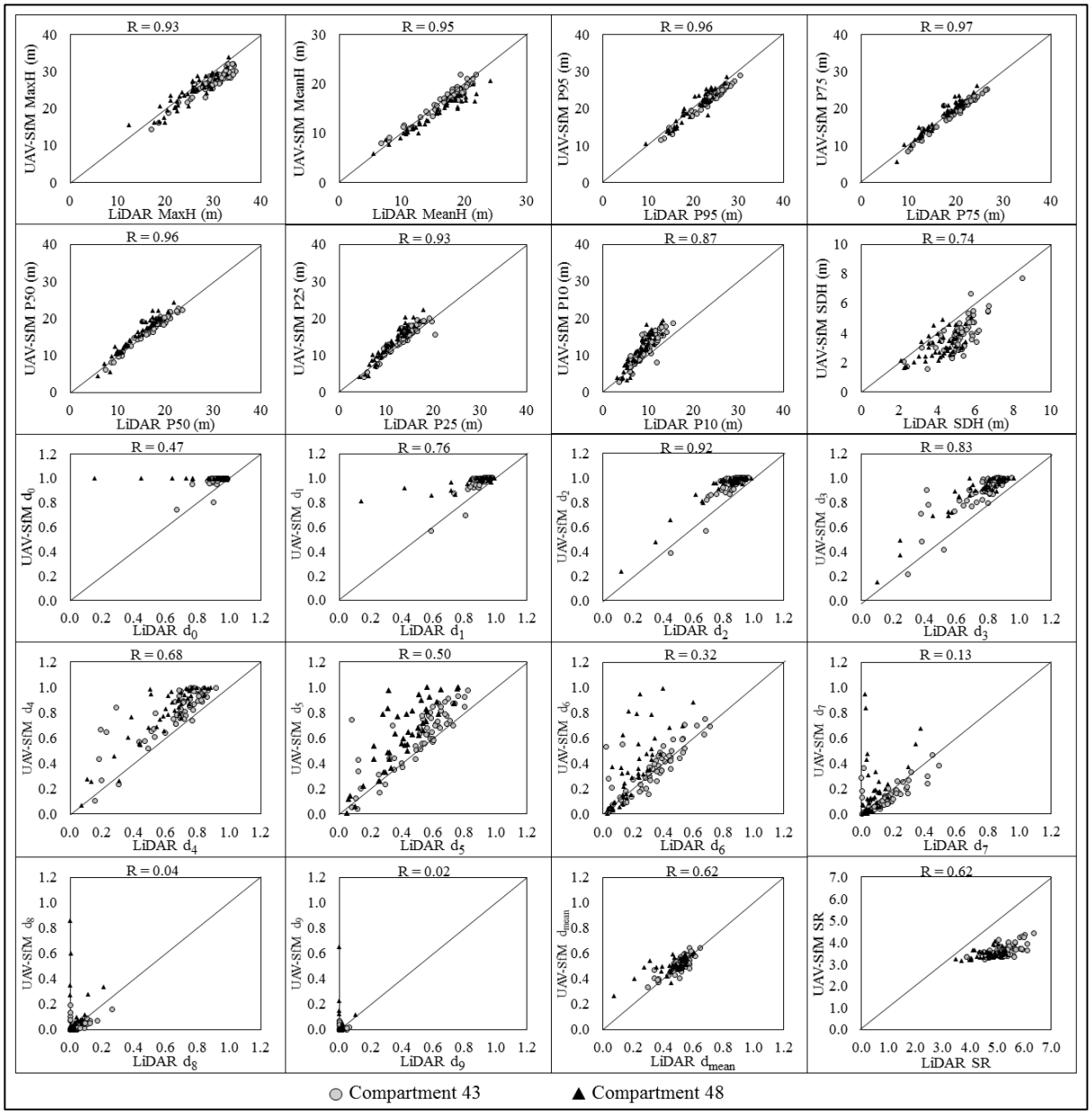

Figure 3.7: Comparison of LiDAR and UAV–SfM forest structural metrics. Each dot represents one sample plot and the plots are coded by forest management Compartment. R represents the Pearson correlation coefficient.

3.3.2. Regression modelling and plot–level validation of forest structural attributes

The regression models selected according to the Akaike's information criterion (AIC) values and penalized for collinearity are summarized in Table 3.3. Different height and density metrics were selected for each model. Nevertheless, every model included at least one height metric and one density metric. Model residuals were tested for violations of regression assumptions. Residuals were normally distributed and no serious problem of heteroscedasticity was found for all the models. Overall, both data sources resulted in models with similar relationships between the estimated and observed values (Figure 3.8). %RMSE of H_{dom} showed the lowest %RMSE (LiDAR H_{dom} and UAV–SfM H_{dom} were 6.3% and 7.4% respectively.) whereas the highest %RMSE values were reported for stem density (22.7% for LiDAR model and 22.3% for UAV–SfM model).

Table 3.3: Summary of regression modelling of forest structural attributes. All regressions were significant at $p < 0.05$.

	Explanatory variable	**RMSE**	**%RMSE**
h_{dom}			
LiDAR model	P95, d_2	1.5 m	6.3
UAV–SfM model	P75, SDH, d_1	1.8 m	7.4
BA			
LiDAR model	MaxH, d_6	4.6 m^2 ha^{-1}	15.8
UAV–SfM model	SDH, P95, d_{mean}	5.4 m^2 ha^{-1}	18.7
D_q			
LiDAR model	MaxH, P10, d_1	3.8 cm	11.5
UAV–SfM model	P95, d_1	3.9 cm	12.1
N			
LiDAR model	P10, d_1, d_8	76 trees ha^{-1}	22.3
UAV–SfM model	SDH, d_1, d_8, d_{mean}	78 trees ha^{-1}	22.7

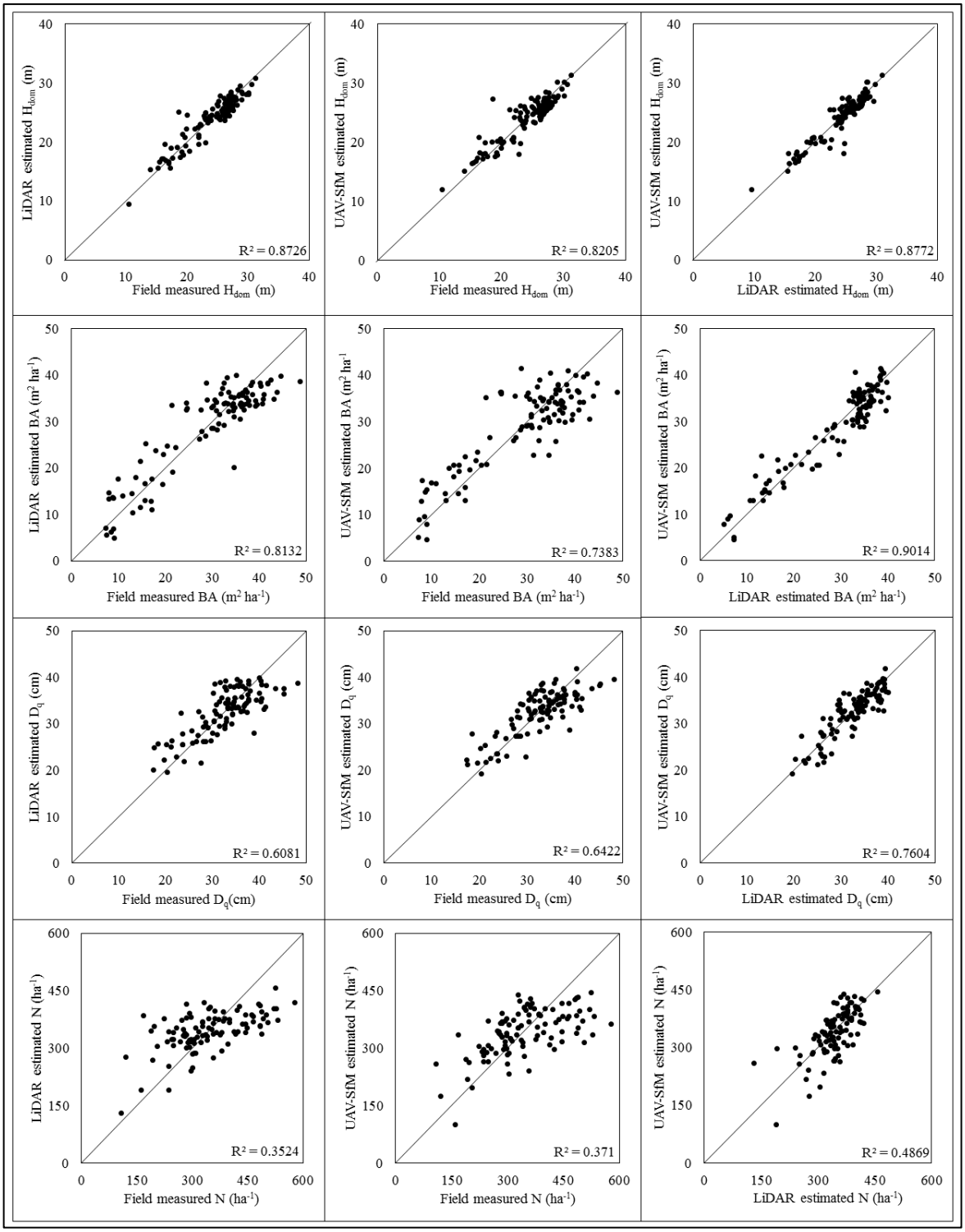

Figure 3.8: Relationship between field–measured and LiDAR–estimated forest structural attributes (left column), field–measured and UAV–SfM–estimated forest structural attributes (center), and LiDAR–estimated and UAV–SfM–estimated forest structural attributes (right column). Each dot represent one field sample plot.

3.3.3. Factors that affect the performance of UAV–SfM$_{CHM}$

Results of GLM analysis are summarized in Table 3.4. Based on the estimated coefficients, I found a statistically significant association between all selected forest structural metrics and the RMSD of canopy height. RMSD showed a positive relationship with the structural metrics of SR (coefficient of determination = 0.23; Figure 3.9), representing the roughness of the canopy through the vertical and horizontal variation in the canopy height, and MeanH (coefficient of determination = 0.19; Figure 3.9). CC was negatively related to RMSD (coefficient of determination = –0.06; Figure 3.9). However, in contrast to structural metrics, no statistically significant associations were found between metrics that explain topographic conditions, such as slope, aspect, or elevation, and RMSD values at the 0.01 confidence level. However, Compartment showed a statistically significant association with RMSD, which indicates an influence of stand or site condition differences between the two Compartments.

Table 3.4: Results of the analysis of RMSD values and forest structural and topographic conditions using GLM.

Variable	Coefficient	Standard error	*t* value	*p* value
(*Intercept*)	–0.48	1.68	–0.28	0.78
Altitude	0.00	0.00	–0.52	0.61
Aspect (North)	0.26	0.44	0.58	0.57
Aspect Northeast)	0.04	0.29	0.15	0.88
Aspect (Northwest)	–0.42	0.34	–1.26	0.21
Aspect (South)	–0.16	0.30	–0.54	0.59
Aspect Southeast)	0.14	0.29	0.49	0.63
Aspect (Southwest)	–0.18	0.28	–0.65	0.52
Aspect (West)	–0.14	0.31	–0.47	0.64
Slope	0.01	0.01	1.10	0.27
MeanH	0.14	0.04	3.99	0.00***
CC	–2.85	0.90	–3.17	0.00**
SR	0.91	0.20	4.57	0.00***
Compartment 48	0.99	0.21	4.82	0.00***

Note: AIC = 297.9. Significance codes: '**' $p < 0.01$, '***' $p < 0.001$.

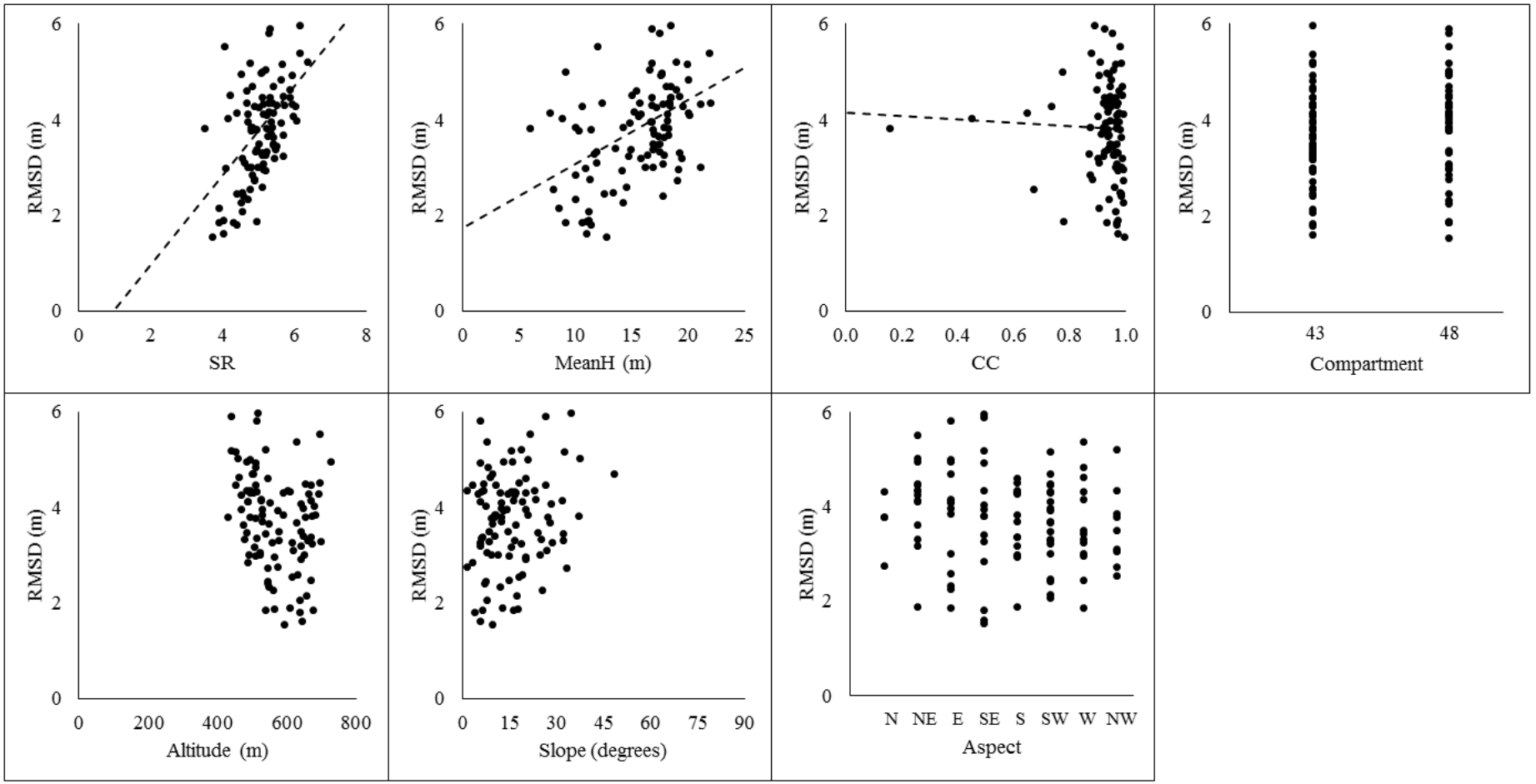

Figure 3.9: Relationships between RMSD and forest canopy structural metrics or Compartment (upper panel). Relationships between RMSD and topographic conditions (lower panel). Each dot represent one sample plot.

3.4. Discussion

3.4.1. Characterization of forest canopy using the UAV–SfM technique

My results demonstrate that the UAV–SfM technique can provide fair characterization of the mixed conifer–broadleaf forest canopy that is comparable to high–cost airborne LiDAR data. In this Chapter, four major characteristics of the UAV–SfM point clouds and CHMs were observed.

First, a limited number of UAV–SfM points denoted the ground, and these were often restricted to large open areas clearly visible from the sky, omitting small canopy gaps (Figure 3.2 and Figure 3.5) from the 3D reconstruction. Unlike LiDAR data, which penetrate the canopy and capture details of the terrain well, digital photogrammetry produces point cloud data based only on the canopy surface that is visible from the sky. Therefore, incomplete details of the terrain can be attributed to occlusion of the terrain by the forest canopy at most viewing angles, particularly in areas with dense canopy cover. This well–known limitation of digital photogrammetry known as dead ground (Wolf, P.; Dewitt, 2000) is caused by the canopy obscuring the ground, resulting in significant omissions. Consistent with previous studies (Jensen and Mathews, 2016; Wallace et al., 2016), my results revealed that the UAV–SfM technique is capable of capturing terrain over certain vegetated surfaces, such as sparse forests with large open areas, but does not function very well in forested areas with dense or closed canopies. This finding highlights the need for an accurate DTM from an alternative source to calculate canopy height with photogrammetric surface models in dense forest areas. In addition, overestimation of UAV–SfM_{CHM} occurred when $LiDAR_{CHM}$ values were near zero (Figure 3.6) as a result of poor reconstruction of small canopy gaps by the UAV–SfM technique and the limited capacity of UAV–SfM data to penetrate the outer canopy and acquire information on lower canopy layers. This limitation is due to leaves and branches of canopy trees that occlude terrain and cast shadows on understorey features. These unreconstructed small canopy gaps resulted in overestimation of CC as well as overestimation of density metrics (in comparison to LiDAR data) in all canopy strata when UAV–SfM data were used, particularly in lower canopy height strata. Previous studies have reported similar overestimations resulting from unreconstructed small canopy gaps regardless of the data collection platform used, e.g., multi–rotor UAV (Wallace

et al., 2016), mini fixed–wing UAV (Lisein et al., 2013), manned aircraft (Gobakken et al., 2015) and satellite (Baltsavias et al., 2008).

Second, the photogrammetric technique introduced underestimations into the UAV–SfM_{CHM} due to unsuccessful reconstruction of the fine peaks of some coniferous trees (Figure 3.2) as well as some isolated tree crowns (Figure 3.5). Mixed forest stands with more coniferous trees were affected more by smoothing in the dense matching process and exhibited large RMSD values. This finding is attributable to the presence of numerous abrupt fine–scale peaks and gaps in the outer canopy that cause object discontinuities or abrupt vertical changes in the canopy. These unreconstructed and partially reconstructed tree crowns in UAV–SfM_{CHM} might result from the built–in algorithm parameters, including the absence of specifically optimized algorithms for trees, inadequate altimetric dilation, and the degree of regularization, in the photogrammetric software package. Leisen et al. (2013) improved conifer reconstruction by optimizing the matching algorithms for conifers, but such optimization introduced omissions of broadleaf trees in their study.

Third, the UAV–SfM technique tends to underestimate the height of the upper canopy layer but overestimate the height of the middle and lower layers of the canopy (Table 3.2). As discussed previously, underestimation of the upper canopy can be attributed to poor reconstruction of fine peaks, whereas overestimation is a result of poor penetration through the upper canopy layer and unreconstructed canopy gaps. Although there is not sufficient evidence in the existing literature, I suggest that it could be possible to minimize these reconstruction problems using higher resolution aerial photographs. The smoothing effect can be minimized when high resolution images are used. Particularly, in comparison to low resolution images, high resolution images can perform better in capturing the fine detailed characteristics of the tree crowns. Also, the ultra–high (original image resolution) or high quality (downscale image by a factor of 4) in point densification might further minimize the reconstruction problems.

Fourth, the surface area ratio metric was significantly underestimated by UAV–SfM data compared to LiDAR data (Table 3.2). The surface area ratio is calculated by dividing the 3D surface area of the forest canopy by the corresponding 2D planimetric area. Therefore, underestimation of the surface area ratio is caused by underestimation of the 3D canopy surface area as a result of a

combination of the factors discussed previously, including poor reconstruction of canopy gaps, unreconstructed or incompletely reconstructed fine peaks, and omission of some isolated tree crowns. Understanding the causes behind overestimation and underestimation of canopy height allows the users of photogrammetric products, in particular forest managers, to more carefully interpret the results of UAV–SfM products.

3.4.2. Estimation and plot–level validation of forest structural attributes

My results for plot–level estimation and validation of the dominant canopy height are consistent with previous studies that used UAV image–based point cloud products. Lisein et al. (Lisein et al., 2013), who used fixed–wing UAV (Gatewing X100) imagery, reported an RMSE value of 1.7 m for dominant height in deciduous broadleaf stands of mixed ages. The mean error and RMSE values obtained for dominant height in my study (mean error = –0.14 m, RMSE = 1.8 m) are lower than those found in previous studies that used digital photogrammetry, e.g. Baltsavias et al. (2008) (RMSE = 6.61 m for deciduous forests using IKONOS imagery); Järnstedt et al. (2012) (RMSE = 5.4 m for state owned forest in Southern Finland using aerial imagery); and Gobakken et al. (2015) (Relative RMSE = 9.3% for mature Norway spruce, pine and mixed forest using aerial imagery). This is also true for BA (a relative RMSE of 36.3% was estimated by Järnstedt et al. (2012) whereas Gobakken et al. (2015) reported a relative RMSE of 18.3%), and N (relative RMSE of 43.7% by Gobakken et al. (2015) and 14.1% by Bohlin et al. (2012). These differences in results can be attributed primarily to data sources, flight configurations, image acquisition parameters, GCPs, and processing workflows (software packages and algorithms), as these parameters directly affect the accuracy of image matching and point densification and thus the quality of the photogrammetric point cloud. Specifically, two major factors facilitated the improvement in results obtained in this study. First, the high quality and large overlap of my UAV imagery allowed us to build a gap–free point cloud data set. Because of the reported impact of image quality and overlap (Wallace et al., 2016; White et al., 2015) on the tie point detection and image matching procedures, the flight plans were designed to achieve a very high overlap between individual images (> 90%), and flights were

undertaken under stable and clear weather conditions for all data acquisition. Therefore, my data set contained only very small areas with no data (accounting for less than 1% of the study area) in my UAV–SfM point cloud data set, which may have been due to shadows and the viewing angle of the camera. Second, choosing appropriate parameter settings for built–in algorithms in the photogrammetric workflow of the Agisoft software package improved my results. It is generally recommended that researchers determine the optimal parameter settings for a particular area based on a preliminary evaluation (i.e., by using sequential selection for a small area), because inappropriate parameter settings can produce unsatisfactory 3D reconstruction even with a robust photogrammetric workflow (Järnstedt et al., 2012; Remondino et al., 2014; Wong, et al., 2016).

However, Jensen and Mathews (Jensen and Mathews, 2016) (RMSE = 1.2 m for Oak–Ash Juniper Savanah and closed canopy woodland using Hawkeye II UAV imagery) reported lower RMSE values for dominant height than mine. Puliti et al. (2015) also reported lower RMSE values for h_{dom} (RMSE = 0.72 m and relative RMSE = 3.5%), and BA (RMSE = 4.5 m^2 ha^{-1}, relative RMSE = 15.4%). This may be because of differences in the forest types studied, as both boreal and woodland forest types have relatively simple structures that differ from those of mixed conifer–broadleaf forests in northern Japan in terms of species composition, height variations, and other factors. Bohlin et al. (2017) concluded that their estimations improved after using textural properties as independent variables. Puliti et al. (2015) concluded that addition of spectral variables as independent variables improved the accuracy of estimations only to a limited degree. Nevertheless, I didn't include textural properties or spectral variables as predictor variables as it was outside the scope of this Chapter.

3.4.3. Influence of forest structural properties and topographic conditions on the performance of canopy height models

In accordance with previous studies (Lisein et al., 2013; Wallace et al., 2016; Wong, et al., 2016), my results reveal the influence of several canopy structural metrics that explain the overall structural complexity of the forest canopy (i.e., structural metrics that are sensitive to both vertical and

horizontal variation in the canopy) on the performance of photogrammetric CHMs (Table 3.4 and Figure 3.9). When the forest canopy has numerous small canopy gaps and peaks, resulting in a rougher canopy surface with significant vertical and horizontal variation, errors tend to be introduced into 3D reconstruction, such as unreconstructed or poorly reconstructed small canopy gaps and peaks and smoothing errors (Figure 3.2, Figure 3.5 and Figure 3.6). These errors result in overestimation or underestimation of canopy cover, height, and 3D canopy surface area, whereas poor penetration of point clouds and shadows cast by dense canopies lead to incomplete information on the middle and lower canopy layers. Similar variations were found in other studies that used different software packages, which suggests that these variations are not related to matching algorithms (Lisein et al., 2013; Remondino et al., 2014; Sona et al., 2014). In contrast to Müller et al. (2014) and Baltsavias et al. (2008), who conducted their studies in mountainous forest environments, I didn't observe a clear relationship between ground slope and RMSD values. This may be because of the narrow range of slopes in my field data set. Understanding the performance of photogrammetric products and their behavior under canopies of varying structural complexities and topographic conditions can support improved management, such as determining how and when to use the UAV–SfM technique for data acquisition and how to interpret the results in light of the structural complexity and conditions of a particular site.

3.5. Conclusion

In this Chapter, I aimed to evaluate the performance of fixed–wing UAV photogrammetric products over mixed conifer–broadleaf forests. The results demonstrated that UAV photogrammetric products, i.e., point clouds, CHMs, and structural metrics have comparable accuracy to the results of high–cost airborne LiDAR observations. Thus, it is proven that UAV–SfM technique is capable of providing an accurate and detailed reconstruction of mixed conifer–broadleaf forest canopy with varying levels of structural complexity. Furthermore, LiDAR and UAV–SfM data provided similar results in terms of area–based predictions of commonly used forest structural attributes, e.g., h_{dom}, BA, Dq, and N. Therefore, it is concluded that although there are differences between ALS and

digital photogrammetric techniques such as SfM, UAV–SfM products developed over the mixed conifer–broadleaf forests in northern Japan performed well in reconstructing 3D forest canopy structure and providing reliable forest canopy structural measurements when combined with $LiDAR_{DTM}$. However, UAV–SfM CHMs were likely to be influenced by the structural complexity of the forest canopy.

Chapter 4 (Abridged version)

Estimation of merchantable volume and carbon stock in living biomass.

This chapter has been accepted for publication by the International Journal of Applied Earth Observation and Geoinformation and will be published soon. For any inquiry or further information, please send an email to sadeepasenarath@yahoo.com

Chapter 5 (Abridged version)

Characterization of forest canopy structure.

This chapter is scheduled to be submitted to a peer review academic journal. For any inquiry or further information, please send an email to sadeepasenarath@yahoo.com

Chapter 6 (Abridged version)

Utility of UAV photogrammetry for uneven–aged forest management planning

This chapter is scheduled to be submitted to a peer review academic journal. For any inquiry or further information, please send an email to sadeepasenarath@yahoo.com

Chapter 7 (Abridged version)

Overall Discussion and conclusions

7.1. Overall discussion

- 7.1.1. Performance of fixed–wing UAV photogrammetry in comparison to airborne LiDAR data
- 7.1.2. UAV photogrammetry for estimating merchantable volume and carbon stock in living biomass
- 7.1.3. UAV photogrammetry for characterizing vertical and horizontal variations of forest canopy structure
- 7.1.4. Utility of fixed–wing UAV photogrammetry in uneven–aged forest management planning
- 7.1.5. General considerations when applying fixed–wing UAV photogrammetry for forestry applications
  - 7.1.5.1. UAV image acquisition and photogrammetric processing
  - 7.1.5.2. Derivation and comparison of structural metrics
  - 7.1.5.3. Requirement of an accurate DTM for normalization of photogrammetric point cloud
- 7.1.6. Comparison of field, LiDAR and UAV data in forestry applications

7.2. Main conclusions

7.3. Limitations

7.4. Directions for future research

The content of this chapter is integral parts of Chapter 4, Chapter 5 and Chapter 6, which are already submitted or schedule to be submitted to peer review academic journals. For any inquiry or further information, please send an email to sadeepasenarath@yahoo.com

Bibliography

1. Aicardi, I., Garbarino, M., Lingua, A., Lingua, E., Marzano, R., Piras, M., 2016. Monitoring Post–Fire Forest Recovery Using Multi–Temporal Digital Surface Models Generated From. EARSeL eProceedings 15, 1–8. https://doi.org/10.12760/01–2016–1–01
2. Albertz, J., 2007. A Look Back; 140 Years of Photogrammetry. Photogramm. Eng. Remote Sens.504–506.
3. Allen, T.F.H., Hoekstra, T.W., 1992. Toward a Unified Ecology. Columbia University Press, New York, NY, USA.
4. Alonzo, M., Andersen, H.–E., Morton, D., Cook, B., 2018. Quantifying Boreal Forest Structure and Composition Using UAV Structure from Motion. Forests 9, 119. https://doi.org/10.3390/f9030119
5. Anderson, K., Gaston, K.J., 2013. Lightweight unmanned aerial vehicles will revolutionize spatial ecology. Front. Ecol. Environ. 11, 138–146. https://doi.org/10.1890/120150
6. Apps, M.J., 2001. Forests, the global carbon cycle and climate change 139–147.
7. Asner, G.P., Mascaro, J., Muller-Landau, H.C., Vieilledent, G., Vaudry, R., Rasamoelina, M., Hall, J.S., van Breugel, M., 2012. A universal airborne LiDAR approach for tropical forest carbon mapping. Oecologia 168, 1147–1160. https://doi.org/10.1007/s00442-011-2165-z
8. Baena, S., Moat, J., Whaley, O., Boyd, D.S., 2017. Identifying species from the air: UAVs and the very high resolution challenge for plant conservation. PLoS One 12, 1–21. https://doi.org/10.1371/journal.pone.0188714
9. Baltsavias, E., Gruen, A., Eisenbeiss, H., Zhang, L., Waser, L.T., 2008. High-quality image matching and automated generation of 3D tree models. Int. J. Remote Sens. 29, 1243–1259. https://doi.org/10.1080/01431160701736513
10. Barker, M.G., Pinard, M.A., 2001. Forest canopy research: Sampling problems, and some solutions. Plant Ecol. 153, 23–38. https://doi.org/10.1023/A:1017584130692
11. Bawa, K.S., Seidler, R., 1998. Natural forest management and conservation of biodiversity in tropical forests. Conserv. Biol. 12, 46–55. https://doi.org/10.1046/j.1523–1739.1998.96480.x
12. Bebi, P., Kienast, F., Schonenberger, W., 2001. Assessing structures in mountain forests as a basis for investigating the forests' dynamics and protective function. For. Ecol. Manage. 145, 3–14. https://doi.org/10.1016/S0378–1127(00)00570–3
13. Bettinger, P., Boston, K., Siry, J.P., Grebner, D.L., 2017. Chapter 1 – Management of Forests and Other Natural Resources BT – Forest Management and Planning (Second Edition). Academic Press, pp. 1–20. https://doi.org/https://doi.org/10.1016/B978–0–12–809476–1.00001–1
14. Bohlin, J., Bohlin, I., Jonzén, J., Nilsson, M., 2017. Mapping forest attributes using data from stereophotogrammetry of aerial images and field data from the national forest inventory 51, 1–18.
15. Bohlin, J., Wallerman, J., Fransson, J.E.S., 2012. Forest variable estimation using photogrammetric matching of digital aerial images in combination with a high–resolution DEM. Scand. J. For. Res. 27, 692–699. https://doi.org/10.1080/02827581.2012.686625
16. Boisvenue, C., Running, S.W., 2006. Impacts of climate change on natural forest productivity – Evidence since the middle of the 20th century. Glob. Chang. Biol. 12, 862–882. https://doi.org/10.1111/j.1365–2486.2006.01134.x
17. Boyd, J., Banzhaf, S., 2007. What are ecosystem services? The need for standardized environmental accounting units. Ecol. Econ. 63, 616–626. https://doi.org/10.1016/j.ecolecon.2007.01.002

18. Bradford, J.B., Kastendick, D.N., 2010. Age–related patterns of forest complexity and carbon storagein pine and aspen–birch ecosystems of northern Minnesota, USA. Can. J. For. Res. 40, 401–409. https://doi.org/10.1139/X10–002
19. Brosofske, K.D., Froese, R.E., Falkowski, M.J., Banskota, A., 2014. A review of methods for mapping and prediction of inventory attributes for operational forest management. For. Sci. 60, 733–756. https://doi.org/10.5849/forsci.12–134
20. Brown, S.L., Schroeder, P., Kern, J.S., 1999. Spatial distribution of biomass in forests of the eastern USA. For. Ecol. Manage. 123, 81–90. https://doi.org/10.1016/S0378–1127(99)00017–1
21. Cambero, C., Sowlati, T., 2014. Assessment and optimization of forest biomass supply chains from economic, social and environmental perspectives – A review of literature. Renew. Sustain. Energy Rev. 36, 62–73. https://doi.org/10.1016/j.rser.2014.04.041
22. Campbell, J., 2002. Introduction to Remote Sensing, 3rd Edition. New York, NY, USA.
23. Carswell, F.E., Meir, P., Wandelli, E. V., Bonates, L.C.M., Kruijt, B., Barbosa, E.M., Nobre, A.D., Grace, J., Jarvis, P.G., 2000. Photosynthetic capacity in a central Amazonian rain forest. Tree Physiol. 20, 179–186. https://doi.org/10.1093/treephys/20.3.179
24. Chianucci, F., Disperati, L., Guzzi, D., Bianchini, D., Nardino, V., Lastri, C., Rindinella, A., Corona, P., 2016. International Journal of Applied Earth Observation and Geoinformation Estimation of canopy attributes in beech forests using true colour digital images from a small fixed–wing UAV. Int. J. Appl. Earth Obs. Geoinf. 47, 60–68. https://doi.org/10.1016/j.jag.2015.12.005
25. Cunliffe, A.M., Brazier, R.E., Anderson, K., 2016. Ultra–fine grain landscape–scale quantification of dryland vegetation structure with drone–acquired structure–from–motion photogrammetry. Remote Sens. Environ. 183, 129–143. https://doi.org/10.1016/j.rse.2016.05.019
26. Dandois, J.P., Ellis, E.C., 2010. Remote sensing of vegetation structure using computer vision. Remote Sens. 2, 1157–1176. https://doi.org/10.3390/rs2041157
27. Dash, J.P., Watt, M.S., Pearse, G.D., Heaphy, M., Dungey, H.S., 2017. Assessing very high resolution UAV imagery for monitoring forest health during a simulated disease outbreak. ISPRS J. Photogramm. Remote Sens. 131, 1–14. https://doi.org/10.1016/j.isprsjprs.2017.07.007
28. Davis, L. S.; Johnson, K.N., 1987. Forest management, 3rd ed. McGraw–Hill Book Company, California, Berkeley, CA, USA.
29. De Dios, J.R.M., Merino, L., Caballero, F., Ollero, A., 2011. Automatic forest–fire measuring using ground stations and unmanned aerial systems. Sensors 11, 6328–6353. https://doi.org/10.3390/s110606328
30. Dempewolf, J., Nagol, J., Hein, S., Thiel, C., Zimmermann, R., 2017. Measurement of within-season tree height growth in a mixed forest stand using UAV imagery. Forests 8, 1–15. https://doi.org/10.3390/f8070231
31. DeWalt, S.J., Maliakal, S.K., Denslow, J.S., 2003. Changes in vegetation structure and composition along a tropical forest chronosequence: Implications for wildlife. For. Ecol. Manage. 182, 139–151. https://doi.org/10.1016/S0378–1127(03)00029–X
32. Dickinson, Y., Zenner, E.K., Miller, D., 2014. Examining the effect of diverse management strategies on landscape scale patterns of forest structure in Pennsylvania using novel remote sensing techniques. Can. J. For. Res. 44, 301–312. https://doi.org/10.1139/cjfr–2013–0315
33. Digby, P.G.N., Kempton, R.A., 1987. Multivariate analysis of ecological communities. Chapman and Hall, London, U.K.

34. Eckert, S., 2012. Improved forest biomass and carbon estimations using texture measures from worldView-2 satellite data. Remote Sens. 4, 810–829. https://doi.org/10.3390/rs4040810
35. Erb, K.–H., Kastner, T., Plutzar, C., Bais, A.L.S., Carvalhais, N., Fetzel, T., Gingrich, S., Haberl, H., Lauk, C., Niedertscheider, M., Pongratz, J., Thurner, M., Luyssaert, S., 2017. Unexpectedly large impact of forest management and grazing on global vegetation biomass. Nature 553, 73–76. https://doi.org/10.1038/nature25138
36. Eriksson, E., Gillespie, A.R., Gustavsson, L., Langvall, O., Olsson, M., Sathre, R., Stendahl, J., 2007. Integrated carbon analysis of forest management practices and wood substitution. Can. J. For. Res. 37, 671–681. https://doi.org/10.1139/X06–257
37. Estes, L.D., Reillo, P.R., Mwangi, A.G., Okin, G.S., Shugart, H.H., 2010. Remote sensing of structural complexity indices for habitat and species distribution modeling. Remote Sens. Environ. 114, 792–804. https://doi.org/10.1016/j.rse.2009.11.016
38. Feng, Q., Liu, J., Gong, J., 2015. UAV Remote sensing for urban vegetation mapping using random forest and texture analysis. Remote Sens. 7, 1074–1094. https://doi.org/10.3390/rs70101074
39. Food and agriculture organization of the United Nations, FRA 2015 Terms and definitions. Forest resources assessment working Paper 180, Food and agriculture organization of the United Nations, Rome. Available at http://www.fao.org/3/a-ap862e.pdf (Last assesed on 27 February 2018)
40. Franklin, J.F., Van Pelt, R., 2004. Spatial aspects of structural complexity in old–growth forests. J. For. 22–28.
41. Franklin, S.E., Ahmed, O.S., Williams, G., 2017. Northern Conifer Forest Species Classification Using Multispectral Data Acquired from an Unmanned Aerial Vehicle 501, 501–507. https://doi.org/10.14358/PERS.83.7.501
42. Fryskowska, A., Kedzierski, M., Walczykowski, P., Wierzbicki, D., Delis, P., Lada, A., 2017. Effective Detection of Sub–Surface Archeological Features from Laser Scanning Point Clouds and Imagery Data. ISPRS – Int. Arch. Photogramm. Remote Sens. Spat. Inf. Sci. XLII–2/W5, 245–251. https://doi.org/10.5194/isprs–archives–XLII–2–W5–245–2017
43. Getzin, S., Nuske, R.S., Wiegand, K., 2014. Using unmanned aerial vehicles (UAV) to quantify spatial gap patterns in forests. Remote Sens. 6, 6988–7004. https://doi.org/10.3390/rs6086988
44. Getzin, S., Wiegand, K., Schöning, I., 2012. Assessing biodiversity in forests using very high–resolution images and unmanned aerial vehicles. Methods Ecol. Evol. 3, 397–404. https://doi.org/10.1111/j.2041–210X.2011.00158.x
45. Ghamry, K.A., Kamel, M.A., Zhang, Y., 2016. Cooperative forest monitoring and fire detection using a team of UAVs–UGVs. 2016 Int. Conf. Unmanned Aircr. Syst. ICUAS 2016 1206–1211. https://doi.org/10.1109/ICUAS.2016.7502585
46. Gini, R., Passoni, D., Pinto, L., Sona, G., 2014. Use of unmanned aerial systems for multispectral survey and tree classification: A test in a park area of northern Italy. Eur. J. Remote Sens. 47, 251–269. https://doi.org/10.5721/EuJRS20144716
47. Gobakken, T., Bollandsås, O.M., Næsset, E., 2015. Comparing biophysical forest characteristics estimated from photogrammetric matching of aerial images and airborne laser scanning data. Scand. J. For. Res. 30, 73–86. https://doi.org/10.1080/02827581.2014.961954
48. Grenzdörffer, G.J., Engel, A., Teichert, B., 2008. The Photogrammetric Potential of Low–Cost UAVs in Forestry and Agriculture. Int. Arch. Photogramm. Remote Sens. Spat. Inf. Sci. Vol. XXXVII 31, 1207–2014. https://doi.org/10.2747/1548–1603.41.4.287

49. Guo, X., Coops, N.C., Tompalski, P., Nielsen, S.E., Bater, C.W., John Stadt, J., 2017. Regional mapping of vegetation structure for biodiversity monitoring using airborne lidar data. Ecol. Inform. 38, 50–61. https://doi.org/10.1016/j.ecoinf.2017.01.005
50. Hall, R.J., Skakun, R.S., Arsenault, E.J., Case, B.S., 2006. Modeling forest stand structure attributes using Landsat ETM+ data: Application to mapping of aboveground biomass and stand volume. For. Ecol. Manage. 225, 378–390. https://doi.org/10.1016/j.foreco.2006.01.014
51. Hame, T., Salli, A., Andersson, K., Lohi, A., 1997. A new methodology for the estimation of biomass of coniferdominated boreal forest using NOAA AVHRR data. Int. J. Remote Sens. 18, 3211–3243. https://doi.org/10.1080/014311697217053
52. Hawryło, P., Tompalski, P., Węzyk, P., 2017. Area–based estimation of growing stock volume in Scots pine stands using ALS and airborne image–based point clouds. Forestry 90, 686–696. https://doi.org/10.1093/forestry/cpx026
53. Hernández–Clemente, R., Navarro–Cerrillo, R.M., Romero Ramírez, F.J., Hornero, A., Zarco–Tejada, P.J., 2014. A novel methodology to estimate single–tree biophysical parameters from 3D digital imagery compared to aerial laser scanner data. Remote Sens. 6, 11627–11648. https://doi.org/10.3390/rs61111627
54. Hill, A., Breschan, J., Mandallaz, D., 2014. Accuracy Assessment of Timber Volume Maps Using Forest Inventory Data and LiDAR Canopy Height Models 2253–2275. https://doi.org/10.3390/f5092253
55. Ho Tong Minh, D., Le Toan, T., Rocca, F., Tebaldini, S., Villard, L., Réjou–Méchain, M., Phillips, O.L., Feldpausch, T.R., Dubois–Fernandez, P., Scipal, K., Chave, J., 2016. SAR tomography for the retrieval of forest biomass and height: Cross–validation at two tropical forest sites in French Guiana. Remote Sens. Environ. 175, 138–147. https://doi.org/10.1016/j.rse.2015.12.037
56. Honkavaara, E., Saari, H., Kaivosoja, J., Pölönen, I., Hakala, T., Litkey, P., Mäkynen, J., Pesonen, L., 2013. Processing and assessment of spectrometric, stereoscopic imagery collected using a lightweight UAV spectral camera for precision agriculture. Remote Sens. 5, 5006–5039. https://doi.org/10.3390/rs5105006
57. Horie K., Miyamoto Y., Limura N., Oikawa N., 2013. List of vascular plant of the University of Tokyo Hokkaido Forest, University of Tokyo Hokkaido Forest. University Forest.
58. Houghton, R.A., Hackler, J.L., Lawrence, K.T., 1999. The U.S. Carbon budget: contributions from land–Use change. Science 285, 574–8. https://doi.org/10.1126/science.285.5427.574
59. Hussin, Y.A., Gilani, H., Van Leeuwen, L., Murthy, M.S.R., Shah, R., Baral, S., Tsendbazar, N.E., Shrestha, S., Shah, S.K., Qamer, F.M., 2014. Evaluation of object-based image analysis techniques on very high-resolution satellite image for biomass estimation in a watershed of hilly forest of Nepal. Appl. Geomatics 6, 59–68. https://doi.org/10.1007/s12518-014-0126-z
60. Huston, M.A., 1994. Biological Diversity. Cambridge University Press, Cambridge, UK.
61. Hyyppä, J., Yu, X., Hyyppä, H., Vastaranta, M., Holopainen, M., Kukko, A., Kaartinen, H., Jaakkola, A., Vaaja, M., Koskinen, J., Alho, P., 2012. Advances in forest inventory using airborne laser scanning. Remote Sens. 4, 1190–1207. https://doi.org/10.3390/rs4051190
62. Iizuka, K., Yonehara, T., Itoh, M., Kosugi, Y., 2017. Estimating Tree Height and Diameter at Breast Height (DBH) from Digital Surface Models and Orthophotos Obtained with an Unmanned Aerial System for a Japanese Cypress (Chamaecyparis obtusa) Forest. Remote Sens. 10, 13. https://doi.org/10.3390/rs10010013

63. Ioki, K., Imanishi, J., Sasaki, T., Morimoto, Y., Kitada, K., 2010. Estimating stand volume in broad–leaved forest using discrete–return LiDAR: Plot–based approach. Landsc. Ecol. Eng. 6, 29–36. https://doi.org/10.1007/s11355–009–0077–4
64. Ioki, K., Tsuyuki, S., Hirata, Y., Phua, M.H., Wong, W.V.C., Ling, Z.Y., Saito, H., Takao, G., 2014. Estimating above–ground biomass of tropical rainforest of different degradation levels in Northern Borneo using airborne LiDAR. For. Ecol. Manage. 328, 335–341. https://doi.org/10.1016/j.foreco.2014.06.003
65. Jaakkola, A., Hyyppä, J., Yu, X., Kukko, A., Kaartinen, H., Liang, X., Hyyppä, H., Wang, Y., 2017. Autonomous collection of forest field reference—The outlook and a first step with UAV laser scanning. Remote Sens. 9. https://doi.org/10.3390/rs9080785
66. Jandl, R., Lindner, M., Vesterdal, L., Bauwens, B., Baritz, R., Hagedorn, F., Johnson, D.W., Minkkinen, K., Byrne, K.A., 2007. How strongly can forest management influence soil carbon sequestration? Geoderma 137, 253–268. https://doi.org/10.1016/j.geoderma.2006.09.003
67. Järnstedt, J., Pekkarinen, A., Tuominen, S., Ginzler, C., Holopainen, M., Viitala, R., 2012. Forest variable estimation using a high–resolution digital surface model. ISPRS J. Photogramm. Remote Sens. 74, 78–84. https://doi.org/10.1016/j.isprsjprs.2012.08.006
68. Jayathunga, S., Owari, T., Tsuyuki, S., 2018. Analysis of forest structural complexity using airborne LiDAR data and aerial photography in a mixed conifer–broadleaf forest in northern Japan. J. For. Res. 29(2), 479–493. https://doi.org/10.1007/s11676–017–0441–4
69. Jensen, J., Mathews, A., 2016. Assessment of Image–Based Point Cloud Products to Generate a Bare Earth Surface and Estimate Canopy Heights in a Woodland Ecosystem. Remote Sens. 8, 50. https://doi.org/10.3390/rs8010050
70. Jing, R., Gong, Z., Zhao, W., Pu, R., Deng, L., 2017. Above–bottom biomass retrieval of aquatic plants with regression models and SfM data acquired by a UAV platform – A case study in Wild Duck Lake Wetland, Beijing, China. ISPRS J. Photogramm. Remote Sens. 134, 122–134. https://doi.org/10.1016/j.isprsjprs.2017.11.002
71. Johnson, D.W., Curtis, P.S., 2001. Effects of forest management on soil C and N storage: Meta analysis. For. Ecol. Manage. 140, 227–238. https://doi.org/10.1016/S0378–1127(00)00282–6
72. Kachamba, D.J., Ørka, H.O., Gobakken, T., Eid, T., Mwase, W., 2016. Biomass estimation using 3D data from unmanned aerial vehicle imagery in a tropical woodland. Remote Sens. 8, 1–18. https://doi.org/10.3390/rs8110968
73. Kane, V.R., Bakker, J.D., McGaughey, R.J., Lutz, J. a., Gersonde, R.F., Franklin, J.F., 2010a. Examining conifer canopy structural complexity across forest ages and elevations with LiDAR data. Can. J. For. Res. 40, 774–787. https://doi.org/10.1139/X10–064
74. Kane, V.R., McGaughey, R.J., Bakker, J.D., Gersonde, R.F., Lutz, J. a., Franklin, J.F., 2010b. Comparisons between field– and LiDAR–based measures of stand structural complexity. Can. J. For. Res. 40, 761–773. https://doi.org/10.1139/X10–024
75. Karna, Y.K., Hussin, Y.A., Gilani, H., Bronsveld, M.C., Murthy, M.S.R., Qamer, F.M., Karky, B.S., Bhattarai, T., Aigong, X., Baniya, C.B., 2015. Integration of WorldView-2 and airborne LiDAR data for tree species level carbon stock mapping in Kayar Khola watershed, Nepal. Int. J. Appl. Earth Obs. Geoinf. 38, 280–291. https://doi.org/10.1016/j.jag.2015.01.011
76. Kasser, M., Egels, Y., 2002. Digital Photogrammetry, Second edi. ed. Taylor & Francis, London. https://doi.org/10.1007/978–3–662–50463–5
77. Keenan, R.J., 2015. Climate change impacts and adaptation in forest management: a review. Ann. For. Sci. 72, 145–167. https://doi.org/10.1007/s13595–014–0446–5
78. Klein, D., Höllerl, S., Blaschke, M., Schulz, C., 2013. The contribution of managed and unmanaged forests to climate change mitigation–A model approach at stand level for the main tree species in Bavaria. Forests 4, 43–69. https://doi.org/10.3390/f4010043

79. Kumar, S., Khati, U.G., Chandola, S., Agrawal, S., Kushwaha, S.P.S., 2017. Polarimetric SAR Interferometry based modeling for tree height and aboveground biomass retrieval in a tropical deciduous forest. Adv. Sp. Res. 60, 571–586. https://doi.org/10.1016/j.asr.2017.04.018
80. Kuuluvainen, T., Tahvonen, O., Aakala, T., 2012. Even–aged and uneven–aged forest management in boreal fennoscandia: A review. Ambio 41, 720–737. https://doi.org/10.1007/s13280–012–0289–y
81. Lähde, E., Laiho, O., Norokorpi, Y., Saksa, T., 1999. Stand structure as the basis of diversity index. For. Ecol. Manage. 115, 213–220. https://doi.org/10.1016/S0378–1127(98)00400–9
82. Latifi, H., Nothdurft, A., Koch, B., 2017. Non–parametric prediction and mapping of standing timber volume and biomass in a temperate forest : application of multiple optical / LiDAR–derived predictors 83, 395–407. https://doi.org/10.1093/forestry/cpq022
83. Leberl, F., Irschara, A., Pock, T., Meixner, P., Gruber, M., Scholz, S., Wiechert, A., 2010. Point Clouds: Lidar versus 3D Vision. Photogramm. Eng. Remote Sens. 76, 1123–1134. https://doi.org/0099–1112/10/7610–1123
84. Lefsky, M.A., Cohen, W.B., Parker, G.G., Harding, D.J., 2002. Lidar Remote Sensing for Ecosystem Studies. Bioscience 52, 19–30. https://doi.org/10.1641/0006–3568(2002)052[0019:LRSFES]2.0.CO;2
85. Lefsky, M.A., Hudak, A.T., Cohen, W.B., Acker, S.A., 2005. Geographic variability in lidar predictions of forest stand structure in the Pacific Northwest. Remote Sens. Environ. 95, 532–548. https://doi.org/10.1016/j.rse.2005.01.010
86. Lehmann, J.R.K., Nieberding, F., Prinz, T., Knoth, C., 2015. Analysis of unmanned aerial system–based CIR images in forestry–a new perspective to monitor pest infestation levels. Forests 6, 594–612. https://doi.org/10.3390/f6030594
87. Levesque, J., King, D.J., 2003. Spatial analysis of radiometeric fractions from high resolution multispectral imagery for modellling individual tree crown and forest canopy structure and health. Remote Sens. Environ. 84, 589–602.
88. Li, A., Dhakal, S., Glenn, N.F., Spaete, L.P., Shinneman, D.J., Pilliod, D.S., Arkle, R.S., McIlroy, S.K., 2017. Lidar aboveground vegetation biomass estimates in shrublands: Prediction, uncertainties and application to coarser scales. Remote Sens. 9. https://doi.org/10.3390/rs9090903
89. Lindenmayer, D.B., Margules, C.R., Botkin, D.B., 2000. Indicators of biodiversity for ecologically sustainable forest management. Conserv. Biol. 14, 941–950. https://doi.org/10.1046/j.1523–1739.2000.98533.x
90. Lindenmayer, D.B., Margules, C.R., Botkin, D.B., 2001. Indicators of biodiversity for ecologically sustainable forest management. Conserv. Biol. 14, 941–950. https://doi.org/10.1046/j.1523–1739.2000.98533.x
91. Lindner, M., Fitzgerald, J.B., Zimmermann, N.E., Reyer, C., Delzon, S., van der Maaten, E., Schelhaas, M.J., Lasch, P., Eggers, J., van der Maaten–Theunissen, M., Suckow, F., Psomas, A., Poulter, B., Hanewinkel, M., 2014. Climate change and European forests: What do we know, what are the uncertainties, and what are the implications for forest management? J. Environ. Manage. 146, 69–83. https://doi.org/10.1016/j.jenvman.2014.07.030
92. Lisein, J., Pierrot–Deseilligny, M., Bonnet, S., Lejeune, P., 2013. A photogrammetric workflow for the creation of a forest canopy height model from small unmanned aerial system imagery. Forests 4, 922–944. https://doi.org/10.3390/f4040922
93. Lowman, M.D., Wittman, P.K., 1996. FOREST CANOPIES : Methods, Hypotheses, and Future Directions A Brief History of Methods of Access. Annu. Rev. Ecol. 27, 55–81.
94. Lowrance, R., Altier, L.S., Newbold, J.D., Schnabel, R.R., Groffman, P.M., Denver, J.M., Correll, D.L., Gilliam, J.W., Robinson, J.L., Brinsfield, R.B., Staver, K.W., Lucas, W., Todd,

A.H., 1997. Water quality functions of riparian forest buffers in Chesapeake bay watersheds. Environ. Manage. 21, 687–712. https://doi.org/10.1007/s002679900060

95. Ma, Z., Hart, M.M., Redmond, R.L., 2001. Mapping vegetation across large geographic areas: integration of remote sensing and GIS to classify multisource data. Eng. Remote Sens. 67, 295–307.
96. Mac Nally, R., Parkinson, A., Horrocks, G., Conole, L., Tzaros, C., 2001. Relationships between terrestrial vertebrate diversity, abundance and availability of coarse woody debris on south–eastern Australian floodplains. Biol. Conserv. 99, 191–205. https://doi.org/10.1016/S0006–3207(00)00180–4
97. MacDicken, K.G., Sola, P., Hall, J.E., Sabogal, C., Tadoum, M., de Wasseige, C., 2015. Global progress toward sustainable forest management. For. Ecol. Manage. 352, 47–56. https://doi.org/10.1016/j.foreco.2015.02.005
98. Maezawa, K., Fukushima, Y., Nakagawa, I., Kawahara, S., 1968. A report on volume table for broad-leaved trees of Tokyo University Forest in Hokkaido. Misc. Inf. Tokyo Univ. For. 17, 77–100.
99. Maezawa, K., Kawahara, S., 1986. A preparation of the volume table for Saghalien Fir (Abies sachalinensis) trees of the University Forest in Hokkaido. Bull. Tokyo Univ. For. 74, 17–37.
100. Maltamo, M., Packalén, P., Yu, X., Eerikäinen, K., Hyyppä, J., Pitkänen, J., 2005. Identifying and quantifying structural characteristics of heterogeneous boreal forests using laser scanner data. For. Ecol. Manage. 216, 41–50. https://doi.org/10.1016/j.foreco.2005.05.034
101. Matese, A., Toscano, P., Di Gennaro, S.F., Genesio, L., Vaccari, F.P., Primicerio, J., Belli, C., Zaldei, A., Bianconi, R., Gioli, B., 2015. Intercomparison of UAV, aircraft and satellite remote sensing platforms for precision viticulture. Remote Sens. 7, 2971–2990. https://doi.org/10.3390/rs70302971
102. McCune, B., Grace, J.B., Urban D. L., 2002. Analysis of ecological communities. MjM Software Design, Oregon, USA.
103. McElhinny, C., Gibbons, P., Brack, C., 2006. An objective and quantitative methodology for constructing an index of stand structural complexity. For. Ecol. Manage. 235, 54–71. https://doi.org/10.1016/j.foreco.2006.07.024
104. McElhinny, C., Gibbons, P., Brack, C., Bauhus, J., 2005. Forest and woodland stand structural complexity: Its definition and measurement. For. Ecol. Manage. 218, 1–24. https://doi.org/10.1016/j.foreco.2005.08.034
105. McGaughey, R., 2016. FUSION/LDV: Software for LIDAR Data Analysis and Visualization. United States Dep. Agric. For. Serv. Pacific Northwest Res. Stn. 211.
106. McNeil, B.E., Pisek, J., Lepisk, H., Flamenco, E.A., 2016. Measuring leaf angle distribution in broadleaf canopies using UAVs. Agric. For. Meteorol. 218–219, 204–208. https://doi.org/10.1016/j.agrformet.2015.12.058
107. Meng, J., Li, S., Wang, W., Liu, Q., Xie, S., Ma, W., 2016. Estimation of forest structural diversity using the spectral and textural information derived from SPOT-5 satellite images. Remote Sens. 8. https://doi.org/10.3390/rs8020125
108. Merilä, P., Mustajärvi, K., Helmisaari, H.S., Hilli, S., Lindroos, A.J., Nieminen, T.M., Nöjd, P., Rautio, P., Salemaa, M., Ukonmaanaho, L., 2014. Above– and below–ground N stocks in coniferous boreal forests in Finland: Implications for sustainability of more intensive biomass utilization. For. Ecol. Manage. 311, 17–28. https://doi.org/10.1016/j.foreco.2013.06.029
109. Messier, C., Puettmann, K.J., 2011. Forests as complex adaptive systems: implications for forest management and modelling. L'Italia For. e Mont. 66, 249–258. https://doi.org/10.4129/ifm.2011.3.11

110. Messinger, M., Asner, G.P., Silman, M., 2016. Rapid assessments of amazon forest structure and biomass using small unmanned aerial systems. Remote Sens. 8, 1–15. https://doi.org/10.3390/rs8080615
111. Michez, A., Piégay, H., Lisein, J., Claessens, H., Lejeune, P., 2016. Classification of riparian forest species and health condition using multi–temporal and hyperspatial imagery from unmanned aerial system. Environ. Monit. Assess. 188, 1–19. https://doi.org/10.1007/s10661–015–4996–2
112. Millar, C.I., Stephenson, N.L., Stephens, S.L., 2007. Climate change and forests of the future: Managing in the face of uncertainty. Ecol. Appl. 17, 2145–2151. https://doi.org/10.1890/06–1715.1
113. Monserud, R. a., Sterba, H., 1996. A basal area increment model for individual trees growing in even– and uneven–aged forest stands in Austria. For. Ecol. Manage. 80, 57–80. https://doi.org/10.1016/0378–1127(95)03638–5
114. Moran, C.J., Rowell, E.M., Seielstad, C.A., 2018. A data–driven framework to identify and compare forest structure classes using LiDAR. Remote Sens. Environ. 211, 154–166. https://doi.org/10.1016/j.rse.2018.04.005
115. Müller, J., Gärtner–Roer, I., Thee, P., Ginzler, C., 2014. Accuracy assessment of airborne photogrammetrically derived high–resolution digital elevation models in a high mountain environment. ISPRS J. Photogramm. Remote Sens. 98, 58–69. https://doi.org/10.1016/j.isprsjprs.2014.09.015
116. Nabuurs, G.J., Thürig, E., Heidema, N., Armolaitis, K., Biber, P., Cienciala, E., Kaufmann, E., Mäkipää, R., Nilsen, P., Petritsch, R., Pristova, T., Rock, J., Schelhaas, M.J., Sievanen, R., Somogyi, Z., Vallet, P., 2008. Hotspots of the European forests carbon cycle. For. Ecol. Manage. 256, 194–200. https://doi.org/10.1016/j.foreco.2008.04.009
117. Nadkarni, N.M., 1994. Diversity of species and interactions in the upper tree canopy of forest ecosystems. Am. Zool. 78, 70–78.
118. Næsset, E., 1997. Estimating timber volume of forest stands using airborne laser scanner data. Remote Sens. Environ. 61, 246–253. https://doi.org/10.1016/S0034–4257(97)00041–2
119. Næsset, E., 2002. Predicting forest stand characteristics with airborne scanning laser using a practical two–stage procedure and field data. Remote Sens. Environ. 80, 88–99. https://doi.org/10.1016/S0034–4257(01)00290–5
120. Næsset, E., 2004. Accuracy of forest inventory using airborne laser scanning : evaluating the first nordic full–scale operational project Accuracy of Forest Inventory Using Airborne Laser scanning : Evalua. Test 37–41. https://doi.org/10.1080/02827580410019544
121. Næsset, E., 2007. Airborne laser scanning as a method in operational forest inventory: Status of accuracy assessments accomplished in Scandinavia. Scand. J. For. Res. 22, 433–442. https://doi.org/10.1080/02827580701672147
122. Næsset, E., Gobakken, T., Holmgren, J., Hyyppä, H., Hyyppä, J., Maltamo, M., Nilsson, M., Olsson, H., Persson, Å., Söderman, U., 2004. Laser scanning of forest resources: the nordic experience. Scand. J. For. Res. 19, 482–499. https://doi.org/10.1080/02827580410019553
123. Näsi, R., Honkavaara, E., Lyytikäinen–Saarenmaa, P., Blomqvist, M., Litkey, P., Hakala, T., Viljanen, N., Kantola, T., Tanhuanpää, T., Holopainen, M., 2015. Using UAV–based photogrammetry and hyperspectral imaging for mapping bark beetle damage at tree–level. Remote Sens. 7, 15467–15493. https://doi.org/10.3390/rs71115467
124. National greenhouse gas inventory report of Japan 2017. National Institute for Environmental Studies, Tsukuba. Available at http://www.cger.nies.go.jp/publications/report/i134/i134.pdf
125. Naughton–Treves, L., Wendland, K., 2014. Land Tenure and Tropical Forest Carbon Management. World Dev. 55, 1–6. https://doi.org/10.1016/j.worlddev.2013.01.010

126. Nelson, H.W., Williamson, T.B., Macaulay, C., Mahony, C., 2016. Assessing the potential for forest management practitioner participation in climate change adaptation. For. Ecol. Manage. 360, 388–399. https://doi.org/10.1016/j.foreco.2015.09.038
127. Nex, F., Remondino, F., 2014. UAV for 3D mapping applications: A review. Appl. Geomatics 6, 1–15. https://doi.org/10.1007/s12518–013–0120–x
128. Noss, R.F., 2001. Beyond Kyoto: Forest Management in a Time of Rapid Climate Change. Conserv. Biol. 15, 578–590. https://doi.org/10.1046/j.1523–1739.2001.015003578.x
129. Nurminen, K., Karjalainen, M., Yu, X., Hyyppä, J., Honkavaara, E., 2013. Performance of dense digital surface models based on image matching in the estimation of plot–level forest variables. ISPRS J. Photogramm. Remote Sens. 83, 104–115. https://doi.org/10.1016/j.isprsjprs.2013.06.005
130. Nyland, R., 2002. Silviculture: Concepts and applications. McGraw–Hill, Boston.
131. Ogaya, R., Barbeta, A., Başnou, C., Peñuelas, J., 2015. Satellite data as indicators of tree biomass growth and forest dieback in a Mediterranean holm oak forest. Ann. For. Sci. 72, 135–144. https://doi.org/10.1007/s13595–014–0408–y
132. Ota, T., Ogawa, M., Shimizu, K., Kajisa, T., Mizoue, N., Yoshida, S., Takao, G., Hirata, Y., Furuya, N., Sano, T., Sokh, H., Ma, V., Ito, E., Toriyama, J., Monda, Y., Saito, H., Kiyono, Y., Chann, S., Ket, N., 2015. Aboveground biomass estimation using structure from motion approach with aerial photographs in a seasonal tropical forest. Forests 6, 3882–3898. https://doi.org/10.3390/f6113882
133. Owari, T., Kamata, N., Tange, T., Kaji, M., Shimomura, A., 2011. Effects of silviculture treatments in a hurricane–damaged forest on carbon storage and emissions in central Hokkaido, Japan. J. For. Res. 22, 13–20. https://doi.org/10.1007/s11676–011–0118–3
134. Parker, G.G., Harmon, M.E., Lefsky, M.A., Chen, J., Pelt, R. Van, Weis, S.B., Thomas, S.C., Winner, W.E., Shaw, D.C., Frankling, J.F., 2004. Three–dimensional Structure of an Old–growth Pseudotsuga–Tsuga Canopy and Its Implications for Radiation Balance, Microclimate, and Gas Exchange. Ecosystems 7, 440–453. https://doi.org/10.1007/s10021–004–0136–5
135. Pasher, J., King, D.J., 2010. Multivariate forest structure modelling and mapping using high resolution airborne imagery and topographic information. Remote Sens. Environ. 114, 1718–1732. https://doi.org/10.1016/j.rse.2010.03.005
136. Pasher, J., King, D.J., 2011. Development of a forest structural complexity index based on multispectral airborne remote sensing and topographic data. Can. J. For. Res. 41, 44–58. https://doi.org/10.1139/X10–175
137. Pelt, R. Van, Nadkarni, N.M., 2004. Development of Canopy Structure in Pseudotsuga menziesii Forests in the South ...
138. Pierzchała, M., Talbot, B., Astrup, R., 2014. Estimating soil displacement from timber extraction trails in steep terrain: Application of an unmanned aircraft for 3D modelling. Forests 5, 1212–1223. https://doi.org/10.3390/f5061212
139. Ploton, P., Barbier, N., Couteron, P., Antin, C.M., Ayyappan, N., Balachandran, N., Barathan, N., Bastin, J.F., Chuyong, G., Dauby, G., Droissart, V., Gastellu–Etchegorry, J.P., Kamdem, N.G., Kenfack, D., Libalah, M., Mofack, G., Momo, S.T., Pargal, S., Petronelli, P., Proisy, C., Réjou–Méchain, M., Sonké, B., Texier, N., Thomas, D., Verley, P., Zebaze Dongmo, D., Berger, U., Pélissier, R., 2017. Toward a general tropical forest biomass prediction model from very high resolution optical satellite images. Remote Sens. Environ. 200, 140–153. https://doi.org/10.1016/j.rse.2017.08.001
140. Poteete, A.R., Ostrom, E., 2004. Heterogeneity, group size and collective action: The role of institutions in forest management. Dev. Change 35, 435–461. https://doi.org/10.1111/j.1467–7660.2004.00360.x

141. Pretzsch, H., 1997. Analysis and modeling of spatial stand structures. Methodological considerations based on mixed beech–larch stands in lower saxony. For. Ecol. Manage. 97, 237–253. https://doi.org/10.1016/S0378–1127(97)00069–8
142. Pukkala, T., Lähde, E., Laiho, O., Salo, K., Hotanen, J.–P., 2011. A multifunctional comparison of even–aged and uneven–aged forest management in a boreal region. Can. J. For. Res. 41, 851–862. https://doi.org/10.1139/x11–009
143. Puliti, S., Ene, L.T., Gobakken, T., Næsset, E., 2017. Use of partial–coverage UAV data in sampling for large scale forest inventories. Remote Sens. Environ. 194, 115–126. https://doi.org/10.1016/j.rse.2017.03.019
144. Puliti, S., Olerka, H., Gobakken, T., Næsset, E., 2015. Inventory of Small Forest Areas Using an Unmanned Aerial System. Remote Sens. 7, 9632–9654. https://doi.org/10.3390/rs70809632
145. R Core Team (2013). R: A language and environment for statistical computing. R Foundation for Statistical Computing, Vienna, Austria. URL http://www.R-project.org/.
146. Reitberger, J., Krzystek, P., Stilla, U., 2008. Analysis of full waveform LIDAR data for the classification of deciduous and coniferous trees. Int. J. Remote Sens. 29, 1407–1431. https://doi.org/10.1080/01431160701736448
147. Remondino, F., Spera, M.G., Nocerino, E., Menna, F., Nex, F., 2014. State of the art in high density image matching. Photogramm. Rec. 29, 144–166. https://doi.org/10.1111/phor.12063
148. Saari, H., Aallos, V.–V., Akujärvi, A., Antila, T., Holmlund, C., Kantojärvi, U., Mäkynen, J., Ollila, J., 2009. Novel miniaturized hyperspectral sensor for UAV and space applications 74741M. https://doi.org/10.1117/12.830284
149. Saatchi, S., Houghton, R.A., Dos Santos Alvalá, R.C., Soares, J. V., Yu, Y., 2007. Distribution of aboveground live biomass in the Amazon basin. Glob. Chang. Biol. 13, 816–837. https://doi.org/10.1111/j.1365-2486.2007.01323.x
150. Sabogal, C., Guariguata, Manuel, R., Broadhead, J., Lescuyer, G., Savilaakso, S., Essoungou, J.N., Sist, P., 2013. Multiple–use forest management in the humid tropics Opportunities and challenges for sustainable forest management, Fao.
151. Salamí, E., Barrado, C., Pastor, E., 2014. UAV flight experiments applied to the remote sensing of vegetated areas. Remote Sens. 6, 11051–11081. https://doi.org/10.3390/rs61111051
152. Santi, E., Paloscia, S., Pettinato, S., Fontanelli, G., Mura, M., Zolli, C., Maselli, F., Chiesi, M., Bottai, L., Chirici, G., 2017. The potential of multifrequency SAR images for estimating forest biomass in Mediterranean areas. Remote Sens. Environ. 200, 63–73. https://doi.org/10.1016/j.rse.2017.07.038
153. Schreuder, H.T., Gregoire, T.G., Wood, G.B., 1993. Sampling methods for multiresource forest inventory. John Wiley & Sons, Inc, New York, NY, USA.
154. Seidl, R., Schelhaas, M.J., Rammer, W., Verkerk, P.J., 2014. Increasing forest disturbances in Europe and their impact on carbon storage. Nat. Clim. Chang. 4, 806–810. https://doi.org/10.1038/nclimate2318
155. Shrestha, G., Stahl, P.D., 2008. Carbon accumulation and storage in semi–arid sagebrush steppe: Effects of long–term grazing exclusion. Agric. Ecosyst. Environ. 125, 173–181. https://doi.org/10.1016/j.agee.2007.12.007
156. Smigaj, M., Gaulton, R., Barr, S.L., Suárez, J.C., 2015. Uav–Borne Thermal Imaging for Forest Health Monitoring: Detection of Disease–Induced Canopy Temperature Increase. ISPRS – Int. Arch. Photogramm. Remote Sens. Spat. Inf. Sci. XL–3/W3, 349–354. https://doi.org/10.5194/isprsarchives–XL–3–W3–349–2015

157. Snavely, N., Seitz, S.M., Szeliski, R., 2008. Modeling the world from Internet photo collections. Int. J. Comput. Vis. 80, 189–210. https://doi.org/10.1007/s11263–007–0107–3
158. Snowdon, P., 1991. A ratio estimator for bias correction in logarithmic regression. Can. J. For. Res. 21, 720–724. https://doi.org/https://doi.org/10.1139/x91–101
159. Sona, G., Pinto, L., Pagliari, D., Passoni, D., Gini, R., 2014. Experimental analysis of different software packages for orientation and digital surface modelling from UAV images. Earth Sci. Informatics 7, 97–107. https://doi.org/10.1007/s12145–013–0142–2
160. Spies, T. a, 1998. Forest Structure : A Key to the Ecosystem. Northwest Sci. 72, 34–39.
161. Spies, T. a, Franklin, J.F., 1991. The Structure of Natural Young, Mature, and Old–Growth Douglas–Fir Forests in Oregon and Washington. Wildl. Veg. Unmanaged Douglas–Fir For. 91–109.
162. Spriggs, R., Coomes, D., Jones, T., Caspersen, J., Vanderwel, M., 2017. An Alternative Approach to Using LiDAR Remote Sensing Data to Predict Stem Diameter Distributions across a Temperate Forest Landscape. Remote Sens. 9, 944. https://doi.org/10.3390/rs9090944
163. Steininger, M.K., 2000. Satellite estimation of tropical secondary forest above–ground biomass: Data from Brazil and Bolivi. Int. J. Remote Sens. 21, 1139–1157. https://doi.org/10.1080/014311600210119
164. Su, Y., Guo, Q., 2014. A practical method for SRTM DEM correction over vegetated mountain areas. ISPRS J. Photogramm. Remote Sens. 87, 216–228. https://doi.org/10.1016/j.isprsjprs.2013.11.009
165. Sumnall, M.J., Hill, R.A., Hinsley, S.A., 2016. Comparison of small–footprint discrete return and full waveform airborne lidar data for estimating multiple forest variables. Remote Sens. Environ. 173, 214–223. https://doi.org/10.1016/j.rse.2015.07.027
166. Takagi, K., Yone, Y., Takahashi, H., Sakai, R., Hojyo, H., Kamiura, T., Nomura, M., Liang, N., Fukazawa, T., Miya, H., Yoshida, T., Sasa, K., Fujinuma, Y., Murayama, T., Oguma, H., 2015. Forest biomass and volume estimation using airborne LiDAR in a cool–temperate forest of northern Hokkaido, Japan. Ecol. Inform. 26, 54–60. https://doi.org/10.1016/j.ecoinf.2015.01.005
167. Tatewaki, M., 1958. Forest Ecology of the Islands of. J. Fac. Agric. Hokkaido Univ. 50, 371–486.
168. The University of Tokyo Hokkaido Forest, 2017. , http://www.uf.a.u–tokyo.ac.jp/files/gaiyo_hokkaido.pdf.
169. Thiel, C., Schmullius, C., 2017. Comparison of UAV photograph–based and airborne lidar–based point clouds over forest from a forestry application perspective. Int. J. Remote Sens. 38, 2411–2426. https://doi.org/10.1080/01431161.2016.1225181
170. Tompalski, P., Coops, N.C., Marshall, P.L., White, J.C., Wulder, M.A., Bailey, T., 2018. Combining multi-date airborne laser scanning and digital aerial photogrammetric data for forest growth and yield modelling. Remote Sens. 10, 1–21. https://doi.org/10.3390/rs10020347
171. Torontow, V., King, D., 2011. Forest complexity modelling and mapping with remote sensing and topographic data: A comparison of three methods. Can. J. Remote Sens. 37, 387–402. https://doi.org/10.5589/m11–047
172. Torresan, C., Berton, A., Carotenuto, F., Di, S.F., Gioli, B., Matese, A., Miglietta, F., Zaldei, A., Wallace, L., Torresan, C., Berton, A., Carotenuto, F., Di, S.F., Gioli, B., Matese, A., Miglietta, F., Vagnoli, C., 2017. Forestry applications of UAVs in Europe : a review Forestry applications of UAVs in Europe : a review. Int. J. Remote Sens. 38, 2427–2447. https://doi.org/10.1080/01431161.2016.1252477

173. Tuominen, S., Balazs, A., Saari, H., Pölönen, I., Sarkeala, J., Viitala, R., 2015. Unmanned aerial system imagery and photogrammetric canopy height data in area–based estimation of forest variables. Silva Fenn. 49. https://doi.org/10.14214/sf.1348
174. Vastaranta, M., Wulder, M.A., White, J.C., Pekkarinen, A., Tuominen, S., Ginzler, C., Kankare, V., Holopainen, M., Hyyppä, J., Hyyppä, H., 2013. Airborne laser scanning and digital stereo imagery measures of forest structure: Comparative results and implications to forest mapping and inventory update. Can. J. Remote Sens. 39, 382–395. https://doi.org/10.5589/m13–046
175. Véga, C., Renaud, J.P., Durrieu, S., Bouvier, M., 2016. On the interest of penetration depth, canopy area and volume metrics to improve Lidar–based models of forest parameters. Remote Sens. Environ. 175, 32–42. https://doi.org/10.1016/j.rse.2015.12.039
176. Verhoeven, G., Doneus, M., Briese, C., Vermeulen, F., 2012. Mapping by matching: A computer vision–based approach to fast and accurate georeferencing of archaeological aerial photographs. J. Archaeol. Sci. 39, 2060–2070. https://doi.org/10.1016/j.jas.2012.02.022
177. Wallace, L., Lucieer, A., Malenovský, Z., Turner, D., Petr, V., 2016. Assessment of forest structure using two UAV techniques: A comparison of airborne laser scanning and structure from motion (SfM) point clouds. Forests 7, 1–16. https://doi.org/10.3390/f7030062
178. Watson, J., Freudenberger, D., Paull, D., 2001. An assessment of the focal–species approach for conserving birds in variegated landscapes in southeastern Australia. Conserv. Biol. 15, 1364–1373. https://doi.org/10.1046/j.1523–1739.2001.00166.x
179. Watts, A.C., Ambrosia, V.G., Hinkley, E.A., 2012. Unmanned aircraft systems in remote sensing and scientific research: Classification and considerations of use. Remote Sens. 4, 1671–1692. https://doi.org/10.3390/rs4061671
180. Westoby, M.J., Brasington, J., Glasser, N.F., Hambrey, M.J., Reynolds, J.M., 2012. "Structure-from-Motion" photogrammetry: A low-cost, effective tool for geoscience applications. Geomorphology 179, 300–314. https://doi.org/10.1016/j.geomorph.2012.08.021
181. White, E.M., 2017. Spending patterns of outdoor recreation visitors to national forests. USDA For. Serv. – Gen. Tech. Rep. PNW–GTR 2017.
182. White, J., Stepper, C., Tompalski, P., Coops, N., Wulder, M.A., 2015. Comparing ALS and Image–Based Point Cloud Metrics and Modelled Forest Inventory Attributes in a Complex Coastal Forest Environment. Forests 6, 3704–3732. https://doi.org/10.3390/f6103704
183. White, J.C., Tompalski, P., Coops, N.C., Wulder, M.A., 2018. Comparison of airborne laser scanning and digital stereo imagery for characterizing forest canopy gaps in coastal temperate rainforests. Remote Sens. Environ. 208, 1–14. https://doi.org/10.1016/j.rse.2018.02.002
184. White, J.C., Wulder, M.A., Vastaranta, M., Coops, N.C., Pitt, D., Woods, M., 2013. The utility of image–based point clouds for forest inventory: A comparison with airborne laser scanning. Forests 4, 518–536. https://doi.org/10.3390/f4030518
185. Wilkes–Allemann, J., Pütz, M., Hirschi, C., 2015. Governance of Forest Recreation in Urban Areas: Analysing the role of stakeholders and institutions using the institutional analysis and development framework. Environ. Policy Gov. 25, 139–156. https://doi.org/10.1002/eet.1668
186. Wolf, P.; Dewitt, B., 2000. Elements of photogrammetry with applications in GIS, Third Edit. ed. McGraw–Hill, New York, NY, USA.
187. Wong, W.V.C. Tsuyuki, S. Phua, M. Ioki, K. Takao, G., 2016. Performance of a photogrammetric digital elevation model in a tropical montane forest environment. J. For. Plan. 21, 39–52.
188. Wong, W.V.C., Tsuyuki, S., Phua, M., Ioki, K., Takao, G., 2013. Forest biophyiscal characteristics estimation using digital aerial photogrammetry and airbone laser scanning for tropical montane forests 10.

189. Woods, M., Pitt, D., Penner, M., Lim, K., Nesbitt, D., Etheridge, D., Treitz, P., 2011. Operational implementation of a LiDAR inventory in Boreal Ontario. For. Chron. 87, 512–528. https://doi.org/10.5558/tfc2011–050
190. Wulder, M.A., Coops, N.C., Hudak, A.T., Morsdorf, F., Nelson, R.F., Newnham, G.J., Vastaranta, M., 2013. Status and prospects for LiDAR remote sensing of forested ecosystems.pdf. Can. J. Remote Sens. 39, S1–S5. https://doi.org/10.5589/m13–051
191. Xie, Y., Sha, Z., Yu, M., 2008. Remote sensing imagery in vegetation mapping: a review. J. Plant Ecol. 1, 9–23. https://doi.org/10.1093/jpe/rtm005
192. Yoga, S., Bégin, J., St–Onge, B., Riopel, M., 2017. Modeling the effect of the spatial pattern of airborne lidar returns on the prediction and the uncertainty of timber merchantable volume. Remote Sens. 9, 1–13. https://doi.org/10.3390/rs9080808
193. Yu, X., Hyyppä, J., Karjalainen, M., Nurminen, K., Karila, K., Vastaranta, M., Kankare, V., Kaartinen, H., Holopainen, M., Honkavaara, E., Kukko, A., Jaakkola, A., Liang, X., Wang, Y., Hyyppä, H., Katoh, M., 2015. Comparison of laser and stereo optical, SAR and InSAR point clouds from air– and space–borne sources in the retrieval of forest inventory attributes. Remote Sens. 7, 15933–15954. https://doi.org/10.3390/rs71215809
194. Yuan, C., Zhang, Y., Liu, Z., 2015. A survey on technologies for automatic forest fire monitoring, detection, and fighting using unmanned aerial vehicles and remote sensing techniques. Can. J. For. Res. 45, 783–792. https://doi.org/10.1139/cjfr–2014–0347
195. Zahawi, R.A., Dandois, J.P., Holl, K.D., Nadwodny, D., Reid, J.L., Ellis, E.C., 2015. Using lightweight unmanned aerial vehicles to monitor tropical forest recovery. Biol. Conserv. 186, 287–295. https://doi.org/10.1016/j.biocon.2015.03.031
196. Zarco–Tejada, P.J., Diaz–Varela, R., Angileri, V., Loudjani, P., 2014. Tree height quantification using very high resolution imagery acquired from an unmanned aerial vehicle (UAV) and automatic 3D photo–reconstruction methods. Eur. J. Agron. 55, 89–99. https://doi.org/10.1016/j.eja.2014.01.004
197. Zellweger, F., Braunisch, V., Baltensweiler, A., Bollmann, K., 2013. Remotely sensed forest structural complexity predicts multi species occurrence at the landscape scale. For. Ecol. Manage. 307, 303–312. https://doi.org/10.1016/j.foreco.2013.07.023
198. Zhang, X., Kondragunta, S., 2006. Estimating forest biomass in the USA using generalized allometric models and MODIS land products. Geophys. Res. Lett. 33, 1–5. https://doi.org/10.1029/2006GL025879
199. Zhao, K., Popescu, S., Meng, X., Pang, Y., Agca, M., 2011. Characterizing forest canopy structure with lidar composite metrics and machine learning. Remote Sens. Environ. 115, 1978–1996. https://doi.org/10.1016/j.rse.2011.04.001
200. Zheng, D., Rademacher, J., Chen, J., Crow, T., Bresee, M., Le Moine, J., Ryu, S.R., 2004. Estimating aboveground biomass using Landsat 7 ETM+ data across a managed landscape in northern Wisconsin, USA. Remote Sens. Environ. 93, 402–411. https://doi.org/10.1016/j.rse.2004.08.008

Appendix

Appendix 1

Basic criteria used in conventional forest stand classification

Stand type		Number of juveniles and small diameter trees	Number of medium and large diameter trees	Number of medium and large diameter trees	Number of juvenile and small diameter trees
		Conifer	Conifer and broadleaf	Conifer ratio	Broadleaf
Conifer–dominating mixed	CDM	High	High	–	–
Young conifer	YC		Low	–	–
Conifer–dominating mixed with poor regeneration	CDM-PR	Low	High	High	–
Broadleaf–dominating mixed	BDM			Low	–
Young broadleaf	YB		Low	–	High
Sparse forest	SF			–	Low

	Number of juvenile and small diameter trees (per ha)		Volume of medium and large diameter trees (m^3/ha)	Volume of medium and large diameter trees (m^3/ha)	Ratio of medium and large diameter conifer (%)
	Conifer	Broadleaf	Conifer dominant	Broadleaf dominant	
High	≥500	≥1000	≥250	≥200	≥70
Medium*	300-500	500-1000	150-250	100-200	30-70
Low	<300	<500	<150	<100	<30

Tree type	DBH (cm)	Height (m)
Juvenile	<5	≥1.3
Small diameter	5-25	
Medium diameter	25-39	
Large diameter	39-59	

* Forest stand type delineation may be changed depending on the situation.

Source: 13th Forest management plan of University of Tokyo Hokkaido Forest (UTHF) 2011–2020.

Reserve forest (RF) delineation is not solely based on the vegetation type and structure, but take several other factors into consideration, e.g., terrain condition (altitude, slope), site condition (poor sites with rocky terrain etc.), stream network, forest road network. There is no fixed criteria, thus the delineation is based on the expertise and the experience of the interpreter (Source: interview with technical staff members of UTHF).

Appendix 2

Appendix 2.1: Number of training samples used for vegetation classification

Ground cover class	Number of training samples (pixels)		
	Compartment 43	Compartment 45	Compartment 48
Broadleaf vegetation	3275	4275	5275
Conifer vegetation	4470	3470	2470
Sasa bamboo	900	1100	1200
Bare earth	630	530	730
Canopy gaps	325	425	225
Total	9600	9800	9900

The interpretation was done manually by considering the spectral values. For this study, I used a total of 29,300 (0.7325 ha) pixels for an area of about 1,000 ha. Training sample area accounted for 0.735% of the total study area. In each location; (1) identified the ground cover (broadleaf, conifer, sasa, bare earth, and canopy gap) type visually, and (2) polygons were drawn to mark pixels that fall into the same ground cover type and specific number was assign for each ground cover type (For example I assigned “1” for broadleaf, “2” for conifers, “3” for Sasa, “4” for Bare earth, and “5” for canopy gaps). This process was repeated for randomly distributed sample locations. It took about 90 min for sample selection for each compartment.

Appendix 2.2: Vegetation classification of compartment 43, 45 and 48 using UAV images acquired in June, 2017.

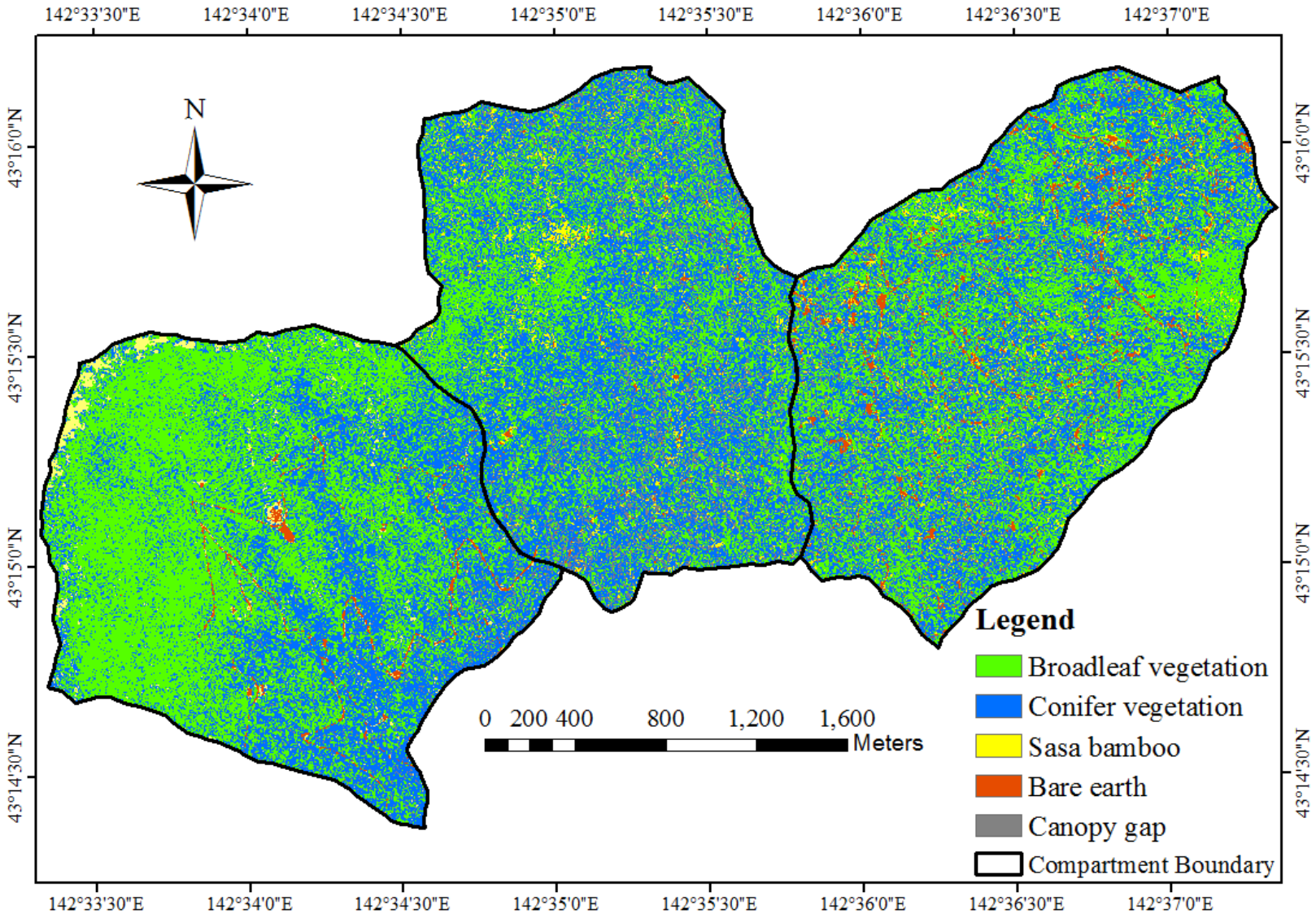

Appendix 2.3: Accuracy Assessment of the vegetation classification

Compartment 43

		Validation (pixel–based)						
	Ground clover class	Broadleaf vegetation	Conifer vegetation	Sasa bamboo	Bare earth	Canopy gaps	Total	User's Accuracy
Classification	Broadleaf vegetation	2415	85	0	0	0	2500	96.6%
	Conifer vegetation	62	1709	199	0	30	2000	85.5%
	Sasa bamboo	15	186	278	0	21	500	55.6%
	Bare earth	0	0	20	220	10	250	88.0%
	Canopy gaps	0	10	10	0	230	250	92.0%
	Total	2492	1990	507	220	291	5500	
	Producer's Accuracy	96.9%	85.9%	54.8%	100.0%	79.0%		

Overall accuracy = 88.2% **Kappa coefficient = 81.9**

Compartment 48

		Validation (pixel–based)						
	Ground cover class	Broadleaf vegetation	Conifer vegetation	Sasa bamboo	Bare earth	Canopy gaps	Total	User's Accuracy
Classification	Broadleaf vegetation	2414	44	42	0	0	2500	96.6%
	Conifer vegetation	58	1786	156	0	0	2000	89.3%
	Sasa bamboo	15	16	448	0	21	500	89.6%
	Bare earth	0	0	12	228	10	250	91.2%
	Canopy gaps	0	0	0	14	236	250	94.4%
	Total	2487	1846	658	242	267	5500	
	Producer's Accuracy	97.1%	96.7%	68.1%	94.2%	88.4%		

Overall accuracy = 92.9% **Kappa coefficient = 89.3**

Compartment 45

		Validation						
	Class	Broadleaf vegetation	Conifer vegetation	Sasa bamboo	Bare earth	Canopy gaps	Total	User's Accuracy
Classification	Broadleaf vegetation		54	64	0	0	2500	95.3%
	Conifer vegetation	102	1537	210	0	40	1889	81.4%
	Sasa bamboo	15	16	448	0	21	500	89.6%
	Bare earth	0	0	20	230	0	250	92.0%
	Canopy gaps	0	43	0	0	217	260	83.5%
	Total	2499	1650	742	230	278	4814	
Producer's Accuracy		95.3%	93.2%	60.4%	100.0%	78.1%	5399	
Overall accuracy = 89.2%					**Kappa coefficient =**		**83.6**	

Validation sample selection and marking procedure was similar to the training sample selection and marking. For each compartment it took about 60 min for sample selection.

In this study, the training and validation sample selection was conducted by the author of this study. Although I tried my best to carry out an unbiased sample selection, some personal bias could still be included in the validation. Therefore, for unbiased validation, the training and validation sample selection could be conducted by two different persons (commonly applied method in many studies).

Appendix 3–6

The content of appendix 3–6 contain information related to Chapter 4, Chapter 5 and Chapter 6, which are already submitted or schedule to be submitted to peer review academic journals. For any inquiry or further information, please send an email to sadeepasenarath@yahoo.com